Modeling Flood Extent of a Large Wetland in a Data-Scarce Region Using Hydrodynamic and Empirical Models

Md Mominul Haque

Thesis submitted in partial fulfillment of the requirements for the Doctorate in Philosophy degree in Civil Engineering

Department of Civil Engineering
Faculty of Engineering
University of Ottawa

Dr. Ousmane Seidou (University of Ottawa) - Primary Supervisor

Dr. Majid Mohammadian (University of Ottawa) - Co-supervisor

DIRECTEUR (DIRECTRICE) DE LA TH`ESE / THESIS SUPERVISORS

EXAMINATEURS (EXAMINATRICES) DE LA THESE /

THESIS EXAMINERS

Dr. Musandji Fuamba (Polytechnique Montréal)

Dr. Hamidreza Shirkhani (University of Ottawa)

Dr. Bahram Daneshfar (University of Ottawa)

Dr. Colin Rennie (University of Ottawa)

Monday, January 13, 2020

DATE DE LA SOUTENANCE / DATE OF ORAL DEFENCE

Abstract

Wetlands are dynamic ecosystems and important sources of natural resources that provide a large array of ecosystem services. Unfortunately, most wetlands are threatened by human and natural stressors, such as damming, irrigation, water abstraction, climate change and variability that compromise the sustainability of the whole system. The Inner Niger Delta (IND), Mali, West Africa, is one of the biggest floodplains in the world, has a vast natural resource that attracts many people to live in and around the delta. The IND is considered a hub of human activities that include agriculture, fishing, transport, and tourism and plays an important role in promoting sustainable development for food security, water management, and the environment. As for most wetlands in the world, the very existence of the IND is at stake with the ever-increasing number of dams and irrigation schemes that are built to feed the growing population in the region. Given the fragility of the system and the multiplicity of water uses in the IND, the current knowledge of the flood dynamics and its relation to ecosystem services and the productivity of economic activity is insufficient. There is no operational hydrodynamic model of the IND, and the Malian authorities rely on simplified models and empirical relations for water resources management in the area. This thesis contributes to a better water resources management of the IND by a) developing the first 2D hydrodynamic model based on a triangular adaptative mesh of the IND that performs well despite the poor quality of available topographic/bathymetric data b) developing an innovative way of accounting for the strong hysteresis phenomenon in the IND in the hydrodynamic modeling that allowed a better reproduction of the hydraulic connectivity between important lakes and the main river and c) developing the first non-stationary relationship between the water levels at a reference station and the flooded area in the IND.

The first part of the thesis deals with the challenge of developing a hydrodynamic model using only two low-resolution satellite-derived Digital Elevation Models: the Shuttle Radar Topography Mission (SRTM), which has a 30m horizontal resolution, and the Multi-Error-Removed Improved-Terrain (MERIT). Given the low vertical accuracy of global DEMs, another DEM was derived using the waterline method, by combining water extent map from satellite images and local water level information. Channel depths were approximated using the hydraulic geometric relationship methods, while the friction coefficient was derived from the global land-use class classification

(GLCC) data. The river network was extracted from the water extent map corresponding to the lowest water level. Six different hydrodynamic models were created by varying the DEM and downstream boundary conditions. Each of the models was calibrated for discharge and water levels. Bayesian Model Averaging (BMA) was finally used to combine the outputs of all six hydrodynamic models into one robust simulation.

In the second part, the effect of hysteresis at the downstream boundary condition of the hydrodynamic model was examined. Existing hydrodynamic models of the IND use a static stage-discharge relationship as a downstream boundary condition during both the rise and recession of the flood, leading to potential inaccuracies in the simulation of the flood extent. This paper explores the improvement in the simulation of the flood and connectivity dynamics resulting from the use of a looped rating curve at the downstream boundary of a hydrodynamic model of the IND. The hysteresis effect is integrated into the rating curve using two methods, one based on dimensionless discharges and levels (DLRC) and the other based on the modified Jones formula (MJRC). Results show that the hysteresis effect is better represented using DLRC and that simulations using any of the modified rating curves improves the accuracy of floodplain extent simulations in the areas close to the downstream station, as well as the timing of the connectivity of the river system to one important lake in the IND. The improvement in water level simulation decreases steadily with distance from the downstream boundary of the modeled area.

The third part of the thesis deals with the development of an improved relation between inundation extent and water levels in the IND. Accurate knowledge of the flooded extent considered crucial for the proper management of natural resources in the IND. Several authors have developed empirical relationships between water levels at key stations in the IND and the flooded extent in an attempt to provide simple tools to link hydraulic parameters to the performance socio-economic activities in the IND. However, simulations from a hydrodynamic model of the IND showed that the relationship between water levels and the inundation extents varies greatly from year to year, and cannot be adequately captured by static formulas. First, it is demonstrated in this paper that if the maximum water level area is known in advance, accurate relationships between water levels and inundation extents can be derived. In the second part of the paper, stepwise regression is used to develop a function that can forecast maximum water levels at Akka using observed streamflow and precipitation upstream of the Delta. The combination of the two results allows a realtime estimation of the inundated area in the IND using observed water levels, precipitation, and streamflow.

Acknowledgement

I would like to express my gratitude to my supervisors, Dr. Ousmane Seidou and Dr. Majid Mohammadian for all the support, encouragement and guidance during my study. All your comments and feedbacks have been very valuable to me.

I would like to thank my thesis evaluation committee members, Dr. Musandji Fuamba, Dr. Colin Rennie, Dr. Bahram Daneshfar and Dr. Hamidreza Shirkhani, for providing precious suggestions and comments on my thesis.

I would also like to convey my appreciation to the University of Ottawa for funding my PhD research including the generous support provided throughout the study. I am grateful to the Public Works Department (PWD) and the Ministry of Housing and Public Works, Bangladesh for all kinds of support I have received during this time.

I like to give my thanks to my wife, Roksana, who gave me continuous support while I pursued this degree. My children (Ardi, Arini and Ayaan) have been my constant source of happiness. Without their constant encouragement, I would not be able to produce this piece of scientific work. Thank you to my brothers Helal, Al Amin, Zahir and my sister, Hasna for all kinds of help and supports. I cannot find the right words to show my appreciation to everybody who has been part of my PhD studies. All I can say is I am thankful for everything.

Finally, I would like to thank my parents for their love and dua throughout my stay and studies. I am missing my mother who could not see the end of the study.

To my mother

Contents

List of Figures

List of Tables

List of acronyms

ASTER	Advanced Spaceborne Thermal Emission and Reflection Radiometer
AMMA	African Monsoon Multidisciplinary Analyses
BMA	Bayesian Model Averaging
CN2	SCS runoff curve number for moisture condition II
ICE- Sat	Ice, Cloud, and land Elevation Satellite
DEM	Digital elevation model
DLR	German Aerospace Centre
DLRC	Dimensionless discharges and water level
DNH	Direction Nationale de l'Hydraulique
d/s	Downstream
ERS	European Remote Sensing Satellite
ENVISAT	Environmental Satellite
ETM	Enhanced Thematic Mapper
GLAS	Geoscience Laser Altimeter System
GLCC	Global Land Cover Characterization
GRDC	Global runoff data center
HL-RMS	Hydrology Laboratory Research Modeling System
HRCDHM	A hydrological model
IND	Inner Niger Delta
JEXA	Japan Aerospace Exploration Agency
JULES	Joint UK Land-Environment Simulator
LiDAR	light detection and ranging
LM	Linear regression model
MERIT	Multi-Error-Removed Improved-Terrain
MJRC	Modified Jones formula
mIGN	Institut national de l'information's datum
MIR	Mid Infrared
MNDWI	Modified Normalized Difference Water Index
MODIS	The Moderate Resolution Imaging Spectroradiometer

NASA	The National Aeronautics and Space Administration
NDMI	Normalized Difference Moisture Index
NDWI	Normalized Difference Water Index
NDVI	Normalized Difference Vegetation Index
NIR	Near Infrared
NSIDC	National Snow and Ice Data Centre
NS	Nash-Sutcliffe coefficient
r	Correlation coefficient
RADARSAT	Radar Satellite system by CSA, Canada
RCHRG_DP	Deep aquifer percolation fraction
RE	Relative error
RES_K	Hydraulic conductivity of the reservoir bottom, mm/hr
RMSE	Root-mean-square-error
RCP	Representative Concentration Pathway
RS	Remote Sensing
SAC-SMA	The Sacramento Soil Moisture Accounting conceptual watershed model
SAR	Synthetic aperture radar
SCS	Soil Conservation Service
SRTM	The Shuttle Radar Topography Mission
SUFI-2	Sequential Uncertainty Fitting program
SWAT	Soil Water Assessment Tools
TOPNET	A hydrological model
TM	Thematic Mapper
u/s	Upstream
UNB	Upper Niger Basin
USACE	the U.S. Army Corps of Engineers
USGS	The United States Geological Survey
WATFLOOD	A hydrological model developed at the University of Waterloo, Canada

List of symbols

h	Depth of water (m) in Eq 2.1
u, v	Velocity components in x and y directions (m/s),
g	Gravity acceleration(m/s^2),
Z	Free surface elevation (m),
t	Time(s) in Eq 2.1- Eq.2.3
n	Manning's coefficient
x, y	Horizontal space coordinates(m),
S_h	Source or sink of fluid,
v_t	Eddy viscosity (m^2/s),
F_x, F_y	Source or sink terms in dynamic equation
C_f	Friction coefficient
∇	Gradient
div	Divergence
τ_x	Friction stresses in x direction
ρ	Density of water (kg/m^3)
K	Conveyance factor,
M	Friction law exponent *(~2/3),*
N	Channel-shape parameter *(~0-1),*
a, c	Rating curve constants in Eq 2.25
b	Water level corresponds to zero discharge in Eq 2.25
h	Measured water level in Eq 2.26
H_{sc}	Scaled water level,
H	Observed water level in Eq 2.27
H_{min}	Minimum water level
H_{max}	Maximum water level
Q_{sc}	Scaled discharge,
Q	Observed discharge in Eq 2.28
Q_{max}	Maximum discharge
Q_s	Discharge obtained from single rating curve.

Q_{loop}	Discharge of loop rating curve in Eq. 2.20
WL_{loop}	Water level of loop rating curve in Eq 2.29
y	Quantity to be forecasted in Eq 2.19
D	Observed data set
K	Number of ensemble model
$p(y\|D)$	Probability density function of BMA prediction for y given data D
$p(f\|D)$	Posterior probability of model prediction f given data D
w	BMA weight
$p(y\|f,D)$	Conditional pdf of y on the condition on f and data D.
$E[y\|D]$	Mean of BMA
$Var[y\|D]$	Variance of BMA
σ^2	Variance associated with model prediction f with respect to data D
a, c, and k	Coefficients in Eq 4.3-Eq 4.5
b, f, and m	Exponents in Eq 4.3-Eq 4.5
x	Simulated value of variable in Eq 2.31- Eq 2.34
y	Observed value of variable in Eq 2.31- Eq 2.34
$\bar{x}$	Average of observed value
$\bar{y}$	Average of simulated values
F_A	Agreement fit measures
F_{UP}	Under-prediction measures
F_{OP}	Over-prediction measures
$E_P \cap E_o$	Intersection between observed and modeled area
$E_P \cup E_o$	Union between observed and modeled area
E_o	Observed flood extent
E_P	Modeled flood extent
SW_t	Final soil water content (mm/d)
SW_0	Initial soil water content (mm/d)
R_{day}	Precipitation(mm/d)
Q_{surf}	Surface runoff (mm/d)
E_a	Evapotranspiration (mm/d)
Q_{gw}	Return flow (mm/d)

Chapter 1

Introduction

1.1 Background

The Inner Niger Delta (IND) is the second-largest wetland in Africa (Ramsar, 2004), and its maximum inundated area can exceed 30,000 km^2 during wet years (Zwarts and Frerotte, 2012). Its main water sources are the Niger and Bani Rivers, which enter the study area at Ké-Macina and Sofara. The Niger River flows through the Delta over several hundred kilometers before exiting at Diré (Fig. 1.1). The maximum inundation area shrinks to around 10,000 km^2 in dry years (Zwarts et al., 2005) under the combined impacts of climate variability, irrigation withdrawals, and dam operation. The IND faces many environmental challenges due to upstream water interventions on the river system, as well as a high precipitation variability. According to Ramsar (2004), the Inner Niger Delta has been threatened for several decades by the degradation of its resources and reduction of flooded areas, because of natural and human-induced changes.

Detailed information on the flood spatial and temporal dynamics, correlations between water levels, and inundation areas are of notable interest to stakeholders (Ogilvie et al., 2015). Various authors (Ogilvie et al., 2015; Mahe et al., 2011; Zwart et al., 2005; Mariko, 2003) analyzed satellite data to understand flood dynamics and established correlation between inundation area and water level. Incomplete data and uncertainty associated with the satellite images upon which the studies were dependent might affect the findings. A two-dimensional hydrodynamic model is needed to represent the propagation and dynamics of the flood. However, modeling activity in data-sparse regions like IND is challenging due to lack of sufficient data upon which a model is developed.

Hydrodynamic modeling is a tool that can be used to simulate inundation, discharge, water level, and other hydraulic variables. In mathematical modeling, the water system is represented by a set of mathematical equations. The equations are solved accurately to get the desired solution. To obtain the solution, several assumptions are made on the boundary conditions, discretization, and numerical techniques. The required data to set-up a hydrodynamic model are topographic and bathymetric data, discharge, stage-discharge data and radar images for calibration and validation of model results. However, the applicability of modern hydrodynamic or flood inundation models is often limited outside the industrialized nations due to a lack of available data (Sanyal and Lu 2004).

Digital elevation models (DEM) derived from LiDAR are generally considered the best source of topographic data (Bates et al. 2003), while single multibeam sonar equipped with Echo-sounder and differential GPS is used for an accurate river cross-section survey (Wilson and Atkinson 2005). Discharge and water level data are generally required at high quality to feed into the models (Hunter et al. 2005). Space-borne radar imaging platforms such as European ERS-1 and ERS-2 satellites, Canadian RADARSAT, European ENVISAT, as well as airborne synthetic aperture radar (SAR) are commonly utilized as sources for obtaining observed flood extents (Schumann et al. .2007, Bates et al., 2006). All the data sources mentioned above are either scarce due to revisit time or non-existent in many developing countries.

Good quality input data is a prerequisite for a hydrodynamic model to produce good quality output. However, modeling activity is challenging in areas where incomplete data or no data are available for the development of a model. Data scarcity is common in developing countries where financial and security constraints often preclude the collection of high-quality data. Often, model developers rely on secondary data sources to develop the model.

In the absence of high resolution topographic data such as LiDAR, there are several alternatives. One of the popular data sources is the Shuttle Radar Topography Mission, SRTM (NASA JPL, 2013) data. One arc- second open-source SRTM data is available worldwide since 2014. Biancamaria et al. (2009), Schumann et al. (2014), and Neal et al. (2012a) used SRTM gridded data for hydraulic modeling of the Ob in western Siberia, the Scioto River in the eastern U.S., and the Niger river (Inner Niger Delta) in Mali, respectively. Even though the SRTM is widely used for research, its use is questionable because of its low vertical accuracy. A global assessment of the performance of SRTM data by Rodriguez et al. (2016) revealed that the data contains a standard deviation of 4.68m, 4.5m, 4.01m, and 4.60m for Africa, Eurasia, North America, and South America respectively. Another source of elevation data is the (Multi-Error-Removed Improved-Terrain) MERIT DEM (Yamazaki et al., 2017), a digital elevation model (DEM) developed from several existing spaceborne DEMs by removing multiple error components such as absolute bias, stripe noise, speckle noise, and tree height bias. Other popular global DEM's for hydrodynamic modeling are ASTER, TanDEM-X-90m DEM (DLR, 2018) and ALOS World 3D-30m (JAXA, 2018).

Remote sensing (RS) data can give valuable support to the delineation of flooded areas, that can be used to calibrate and validate hydrodynamic models. Researchers commonly use satellite images to derive an inundation extent for flood monitoring (Ogilvie et al., 2015), hydraulic model calibration (Karim et al. 2011), and validation purpose (Neal et al., 2012). RS data is available globally with considerable spatial coverage. It is often used as a source of data for large scale flood mapping. These RS observations can be obtained using optical sensors, passive microwave instruments or synthetic aperture radars (SAR). Although researchers stres to use SAR image, the costly procedure of acquiring radar imagery makes it difficult to have the data over developing countries. Although optical remote sensing techniques are hampered by the presence of cloud, the easy retrieval, processing, and interpretation of the images make more frequently used for flood modeling (Malinowski & Schwanghart, 2017). The Landsat and MODIS images, which are accessible at no cost, are often used inundation modeling in the developing world.

Several studies (most notably by Dadson et al., 2010; Haag, 2015; Neal et al., 2012) contributed towards the understanding of the hydrodynamic behavior of the IND. However, these studies did not lead to a well-calibrated model of the IND because of limitations such as to the use of a low-resolution structured grid and numerical approximation of LISFLOOD- FP as in Neal et al., (2012), the use a the simplified inundation fraction method in Dadson et al., (2010), or an unsuccessful calibration as in Haag, (2015). A major objective of this study aims to develop a better model by adopting a sophisticated modeling tool, TELEMAC 2D, a suite of finite element computer program that solves the shallow water equations over an unstructured grid using a finite element method.

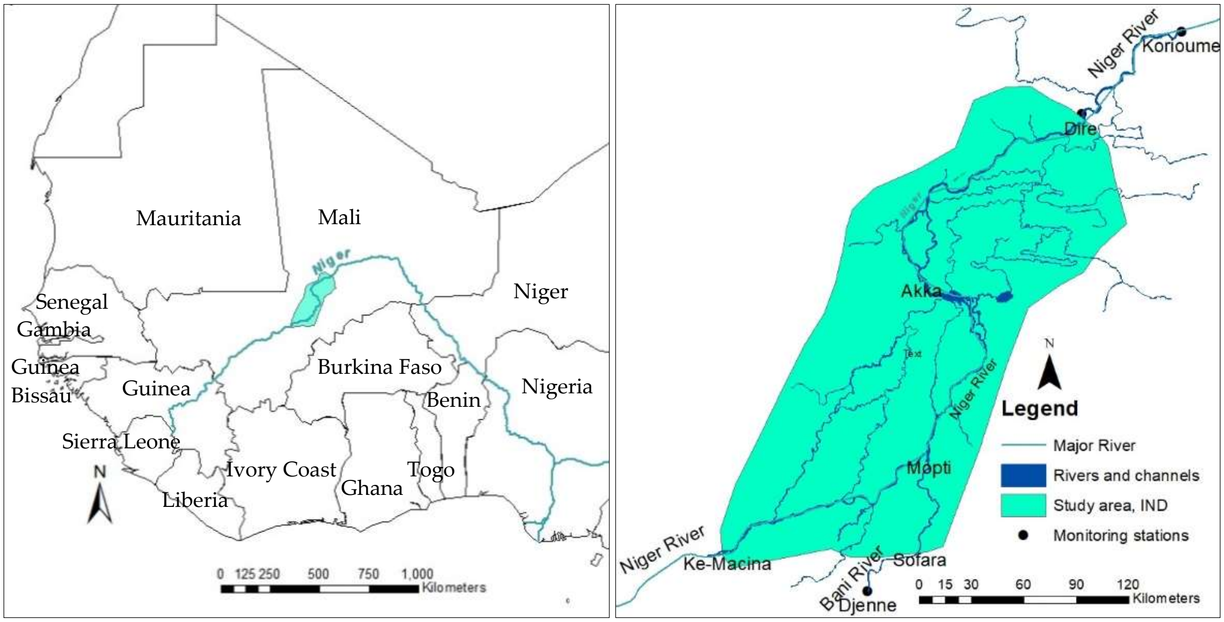

Fig. 1.1: Location map of the study area, the Inner Niger Delta, Mali

None of the previously developed hydrodynamic models explicitly accounted for the strong hysteresis phenomenon observed at hydrometric stations in the IND. Fig. 1.2 presents the non-looped rating curve used in Haque et al. (2019a) along with the actual looped rating curve at the Diré hydrometric station. Horritt (2000) has examined the effect of the hysteresis phenomenon on hydrodynamic simulations and found that the accuracy of the simulations near the downstream boundary might be strongly affected when a hysteresis effect is present. He also mentioned that the impact of the downstream boundary condition for dynamic circumstances would, of course, be distinct, and its impact may extend further upstream. In the particular case of the IND, ignoring the hysteresis effect leads to significant errors in the simulation of water levels downstream, which in turn affects the connectivity between the main river and important water bodies. This led to the second objective of the thesis: better reproduction of the hysteresis phenomenon in the simulations, and hence a better capture of the connectivity to key water bodies in the IND.

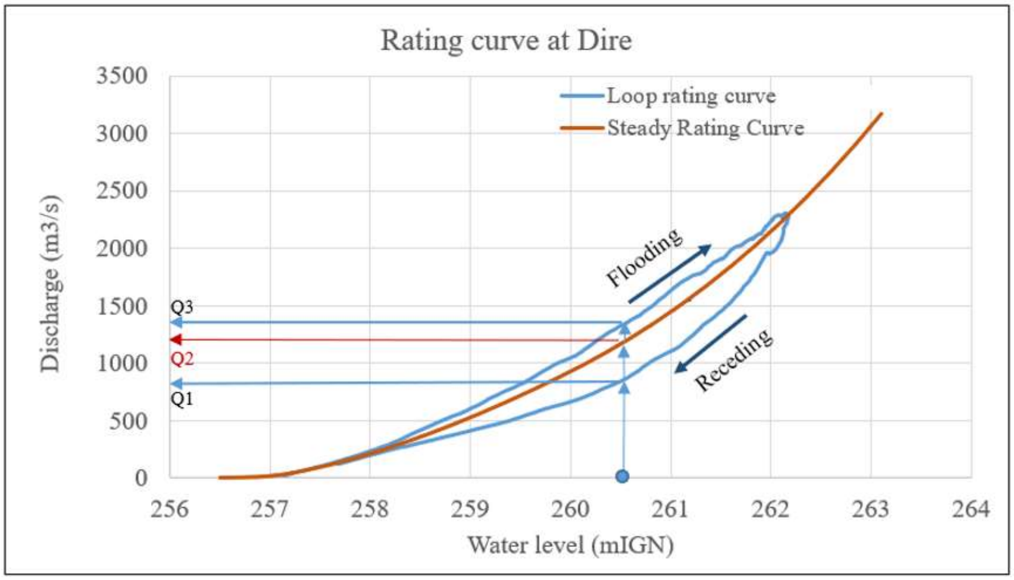

Fig. 1.2: Comparison of looped and single (steady) rating curves at Dire for 2001-2002

The operation of the hydrodynamic model developed in this thesis requires the availability of a computing platform with parallel processing capability, the availability of real-time water levels, streamflow and precipitation measurements, as well as precipitation forecasts. These requirements are, of course, not fulfilled by Malian technical services. These services routinely use empirical relationships between water levels observed at one or several hydrometric stations in the IND, and inundation extent. Such relations have been developed by several authors such as Ogilvie et al. (2015), Mahe et al. (2011), Zwarts et al. (2005), and Mariko (2003). The hysteresis phenomenon is taken into account by having one equation for the rising flood, and an equation for the recession. These equations are the same for any year, while the simulations with the hydrodynamic model showed that the relation fluctuates from year to year. The third and final objective of the thesis was to derive a new relationship that can vary from year to year according to the hydraulicity. Such equation would be easier to use for technical services in Mali and would provide more precise estimations of the inundation extent.

1.2 Objectives

The objective of this study is to develop tools that can improve water resources management in the IND.

The specific objectives are:

- Develop a methodology that allows the use of two-dimensional hydrodynamic modeling in a data-scarce area to simulate variables such as water level, depth, discharge, and inundation extent precisely. This involves finding ways to account for the low quality or unavailability of key data sets and combining multiple uncertain models into a more robust one using Bayesian Model Averaging;
- Account for the hysteresis phenomenon in hydrodynamic modeling to better simulate water levels and connectivity between the main river and water bodies downstream of the study area;
- Develop a better empirical relation between water levels and inundation extent in the IND.

1.3 Scope of the study

Integrated water management is a complex problem, especially in an area such as the IND, where there are multiple users and multiple issues. In this thesis, we will develop tools that can help decision-makers better understand and predict the flood dynamics and extent in the IND. We will demonstrate that the tools indeed provide more and better information in the Delta, but we will not attempt to evaluate or recommend a water management strategy for the IND.

1.4 Methodology

A two-dimensional hydrodynamic model using TELEMAC 2D was set up for the study area to simulate several variables, and they are discharge, flow velocity, water level, inundation extent, etc. In the absence of elevation data, we used the global digital elevation models of SRTM and MERIT DEM. As vertical accuracy of these data is not guaranteed, a new elevation data set is created using the waterline method (Cracknell et al. 1987, Koopmans and Wang 1995, Mason et al. 1995, Ramsey 1995) from the combined uses of water extent map derived from Landsat images and water levels. Given that observed discharge data are only available from three locations, a Soil Water Assessment Tool (SWAT) hydrological model (Seidou, 2019) of the Niger at Diré was developed and calibrated to generate discharge at the remaining locations of the model. The bathymetry was derived from the hydraulic geometric relationship (Leopold and Maddock, 1953), and the river network was extracted from the satellite imagery corresponding to the lowest water level. Simulations were performed under various conditions. Roughness was estimated from USGS Global Land Cover Characterization (GLCC) database (Loveland et al. 2000) and associated manning's coefficient. The elevation dataset was adjusted during calibration. In each run of the model, simulated inundation was compared with satellite image, the over-predicted and under-predicted areas were calculated, the elevation of those areas was adjusted by adding or subtracting the simulated water depth.

Bayesian Model Averaging (BMA) was applied to the simulated time series of water levels and discharges to reduce uncertainty. To implement the methods, six models were set up from the combination of three DEM (SRTM, MERIT DEM and the waterline DEM) and two boundary conditions (water level as a function of discharge and discharge as a function of water level). Each of the models was calibrated against discharge and water level. Given that we have three models, each of the models was run two times with two sets of boundary conditions at the downstream location. In this way, six scenarios were obtained from the models. Simulation outputs from different scenarios were then combined through BMA.

Given that the hysteresis effect is present at all the stations, it results looping in the stage-discharge relationship (Q-H). If a stream location has a loop rating curve, then placing a single-valued rating curve as the boundary condition can introduce errors in the simulation. USACE (1993) stated that stream location exhibiting loop rating could cause local effects on water level in the vicinity of the curves. The Q-H relationship was characterized, and a function was developed for the loop rating curve. The derived rating curve was prescribed at the outlet boundary by modifying the respective source code related to the stage-discharge curve. Simulation results using steady and loop rating curve at the downstream boundary were compared to see if loop rating improves the simulation performance.

An improved relation between water levels at Mopti and inundation extent was developed. Previous studies (Ogilvie et al., 2015; Mahe et al., 2011; Zwart et al., 2005; Mariko, 2003) proposed static relationships between water levels in the IND and the inundation extent. First, the domain of the hydrodynamic model was extended to match that of these authors. The new model was calibrated and validated, and the new relationship was derived as follow:

1. The development, calibration, and validation of a hydrodynamic model and the development of a relationship between simulated water levels at Mopti and inundation extent in the IND, conditioned on the knowledge of yearly maximum water levels $H_{\max}$ and yearly maximum inundation extents $I_{\max}$;
2. The development, calibration, and validation of a linear model that can forecast $I_{\max}$and $H_{\max}$given precipitation and streamflow measured on the upper Niger river basin (UNB) before the flood season;
3. The combination of the relationships developed in points 1 and 2 to obtain a relationship between water levels at Mopti and inundation extent in the IND that changes from year to year. The inundation extent predicted by the new relationship is then compared to the predicted relationships developed by other studies, and with the inundation extent obtained from MODIS satellite imagery.

1.5 Novelty

The material presented in this thesis is novel in several aspects:

1. Originality in terms of the nature of work
   - The area modeled in this study is a large floodplain of about 30,000 sq. km. Model setup, simulation, and calibration of such a large area are rare especially in a region where data scarcity is a major challenge. The authors had to resort to alternative methodologies to derive topographic and bathymetric data.
   - The first-ever 2D hydrodynamic model of the Inner Niger Delta based on triangular mesh in unstructured grid was developed in this thesis
   - A forecasting model was proposed to forecast the maximum inundation extent in the Delta using observed precipitation and streamflows in the Upper Niger Basin.

- The first non-stationary relationship between water levels at Mopti and inundation extent in the IND was developed, along with a forecasting model for the maximum water level and inundation extent. This relationship can be used to plan socio-economic activities ahead of time.

2. Originality in terms of methods/ approaches taken
   - The study provided a systematic approach to model a floodplain in a data-scarce environment, including data acquisition, processing, simulation, calibration, and validation, and can be replicated to other places to model floodplains.
   - The waterline method was used to derive topographic data of the region with the use of a water map derived from Satellite images and water level measurement.
   - Bathymetric data were estimated from the hydraulic geometric relationship and later adjusted during the calibration procedure.
   - The study makes use of the global land cover data, GLCC, to estimate the roughness parameter to be used for the model. In this way, distributed Mannings coefficients are obtained throughout the floodplain and used for the model.
   - Inundation extents for the IND were derived from the Landsat and MODIS image and used for the calibration of the model. The inundation map is compared with the simulated inundation to obtain an over-predicted, agreed, and under-predicted area. The elevation data at the over-predicted and under-predicted areas are adjusted based on the simulated water depth at the simulation.
   - Bayesian Model Averaging (BMA) is applied to improve the multiple imperfect simulations from hydrodynamic models. Several variations of the model were created with a varying source of elevation and downstream boundary conditions, then combined with BMA. This is the first time BMA is used to combine hydrodynamic models
   - TELEMAC2D was modified to use a looped rating curve as a downstream boundary condition. The modification led to a better simulation of water levels and hydraulic connectivity in the IND.

3. State of the art techniques

The study uses the following state of the art techniques to conduct the research: application of a two-dimensional model, TELEMAC 2D which solves the governing equations in finite element method using unstructured grids, remote sensing and global DEM data retrieve, analysis and processing with computer applications: Blue Kenue, ArcGIS, MATLAB, FORTRAN, etc.

1.6 Outcome

The main outcomes of the present thesis are one published and two submitted journal papers. The papers above form Chapter 4-6 of this thesis. The papers are as follows:

- Haque, M.M., Seidou, O., Mohammadian, A., Djibo, A.G., Liersch, S., Fournet, S., Karam, S., Perera, E.D.P., Kleynhans, M. (2019) Improving the Accuracy of Hydrodynamic Simulations in Data Scarce Environments Using Bayesian Model Averaging: A Case Study of the Inner Niger Delta, Mali, West Africa. *Water*, *11(9)*, 1766. https://doi.org/10.3390/w11091766.

- Haque, M.M., Seidou, O., Mohammadian, A. (2019b) Effect of rating curve hysteresis on flood extent simulation with a 2D hydrodynamic model: a case study of the Inner Niger Delta, Mali, West Africa, *Journal of African Earth Sciences* (Revised)

- Haque, M.M., Seidou, O., Mohammadian, A., Djibo, A.G., (2019c) Development of an improved relationship between water levels and flooded area in Inner Niger Delta, Mali, West Africa, *Journal of Hydrology: Regional Studies* (Revised)

1.7 Thesis Outline

The thesis is organized in seven chapters, as follows:

Chapter 1 provides the background and objectives of this research work. This chapter contains the problem statement, the objectives, scope of the research, major outcomes, and the overall organization of the thesis.

Chapter 2 is a comprehensive literature review. The chapter starts with a brief overview of hydrodynamic modeling in large flood plains worldwide, followed by an overview of the previous studies in IND. A description of the data requirements for hydrodynamic modeling in data-scarce region is presented. The theory behind the statistical methods, including stepwise regression, simple/multiple linear regression, polynomial regression is presented. A description of model evaluation performance measures is provided.

Chapter 3 presents the characteristics of the study area that are relevant to this work, such as precipitation, evaporation, water balance, etc. The various data sets used in the study are presented. These data sets include observed discharge and water levels, simulated discharges at ungauged locations, and inundation extent derived from satellite images.

Chapter 4 focuses on the development of multiple hydrodynamic models and the combination of their output using Bayesian Model Averaging (BMA). Six different hydrodynamic models of the study area were developed using three different DEMs and two different downstream boundary conditions. The simulated water levels and discharge time series were combined with BMA to get an improved result. The way to identify which individual models are better for a particular variable (such as discharge and water level) in a particular location are discussed

Chapter 5 focuses on the improvement of the hydrodynamic model's simulations by incorporating an improved rating curve (looped rating) at the downstream boundary. It is shown that simulations using looped rating curves improve the accuracy of floodplain extent simulations in the areas close to the downstream station, as well as the timing of the connectivity of the river system.

Chapter 6 focuses on how to produce a time-varying relationship between water levels and simulated inundation areas from the hydrodynamic model. Calibration and validation of the real-time relationship curve are presented. This chapter contains a method for forecasting the maximum water level and corresponding maximum inundation. These results are useful for decision-makers in the sense that they can forecast how far a flood is likely to spread, and optimize activities that are sensitive to flood extents such as rice planting or forage management.

Chapter 7 summarizes the major findings and gives conclusions of this research work. This chapter also provides commendations for further studies.

Chapter 2

Literature review

Hydrodynamic modelling in data-scarce region is a challenging task due to incomplete data or no data available for the development of a model. The required data to set-up a hydrodynamic model are: topographic and bathymetric data, discharge, stage-discharge data and satellite-derived inundation extent etc.

2.1 Modeling studies in data sparse region

Despite the limitation due to the availability of data, there have several modeling studies been conducted in large floodplains in data-sparse regions. Komi et al., (2017) developed a hydraulic model to predict flood extent for a 140 km reach of the Oti River, West Africa. Biancamaria et al. (2009) studied the hydrodynamics of a 900km reach of Ob river in Western Siberia, Wilson et al., (2007) conducted a floodplain modeling study of a 240 x 125 km section of the central Amazon floodplain in Brazil. Yan et al. (2014) carried out research on a 280 km river reach of Blue Nile, Sudan. The LISFLOOD-FP modeling tool was popular among the authors of large-scale flood modeling. However, the simulations contain large uncertainties because LISFLOOD-FP uses a simplified form of the St-Venant equations, which are simplified by diffusive and kinematic approximations.

2.2 Hydrodynamic modeling of the IND

Dadson et al. (2010) modeled evaporation and inundation patterns in the IND using the Joint UK Land-Environment Simulator (JULES) land surface model together with the CEH Grid-to-Grid (G2G) 1D kinematic wave river routing model (Bell et al., 2007). The model was driven by meteorological data from the ALMIP experiment (AMMA Land Surface Model Intercomparison Project, wherein AMMA stands for African Monsoon Multidisciplinary Analyses). Their model simulations are shown in Fig. 2.1. The monthly mean discharge at Tilembeya (about 50 km d/s of Ke-Macina on Niger River) from 2000- 2006 is presented along with the observed discharge obtained from Global Runoff Data Centre. They obtained an NS coefficient of 0.70, and model overestimated the June-November flow. The inundated area in that model was described as a fraction of land that is inundated on a 25km grid. Fig. 2.1 shows the model prediction for discharge and inundation area.

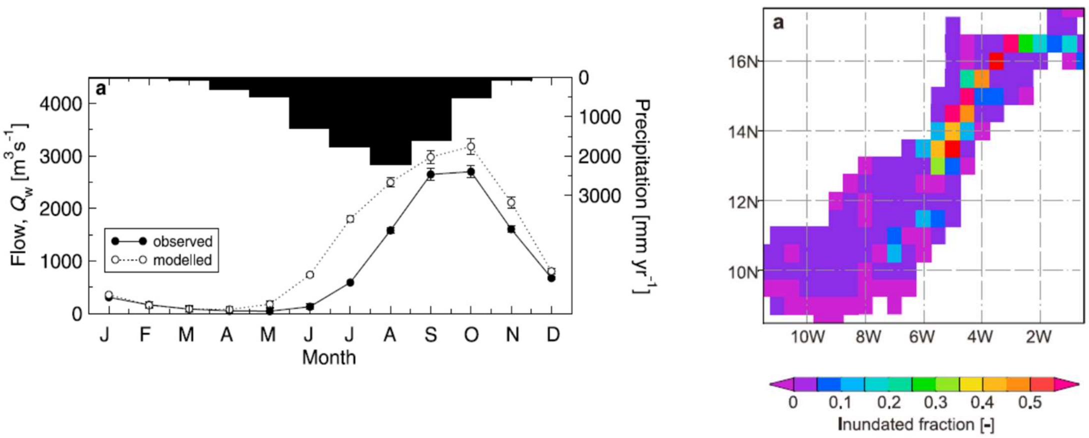

Fig. 2.1: Comparison of modeled discharge (left) and inundation pattern (right)

Fig. 2.1 shows that the model is not able to correctly predict the discharge at the station and that the generated inundation map has a coarse resolution. Discrepancies between simulations and observations arise from the use of a 1D kinematic wave model, which is not able to account for flow interaction in the lateral direction and is difficult to use in areas with relatively flat floodplain. Another drawback of the model is that it did not produce spatial distribution of flood areas because the inundation fraction method is not able to identify flooding and drying part of the lands in the 25km pixel.

Haag (2015) developed a hydrodynamic model (D-Flow Flexible Mesh) to simulate the flow variables and inundation extent of IND. D-Flow FM implements a finite volume solver on an unstructured grid. Simulation results from the model are shown in Fig. 2.2. The model overpredicts the discharge at Mopti and Dire, and there is little correlation between simulated and observed discharged from GRDC (Global Runoff Data Centre) data. The simulated inundation for 16th March 1996 and 22nd October 1996 is presented, which represents the recession (dry) and flood (wet) time, respectively. Surprisingly, the inundation extent on both days is almost the same. In reality, more areas become inundated during October at the upstream part of the IND (from Ke-Macina to Akka), and the model was supposed to simulate more inundation area in that part. The reason behind the problem is that it was not properly calibrated for discharge. The calibration was also not performed for the inundation area using satellite-derived water extent information. Other causes include low-resolution HydroSHED DEM (450m) and the model grid (minimum cell about 675m), which is too coarse for flood mapping.

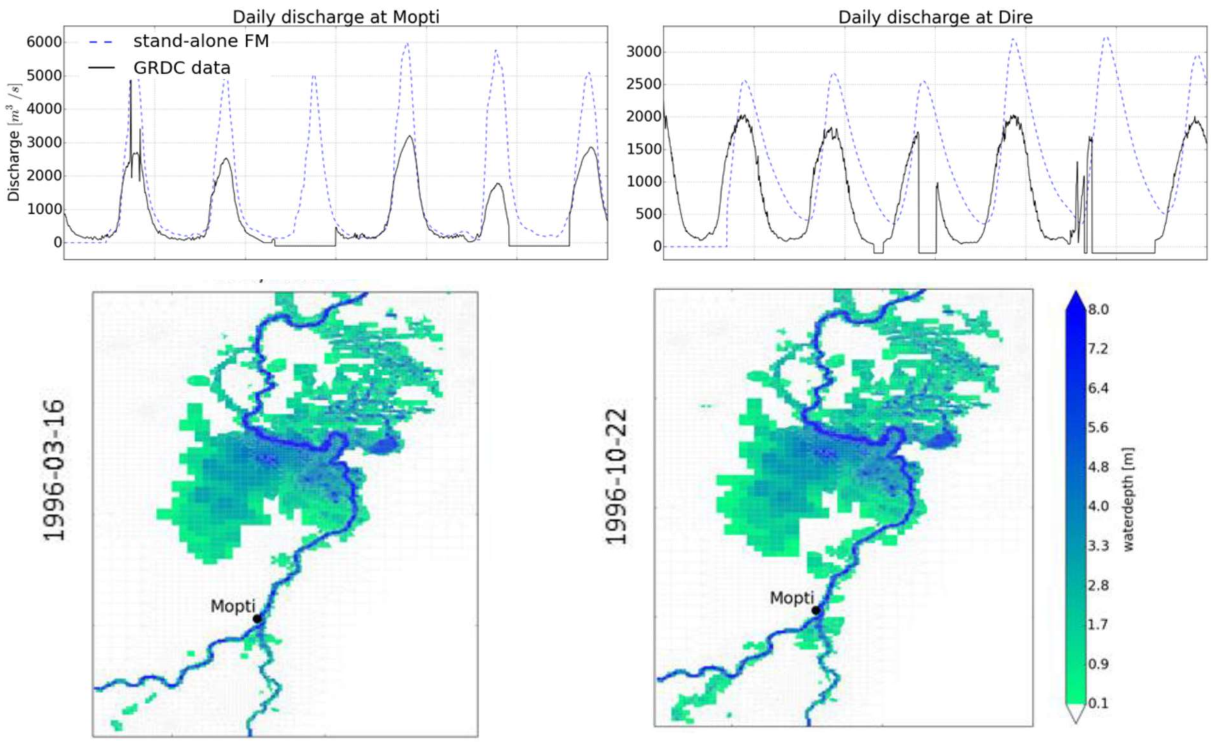

Fig. 2.2: Discharge (top) and inundation (bottom) as modeled by the D-Flow FM model (Haag, 2015)

Neal et al. (2012) developed a hydrodynamic model of the IND using an upgraded version of LISFLOOD-FM (Bates and de Roo, 2000) that uses a sub-grid structure for simulating flows in channels with a much smaller size than the actual grid resolution of the model. The authors were successful in representing narrow channel representation into the model. However, the performance of the model in predicting water level and the inundation extent was not very satisfactory. The model was able to simulate the discharge up to NS 0.91 at Dire, but information about model performance at other hydrometric stations in the IND was not provided. Model predictions for water level and inundation extent were unsatisfactory (Fig. 2.3).

Water Level

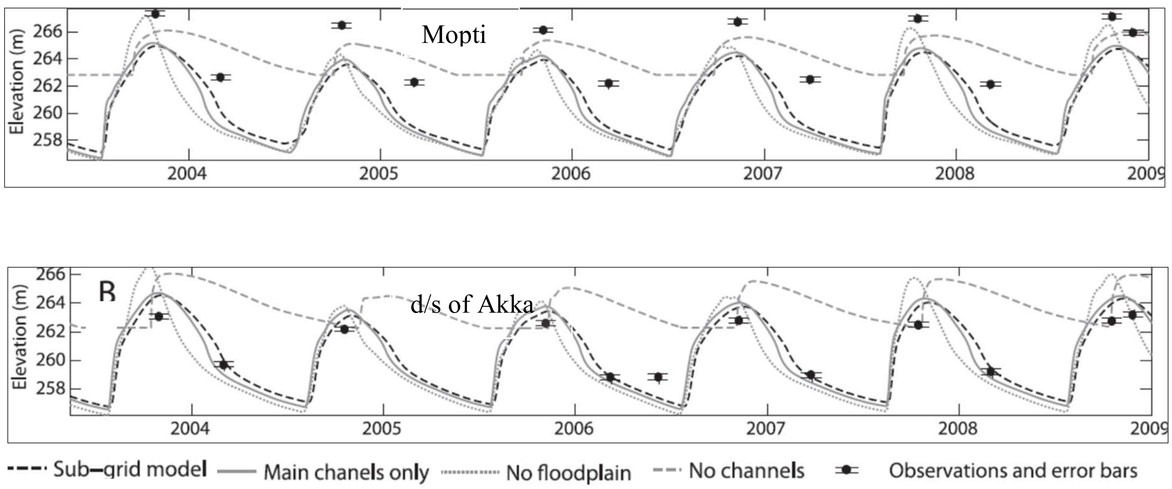

Inundation Extent

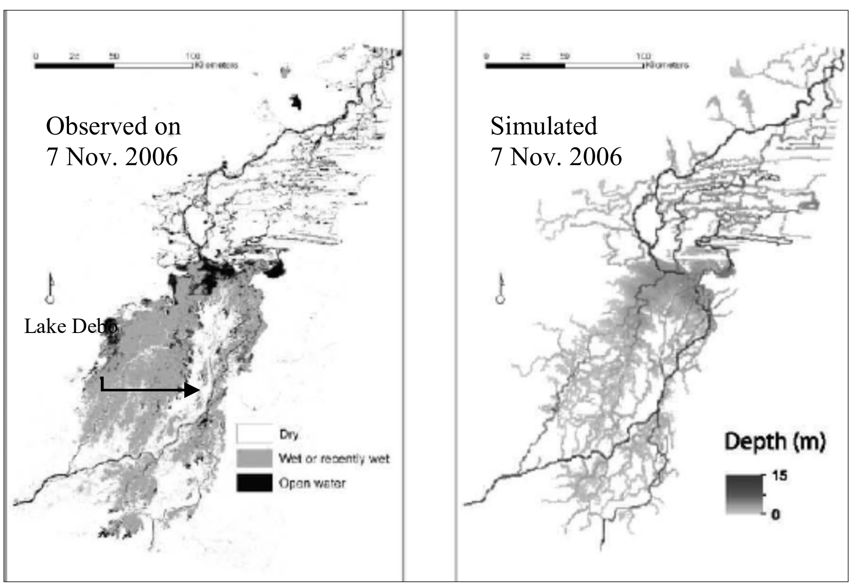

Fig. 2.3: Water level (top) and inundation extent (bottom) simulation on a sub-grid model of Neal et al. 2012

It is shown in Fig. 2.3 (top) that simulated water levels at upstream and downstream of Lake Debo were under-predicted (up to -2.0m) and over-predicted (up to +1.7m). These discrepancies affected the simulated flood extent, leading to less flooded areas in the upstream and more flooded areas in the downstream areas. The authors compared the simulated inundation on 7th November 2006 with the observed inundation derived from Landsat image (Fig. 2.3 (bottom)). The upper part of IND, upstream of Lake Debo, shows less inundation, while the lower part shows higher than the observed. Although the authors mentioned that the elevation data was the reason for the not so good prediction, other causes may be the use of the simplified form of the St-Venant equations and the finite difference method to solve the shallow water equation over a grid of coarse (1.0km) resolution.

Zsufa et al. (2013) developed a hydrodynamic model to investigate the pollution and habitat conditions of the IND. They used River 2D (Steffler and Blackburn, 2002) in their study. They selected a small study area in the vicinity of Niger and Bani river confluence near the town of Mopti. The simulated water depth at a total flow of 3000m^3/s at Mopti under steady-state condition is shown in Fig. 2.4. The authors expressed the need for a full-scale model for IND, considering all river flows and evaporation loss.

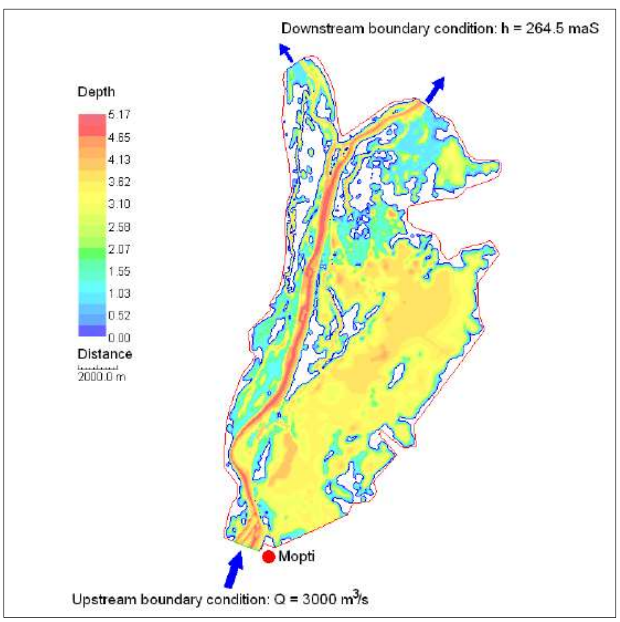

Fig. 2.4: Simulated water depth in the model area by Zsufa et al. (2013)

A high-resolution 2D hydrodynamic model, which can simulate the flow dynamics of the IND properly, is still absent. The present study is an endeavor to model the area with improved modeling techniques.

2.3 Hydrodynamic model selection for flood wave propagation

There are several modeling tools available to model a floodplain. The simplest way to model a floodplain is to apply a one-dimensional (1D) modeling tool. The more complex approach uses two dimensional (2D) or three dimensional (3D) models.

Traditionally, 1D river models have been used to model fluvial flooding events and flood forecasting purposes. 1D models are developed from a set of cross-sections of the river and floodplain, and water levels are calculated using the 1-dimensional form of the governing equations. A 1D model is good at representing the in-channel water level and flows by calculating a single water level, velocity, and flow rate for each cross-section. As far as topographic data is concerned, 1D models only require cross-sections data, which was a major advantage when access to topographic data was limited in data-sparse regions.

While 1D models perform well when the flow is restricted between channel banks, 2D modeling was shown to better estimate flows in floodplains, where the flow is considered largely 2-dimensional (e.g., Andersson and Bates, 1993; Cook and Merwade, 2009). 2D hydraulic models consist of a 2D computational mesh/grid and solve the two-dimensional form of continuity and momentum equation for water level, flow rate and other variables in each grid cell. 2D models need topographical and bathymetric data, covering the whole area that is to be modeled. A brief description of modeling tools is given in Table 2.1.

Table 2.1: Floodplain modeling tools (Bates and DeRao, 2000)

Type/name of the model	Channel routing	Floodplain routing	Discretization
1D models (MIKE11, HEC-RAS)	Full solution of the 1D St. Venant equations	Full solution of the 1D St. Venant equations	Treats domain as a series of cross-sections perpendicular to the flow direction. Areas between cross-sections are not explicitly represented
2D Models (TELEMAC-2D, MIKE21, Delft 3D)	Full solution of the 2D St. Venant equations with turbulence closure	Full solution of the 2D St. Venant equations with turbulence closure	Structured grids (finite difference methods) or unstructured grids (finite volume and finite element methods) using a variety of geometries, but typically, triangles or quadrilaterals.
Sub-grid model (LISFLOOD-FP)	Two-dimensional kinematic wave solved using an explicit finite difference procedure using designated channel cells	Uniform flow formulae (Manning equation)	Raster-based discretization derived automatically from a DEM.

Choosing an appropriate model among the plenty of available tools is an important part of the modeling study. The selection is based on how a model can represent the physical system and what are the numerical schemes upon which the model is developed. To narrow down the selection, it is preferred to apply a 2D hydrodynamic model as we are interested in modeling a large flood plain in which depth-averaged- shallow water equations are to be solved in the horizontal x and y directions. We then move to choose a 2D model that can solve the equations in the unstructured grid in the finite element method.

Cook and Merwade (2009) found that finite element methods are less sensitive to the resolution of terrain models and, therefore, effective in containing the uncertainty in the model outcomes arising from the error in the terrain input. An unstructured grid can account for the variation of the geometry in the channel and over the floodplain. TELEMAC 2D uses sophisticated numerical schemes, and it solves the systems of equations with finite element methods in unstructured grid. TELEMAC-2D is physically realistic and has certain advantages: It is can handle terrain data with varying resolution (Di Baldassarre et al. 2010) and is applicable in studies where high-resolution DEMs are not available. Sanyal et al. (2014) showed that a complex model such as TELEMAC-2D is more appropriate than 1D-2D models for simulating floodplain inundation for complicated channel networks and low-quality input data.

Process representation is important for hydraulic modeling. The detailed geometry of the river channel and bathymetry is the most important input in any hydraulic model (Pappenberger et al. 2005). Channel representation is another difficult part of the hydrodynamic modeling. To tackle this issue, Neal et al. (2012) developed a sub-grid channel hydraulic model- LISFLOOD-FP model, where any river channel whose width is narrower than the spatial resolution of the topography data on low-resolution terrain data can be represented. LISFLOOD-FP has been applied by many authors such as Wilson et al., (2007), Biancamaria et al., (2009), Komi et al., (2017), Yan et al., (2014), Neal et al. (2012).

Sanyal et al. (2014) applied both the LISFLOOD-FP and TELEMAC-2D models for an inundation modeling of a large ungauged river, the Damodar River, in India. The authors compared the simulation result obtained from both the models and concluded that the TELEMAC-2D is more suitable than the LISFLOOD-FP model for simulating extensive floodplain inundation in a data-scarce region.

Based on the fact that a 2D model is appropriate for a floodplain modeling and process representation can better be done with the finite element method with the unstructured grid, we choose to apply TELEMAC 2D. No modeling was conducted previously in the study area with this modeling tool.

2.4 Governing equations in the hydrodynamic model

TELEMAC-2D solves the depth-integrated Shallow Water Equations (SWEs) using the finite element method on an irregular mesh. At each computational node of the mesh, TELEMAC-2D estimates the depth of flow and two horizontal velocity components. The governing equations considered are:

Continuity Equation:

$$\frac{\partial h}{\partial t} + u.\nabla(h) + hdiv(u) = S_h \tag{2.1}$$

x-Momentum

$$\frac{\partial u}{\partial t} + u \cdot \nabla(u) = -g\frac{\partial Z}{\partial x} + F_x + \frac{1}{h}div(hv_t\nabla u) \tag{2.2}$$

y-Momentum

$$\frac{\partial v}{\partial t} + u \cdot \nabla(v) = -g\frac{\partial Z}{\partial y} + F_y + \frac{1}{h}div(hv_t\nabla v) \tag{2.3}$$

in which, h (m) depth of water, u, v (m/s) velocity components, g (m/s^2) gravity acceleration, Z (m) free surface elevation, t (s) time, x,y (m) horizontal space coordinates, S_h (m/s) source or sink of fluid, v_t (m^2/s) eddy viscosity (1.0 m^2/s), F_x, F_y are the source or sink terms in dynamic equation, representing bottom friction, h, u, and v are the unknowns.

Bottom Friction

Friction is a major unknown parameter in a hydraulic study. Friction laws themselves are mostly empirical. Therefore, the friction coefficient is often considered as an important calibration parameter. The friction force is expressed as follows (Hervouet, 2007):

$$F_x = \tau_x * \Delta x * L \text{ (x} - \text{direction)} \tag{2.4}$$

$$\tau_x = -\frac{u}{2}\rho * C_f * \sqrt{u^2 + v^2} \tag{2.5}$$

The coefficient, C_f is hardly used in free surface hydraulics and is usually replaced by others. The best known are the Chezy (c), Mannings (n), and Strickler coefficient (s). Theses coefficients are bounded to the C_f by the following formula:

$$C_f = \frac{2g*n^2}{h^{\frac{1}{3}}} \tag{2.6}$$

So, friction forces in x and y directions are:

$$F_x = -\frac{u*g*n^2}{h^{\frac{4}{3}}} * \sqrt{u^2 + v^2} \tag{2.7}$$

$$F_y = -\frac{v*g*n^2}{h^{\frac{4}{3}}} * \sqrt{u^2 + v^2} \tag{2.8}$$

With:

C_f = friciton coefficient (dimensionless)

h= depth of flow for shallow water flow

τ_x = friciton stress in x direction

ρ = density of water (kg/m^3)

Δx *and* L = length and width of infinitesimal reach

u and *v* are the velocity in *x* and *y*-direction respectively

In TELEMAC 2D, the SWE's are solved using a fractional step method (Marchuk, 1975), whose main principle is that the hyperbolic and parabolic parts of the SWE's should be treated separately. The solution comprises two steps: a solution of advection terms, and the solution of the propagation, diffusion, and source terms. Several schemes are available for the advection step, where the Method of Characteristics has been applied to solve the advection of *u* and *v*. The Streamline Upwind Petrov-Galerkin (SPUG) method (Brookes and Hughes, 1982) has been applied to solve the advection of h in the continuity equation. Variational formulations and space discretization transform the continuous equations into a linear triangular element, where the dependent variables *u*, *v,* and h are expanded using equal order interpolation functions. In the second step, the propagation, diffusion, and source terms are coupled through an implicit time scheme, and the resulting linear system is solved with a variant of the conjugate gradient method (Bates et al., 1997).

2.5 Open-access remote sensing data for flood modeling and management

2.5.1 Topographic data

Topographic data comes from Digital Elevation Models (DEM). DEM is a gridded digital representation of terrain, with each pixel value corresponding to a height above a datum. DEMs can be created from ground surveys, digitizing existing hardcopy topographic maps, or by remote sensing techniques (Hawker et al. 2018). The topography is the key factor in estimating the extent of the flood (Horritt and Bates, 2002). Generally speaking, the quality of flood predictions increases with higher resolution DEMs. Expensive data acquisition process and inaccessibility in some of the regions make field survey virtually impossible in the developing countries. So, the developing countries mostly rely on data from secondary sources such as processed data from by remote sensing method.

Remote sensing techniques comprise photogrammetry, airborne and space-borne Interferometric Synthetic Aperture Radar (InSAR), and Light Detection and Ranging (LiDAR) (Hawker et al. 2018). High Resolution (each grid length<10 m) LiDAR has higher precision and accuracy and is suitable for applications, such as flood modeling, that rely on the accurate derivation of surface characteristics. Global LiDAR coverage with the limited amount of LiDAR data (0.005% of the earth's land area) that is currently available almost exclusively found in developed countries. Space-borne InSAR is the most common technique to create global DEMs and is the technology behind the most widely used open-access global DEM, e.g., the Shuttle Radar Topography Mission (SRTM). An overview of free global DEMs is given in Table 2.2.

In data-sparse regions, a limited number of global DEM products dictates that only a single DEM is used, with this most commonly being SRTM (Yan et al., 2015). Following its acquisition in 2000, SRTM remains the world's most popular DEM due to its availability, resolution, vertical accuracy, and lower artifacts and noise compared to alternative global DEMs (Hawker et al. 2018; Rexer and Hirt, 2014; Jarihani et al., 2015). Yet, recently released products such as MERIT and TanDEM-X 90 could change that scenario.

Table 2.2: List of global digital elevation model (Source: Hawker et al. 2018)

Dataset	Sensor/Satellite	Resolution (m)	Vertical accuracy	References
ALOS AW3D30	Optical	30	4.4m (RMSE)	Tadono et al. (2016)
ASTER GDEM	Optical	30	17m (95% conf.)	Tachikawa et al. (2011)
Bare Earth DEM	SRTM	90	5.9m (RMSE)	O'Loughlin et al. (2016)
EarthEnv	ASTER &SRTM	90	4.15m(RMSE)	Robinson et al. (2014)
MERIT	AW3D30, SRTM and Viewfinder Panorama	90	5m (LE90)	Yamazaki et al. (2017)
SRTM	SAR C Band	30, 90	6m (MAE)	Farr et al. (2007)
TanDEM-X 90	SAR X Band	30, 90	unknown	Rizzoli et al. (2017)
Viewfinder Panorama	ASTER, SRTM, and other sources	90	Not reported	De Farranti (2014)

2.5.2 Radar altimetry for water level data

Water level data is essential for hydrodynamic modeling. Radar altimetry provides an alternative option in getting data in the absence of in-situ records. Radar altimetry missions now routinely measure freshwater surface elevation of large rivers, lakes, and water bodies (Ekeu-wei and Blackburn, 2018; Koblinsky et al. 1993). Table. 2.3 summarizes a list of radar instruments with the accuracy of the altimetry water level.

O'Loughlin et al. (2016) reported that a short energy pulse is transmitted, which is then reflected by the water surface back to the sensor. If the position of the satellite is known, then the distance from the altimeter to the surface is proportional to the time delay between transmission and return of the reflected energy. O'Loughlin et al. (2016) suggested that the water bodies should be wider (2-3 times) than that of the ground footprint for better accuracy.

The vertical accuracy of altimetry water levels contributes to uncertainties in hydrologic and hydraulic modeling simulations (O'Loughlin et al. 2016). These inaccuracies are attributed to the different sensor types, the distance between in-situ and virtual station, and location of altimetry track intersection, instrument noise, topography and heterogeneity of reflecting land surfaces (Belaud et al. 2010, Ponte et al. 2007, Tourian et al. 2016). Despite these limitations, altimetry is widely used in hydrology, particularly in the context of hydrodynamic modeling in data-sparse regions (Ekeu-wei and Blackburn, 2018). Many authors (Domeneghetti et al. 2014, Belaud et al. 2010, Yan et al., 2015) utilized water level data estimated using radar altimetry in their hydrodynamic study. Domeneghetti et al. (2014) suggested that altimetry data should be applied in combination with measured data; Sun et al. (2015) advised if there is measured data, it should be given more weight.

Table. 2.3: List of principal altimetry instruments for water level information (Source: O'Loughlin et al., 2016 and Ekeu-Wei and Blackburn, 2018)

Satellite Mission	Ground footprint (m)	Revisit time (days)	Operation time line	Accuracy (m)	Reference
TOPEX/Poseidon	~600	9.9	1993–2003	0.35	Frappart et al., 2006
ERS-1	~5000	35	1991–2000	N/A	Da Silva et al., 2010
ERS-2	~400	35	1995–2003	0.55	Frappart et al., 2006
ENVISAT	~400	35	2002–2012	0.28	Frappart et al., 2006
Jason-1	~300	10	2002–2009	1.07	Jarihani et al., 2015
ICE Sat/GLAS	~70	-	2003–2009	0.10	Urban et al., 2008
Jason-2	~300	10	2008 *	0.28	Jarihani et al., 2015
Sentinel 3 SRAL	~300	27	2016 *	0.03	Da Silva et al., 2010
SWOT	~10-70	21	2020 +	0.10	Fu et al., 2009

2.5.3 Flood extent detection using remote sensing

Remote sensing provides a useful tool to observe the spatial and temporal distribution of floods. Optical, passive microwave, and radar instruments are being used for inundation extent mapping and monitoring purposes. Due to its consistent observation, remote sensing inundation information has been used in recent studies to complement in-situ data for hydrological and hydrodynamic modeling in data-scarce regions (Malinowski & Schwanghart, 2017).

Synthetic Aperture Radar (SAR) and optical images have been applied with varying precision in the study of floodplains. Table. 2.4 summarizes a list of sensors used for flood extent delineation purpose. Flood mapping using optical imagery has proved to be relatively successful (e.g., Wang 2004; Marcus and Fonstad 2008; Proud et al. 2011). However, flood mapping may sometimes be hampered due to the inability of the optical image to penetrate the cloud. Consequently, several authors (Schumann et al. 2012; Di Baldassarre and Uhlenbrook 2012; Yan et al. 2015) have focused exclusively on radar sensors.

Though SAR images are not disturbed by cloud cover, they remain very sensitive to the water surface effects resulting from wind and currents, which impede water body identification. Conversely, optical images are highly affected by cloud presence but are less sensitive to surface properties and are therefore suited to delineating water bodies in semi-arid areas with low annual cloud cover (Ogilvie et al., 2015). Optical remote sensing images are the frequently used data for inundation mapping because optical images are easy to interpret and process for inundation retrieval (Malinowski & Schwanghart 2017).

Table. 2.4: Summary of satellite uses in flood extent study (Source: Grimaldi et al. 2016)

Satellite (Sensor)	Agency	River/ location	References	Cost
MODIS (AQUA & TERRA) (Optical)	NASA (1999-present)	1.Fitzroy river (Australia); 2.Mengwa area, Huaihe River (China) 3.Mekong River (Laos, Cambodia, Thailand) 4. Niger river (Mali)	1.Karim et al. (2011); 2.Lai et al. (2014), 3. Sakamoto et al. (2007) 4. Ogilvie et al, (2015)	Free
LANDSAT (5,7,8) (Optical)	NASA (1984-present)	Niger River (Mali)	Zwarts et al. (2005) Neat et al. (2012)	Free
ERS-1 (SAR)	ESA (1991–2000)	1.Meuse River (NDL); 2.Thames River(UK)	1.Hunter et al. (2005); 2.Mason et al. (2009)	Free
ERS-2 (SAR)	ESA (1995–2011)	1.Dee River (UK); 2.Alzette River (Luxembourg)	1.Stephens et al. (2012); 2.Matgen et al. (2004); 2.Di Baldassarre et al. (2009b); 2.Schumann et al. (2009b)	Free
ENVISAT-ASAR (SAR)	ESA (2002-2012)	1.Dee River (UK); 2.Alzette River (Luxembourg), 3.Mekong River (Laos, Cambodia, Thailand)	1.Schumann et al. (2009b), 2.Di Baldassarre et al. (2009b), 2.Matgen et al. (2004); 2.Schumann et al. (2009b) 3.Dung et al. (2011)	Free
RADARSAT (SAR)	CSA (1995-2013)	1.Upper Severn River (UK) 2.Moselle River (France–Germany)	1.Horrit (2006) 2.Hostache et al. (2010)	not free
Sentinel-1	ESA (2014-present)	1.Bangladesh 2.India	1.Uddin et al. (2019) 2. Anusha & Bharathi (2019)	Free
Sentinel-2	ESA (2014-present)	1.Italy and Spain 2.Turkey	1. Noti et al. (2018) 2. Kaplan, K and Avdan, (2017)	Free

2.5.4 Detection of flooded areas

The inundation interpretation of optical images is performed using standardized indices. In the past two decades, spectral indices have been exploited to separate water pixels from non-water pixels in optical remote sensing. The commonly used indices are: the Modified Normalized Difference Water Index (MNDWI) (Xu 2006), the Normalized Difference Moisture Index (NDMI) (Wilson et al. 2002), the Normalized Difference Water Index (NDWI) (McFeeters 1996) and the Normalized Difference Vegetation Index (NDVI) (Rouse et al. 1973) indexes.

The equations for MNDWI, NDMI, NDWI, and NDVI indexes are given below:

$$MNDWI = \frac{Green-MIR}{Green+MIR} \tag{2.9}$$

$$NDMI = \frac{NIR-M}{NIR+MIR} \tag{2.10}$$

$$NDWI = \frac{Green-NIR}{Green+NIR} \tag{2.11}$$

$$NDVI = \frac{NIR-Red}{NIR+R} \tag{2.12}$$

For MODIS images, the Green, NIR, and MIR represent reflectance from Band 4 (545nm- 565nm), Band 2 (841nm to 876nm), and Band 6 (1628nm to 1652nm) respectively. Ogilvie et al. (2015) analyzed MODIS images to study the spatial and temporal dynamics of flood across the Niger Inner Delta throughout 2000 - 2011. They combined MNDWI and NDMI to delineate water extent. Water was classified when the pixel had the threshold value of 0.15 for NDMI, and for the MNDWI, classifying pixels above the threshold of -0.34 was considered a flooded area.
For Landsat 7, ETM images, Green, Red, and NIR (near-infrared) represent the reflectance of Band 2, Band 3, and Band 4, respectively. Neal et al. (2012) derived inundation extent using Landsat 7 ETM image for Inner Niger Delta. They classified open water if NDWI index is greater than zero and if the NDVI index is greater than 0.5.

Previous researchers (Ogilvie et al. 2015; Mariko 2003; Zwarts et al. 2005) were successful in extracting the inundation extent of IND using Landsat and MODIS images. Given that the main hindrance of optical imagery is the presence of clouds, it is possible to overcome the difficulties by processing cloud-free images. Ogilvie et al. (2015) derived a time series of cloud coverage for the period of 2000-2011 over the IND is shown in Fig. 2.5. It is shown that cloud presence remained low (3.9% of the IND area on average) between September and April but rose considerably (up to 23% of the IND area) during the months of May-August. Ogilvie et al. (2015) also mentioned that the period of 2001-2002 and 2008- 2009 had least cloud years over the IND area among their study period of 2000-2011.

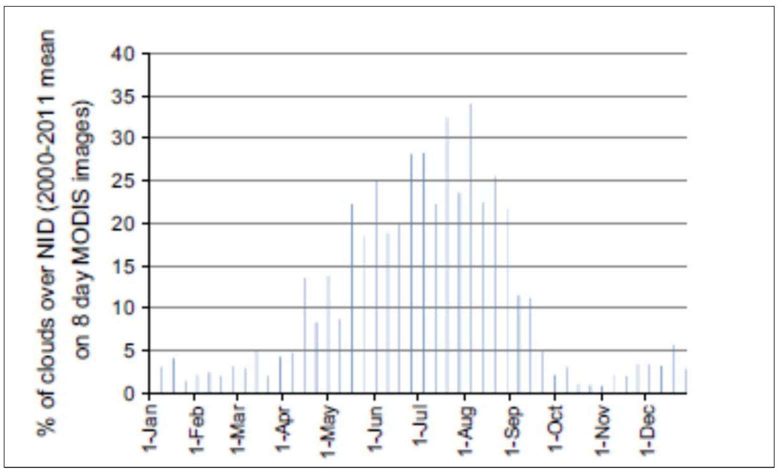

Fig. 2.5: Mean cloud coverage over the IND area on MODIS images throughout 2000- 2011 (Ogilvie et al., 2015).

It is found that the 2001-2002 and 2008-2009 years experienced relatively less cloud. Our study uses these two years as calibration and validation periods. MODIS and Landsat images during the months September- February will be considered for extracting water extent as these months show less cloud than the other months.

2.6 Statistical methods

2.6.1 Simple linear regression

The most common models used in hydrology assume a linear relationship between two variables. Generally, the objective of such a model is to provide a means of predicting one variable (dependent) from the knowledge of the second variable (independent). The statistical procedure applied to determine the relationship between the two variables is known as regression (Haan, 2002).

The simplest linear regression model can be written as follows:

$$Y = a + bX \tag{2.13}$$

where Y is called the dependent variable and X the independent or explanatory variable, the terms a and b are the parameters of the model. The parameter a is called the intercept term, and the parameter b is called slope parameter. These parameters are referred to as regression coefficients.

Haan (2002) describes the following task to complete when fitting a regression model:

- Estimation of the parameters in the regression equation (least square method)
- Model evaluation with the coefficient of determination (R^2)
- Testing of the regression line and the coefficients by calculating confidence interval and test of hypotheses.
- Model application

2.6.2 Multiple Regression

Multiple regression is the statistical procedure where we can predict the values of a response (dependent) variable from a collection of the predictor (independent) variable values. The general purpose of multiple regression is to find a relationship between several independent or predictor variables and a dependent variable. The multiple linear regression equation is as follows:

$$Y = b_o + b_1X_1 + b_2X_2 + \cdots .. + b_nX_n \tag{2.14}$$

where Y is the predicted or expected value of the dependent variable, X_1 through X_n are *n* distinct independent or predictor variables, b_o is the value of Y when all of the independent variables (X_1 through X_n) are equal to zero (intercept), and b_1 through b_n are the estimated regression coefficients. The followings are the main steps in multiple regression analysis:

- Determine parameters in the regression equation (by using the least square method, method of moments, or maximum likelihood method). Linear regression models are often fitted using the least-squares approach.
- Determine the percent of the variability in Y that is accounted for by multiple regression, R^2
- Test statistical significance of the multiple regression (p-value)
- Determine the relative importance of different independent variables X in explaining Y.

Various authors such as Patel et al. (2016), Archer and Fowler (2008), and Korecha & Barnston (2006) developed regression models for streamflow estimation, flood forecasting, and seasonal precipitation forecasting, respectively.

.

One of the major advantages of the multiple regression method is that investigators are provided with an opportunity so that they can structure their models based on their knowledge and experiences with the physical system being modeled. On the other hand, one of the major and frequent disadvantages is that regression coefficients may be irrational when two or more predictor variables are highly correlated with each other (Mc-Cuen et al. 1979).

2.6.3 Polynomial regression

Polynomial regression is a statistical technique that deals with the non-linear relationship between different variables. The typical form of polynomial regression consists of different powers of independent variables, X_n^n with a dependent variable, Y. If the equation has only independent variables of degree of 1, it will be a multiple linear regression. A non-linear regression is obtained if the power of different independent variables, X_n, is not equal to 1. In hydrology, it is an important statistical technique because most of the correlations between different variables are non-linear. The general form of polynomial regression can be shown as follows:

$$Y = b_o + b_1 X_1^1 + b_2 X_2^2 + b_2 X_2^2 + \cdots + b_n X_n^n \quad (2.15)$$

Polynomial regression also uses the least-square method to find the most suitable coefficients of a and b. The processes of finding the coefficients of independent variables and interception are similar to multiple linear regression, the only difference being the degrees of independent variables.

2.6.4 Stepwise Regression

Stepwise regression is another statistical technique that can be used for developing a prediction equation relating a dependent variable to one or more predictor variables (Mc-Cuen et al. 1979). Even though it is a type of multiple regression analysis, it differs on the fact that the stepwise regression uses statistical criteria for selecting which of the available predictor variable will be included in the final regression equation; in contrast, multiple regression analysis includes all the available variables in the equation. This approach is probably the best way to pick the correct predictors for a system (Wang et al., 2009).

This regression analysis starts with no candidate variable in the model. Variables are then added one by one at each iteration according to their level of significance in the analysis. At each step, the *p*-value of an *F*-statistic is computed to test the new regression models. If any predictor, not in the model, has *p*-values less than a specific value (say 0.05) then that predictor is added to the model. If the *p*-value of the predictor is greater than the threshold (0.05) then that predictor is not included in the analysis. At the first step, the prediction is equal to the sample mean of the predictand ($\hat{y}$) as shown in the following equation:

$$\hat{y} = b_0 \tag{2.16}$$

Candidate variables are then added to it one at a time, and if there are *N* variables*,* *N* equations need to be constructed and tested. Consequently, the predictor with the best linear regression among the candidate predictors is then chosen, which satisfies the level of significance, coefficient of determination (R^2), and the largest F ratio. At this stage of the screening procedure, the prediction equation becomes:

$$\hat{y} = b_0 + b_1 x_1 \tag{2.17}$$

x_1 is the predictor which meets those criteria.

The remaining (N-1) candidate variables are then added to the above equation to determine the next best predictor applying the same criteria as described in the previous step. The procedure is then recognized as the next best predictor (x_2) and added to the model as follows:

$$\hat{y} = b_0 + b_1 x_1 + b_2 x_2 \tag{2.18}$$

All the subsequent steps follow this pattern until all predictors are tested. As one candidate variable is added to the previous equation each time, all regression coefficients and the intercepts term change.

Stepwise regression is very popular among researchers so that they can choose the best predictors among the large predictor data set. Sittichok et al. (2014), and Gado Djibo et al. (2015) applied this method to screen potential predictors for the development of rainfall forecast models.

2.6.5 Multi-modeling technique and Bayesian Model Averaging (BMA)

Multi-modeling is a technique to join the results of individual models into a robust one. Different models have different strengths in capturing different hydraulic aspects. Relying on a single model can lead to a faulty prediction of an event. Due to the incomplete representation of processes in the models, predictions from a single model often lead to bias of the forecast (Zhu et al., 2013). Georgakakos et al. (2004) stated that combining simulations from multiple models may better account for uncertainties in physical processes and model structure. This has motivated several researchers to adopt a multi-model ensemble method.

Various multi-modeling techniques have been developed to improve the streamflow and water level predictions (Georgakakos et al. 2004; Ajami et al. 2006; Duan et al. 2006). There are several methods available to combine results, among them the notables are: Simple model average by Georgakakos et al. (2004), Weighted average method (WAM) by Shamseldin et al. (1997), Multi-model super-ensemble (MMSE) by Krishnamurti et al. (2000), Bayesian model averaging (BMA) by Hoeting et al. (1999).

Ajami et al. (2005) applied the multi-modeling approach on five basins of the Arkansas Red river basin. They combined the simulation output of seven hydrological models such as SWAT, SAC-SMA, NOAH Land Surface Model, HRCDHM, HL-RMS, TOPNET, and WATFLOOD. They combined the simulations with multimode techniques: SMA, MMSE, Modified Multi-Model Super Ensemble (M3SE) and the WAM. This study revealed that the multi-model predictions obtained from single model predictions are generally better than any single member model predictions. They suggested that at least four models be included for the methods. Although the study reveals that multi-model prediction is better than the single model, however, it was not able to identify the strength of individual models to be given priority during the combination. BMA overcomes this deficiency by weighing a model by its performance and likelihood of predicting the observation, resulting in a probabilistic forecast. BMA is a statistical methodology that aims to combine inference and predictions of several different models and to jointly assess their productive uncertainty. Various case studies show that BMA can produce more reliable predictions than other multi-model methods (Raftery et al., 2003, 2005; Duan et al., 2007; Vrugt and Robinson, 2007).

Beckers et al. (2015) applied BMA to a set of water-level forecast models used in the Flood Forecasting and Warning System for Rhine and Meuse rivers (FEWS NL). Four meteorological models were combined with both a hydrological model (HBV) and a combination of hydrological-hydraulic models (HBV/SOBEK) to produce eight competing model forecasts. An additional forecast was obtained using a statistical model called Lobith. HBV discharges were translated into water level values using an empirical water-level discharge relationship. It was found that BMA is a promising method to produce a calibrated probabilistic forecast from a collection of competing forecast models.

This study makes use of BMA to combine the water levels and discharge time series simulated by 2D hydraulic models. It is believed that the method will increase the predictive performance of the combined result. Nobody previously applied this method in that area. As it is known that elevation data is an important source of error and can propagate into the result; consequently, results from several models with different elevation sources can remove the bias and improve the accuracy.

The weight of the individual model will be determined and will be applied to see if we can apply the weight for future prediction.

2.6.6 The theoretical background of BMA

Let *y* be the forecasted and $D = \left[y_1^{obs}, y_2^{obs} \dots \dots .. y_T^{obs}\right]$ to be the training data with length *T*. Let *K* models be denoted by $f = [f_1, f_2, f_3, \dots \dots, f_K]$. Based on the observations *D*, the BMA probability density function (pdf) of *y* is given by:

$$p(y|D) = \sum_{k=1}^{K} p(f_k|D) \; . \;\; p_k(y|f_k, D) \qquad (2.19)$$

Where,

$p(y|D)$ is the pdf of BMA of *y* given data *D*.

$p(f_k|D)$is the posterior probability of model prediction f_k given the observational data D, also known as BMA weight w_k.

$p_k(y|f_k, D)$ is the conditional probability density function (pdf) of y on the condition on the model prediction f_k and observational data set *D*.

If we denote $w_k = p(f_k|D)$, the sum of w_k equal to 1 i.e. $\sum_{k=1}^{K} w_k = 1$.

So, $p(y|D)$ can be written in the following form:

$$p(y|D\ ) = \sum_{k=1}^{K} w_k \; . \;\; p_k(y|f_k, D) \qquad (2.20)$$

The mean and variance of the BMA prediction can be expressed as:

Mean of BMA:

$$E[y|D] = \sum_{k=1}^{K} p(f_k|D) \,.\, E[p_k(y|f_k, D)] = \sum_{k=1}^{K} w_k f_k \tag{2.21}$$

Variance of BMA:

$$Var[y|D] = \sum_{k=1}^{K} w_k (f_k - \sum_{k=1}^{K} w_k f_k)^2 + \sum_{k=1}^{K} w_k \sigma_k^2 \tag{2.22}$$

Where, σ_k^2 is the variance of y with respect to models f_k and data D.

The successful implementation of the BMA requires estimates of the weights, w_k and standard deviations, σ_k of the conditional pdfs of the ensemble members. Their values can be estimated through the maximum likelihood method (Raftery et al. 2005).

Let, $\theta = \{w_k, \sigma_k, \;\; k = 1, \dots K\}$

The logarithmic likelihood function can be approximated as follows:

$$l(\theta) = \sum_{t=1}^{T} log\left(\sum_{k=1}^{K} w_k \,.\; p_k(y|f_k, D)\right) \tag{2.23}$$

Equation (2.23) cannot be solved analytically for θ. The BMA weights can be calculated by two approaches, such as the Markov Chain Monte Carlo (MCMC) (Vrugt et al. 2008) algorithm and Expectation-Maximization (EM) (McLachlan and Krishnan, 1997) algorithm. We applied the EM algorithm, as recommended by Raftery et al. (2005), to get the optimum value of θ.

2.7 Improved boundary condition

Boundary conditions are a required component of hydrodynamic models. There are two types of boundary conditions in a hydraulic model. One is the inlet boundary where discharge is prescribed. Another is the outlet boundary where water level or stage-discharge curve is prescribed. Uncertainty can result from inappropriate boundary conditions. The uncertainties in the boundary conditions are very often neglected (Pappenberger et al., 2006). The dominant part of the discharge at the inlet boundary in our model is coming from observations and considered as error-free.

In this thesis, a rating curve was prescribed at the downstream boundary of all hydrodynamic models. As the study area is dominated by the hysteresis effect, a looped rating curve is characterized and prescribed at the downstream boundary. The two methods used to derive the looped rating curves are described in the following section:

2.7.1 The Jones formula

The Jones formula (Jones, 1916) is the best-known formula for loop rating curve derivation. Herschy (1995) suggests using the Jones formula for correcting the steady-state rating curve when loop flow is present and significant.

Jones (1915) used the following equation for loop flow computation:

$$Q_L = Q_s \left[1 + \frac{1}{S_0 c} \frac{\partial h}{\partial t}\right]^{1/2} \tag{2.24}$$

In which, Q_s is single rating discharge, can be obtained from the single rating curve, S_0 the mean slope of the stream and c the kinematic wave speed, $\partial h/\partial t$ rate of change of stage.

Q_s can be approximated by the following power-law function (Herschy, 1978; Dymond and Christian, 1982; ISO, 1998):

$$Q_s = a(h - b)^c \tag{2.25}$$

Petersen-Øverleir (2006) simplified the loop rating equation in the following way:

$$Q_L = a(h - b)^c \left[1 + \theta(h - b)^{-M} \frac{\partial h}{\partial t}\right]^{1/2} \tag{2.26}$$

where $\theta = \frac{(1+N)^{M+1}}{K S_0^{\frac{3}{2}}(M+N+1)}$

K conveyance factor, *M* friction law exponent *(~2/3), N* channel-shape parameter *(~0-1),* a and c are rating curve constants and can be estimated from a steady rating curve analysis, b is the water level corresponds to zero discharge

2.7.2 Dimensionless form of Q and WL

Mishra and Seth (1998) stated that hysteresis is represented by dimensionless quantity derived from stage and discharge values. The equations used to transform discharges and water levels into their dimensionless forms are given in the following section.

Observed water levels for each of the year are transformed into a scale of 0-1 by using the following formulae:

$$(H_{sc})_i = \frac{H_i - H_{min}}{H_{max} - H_{min}} \tag{2.27}$$

In which, H_{sc} is scaled water level, H is the observed water level, H_{min} is the minimum and H_{max} is the maximum water level, i is the i^{th} data of the respective year.

Observed discharge for each of the year is transformed into scale by using the following formulae:

$$(Q_{sc})_i = \frac{Q_i - Q_s}{Q_{max}} \tag{2.28}$$

In which, Q_{sc} is scaled discharge, Q is observed discharge, Q_{max} is the maximum discharge, i is the i^{th} data of the respective year, Q_s is the discharge obtained from a single static rating curve.

The scaled values can be used to obtain the loop rating curve with the following equation:

$$WL_{loop} = (H_{sc})_i * (H_{max} - H_{min}) + H_{min} \tag{2.29}$$

$$Q_{loop} = (Q_{sc})_i * Q_{max} + Q_s \tag{2.30}$$

in which Q_{loop} and WL_{loop} are discharge and water level of loop rating curve, respectively. The other terms are described in the previous section.

2.8 Performance assessment for discharge and water level simulation

Models performance can be evaluated with various techniques as described in the flowing sections

2.8.1 Pearson correlation coefficient

Pearson correlation coefficient (r) is the ration of the sample covariance to the product of the standard deviations of the observed and simulated values (Wilks, 2011). The coefficient of determination (R^2) is the square value of the Pearson correlation coefficient. The general form of the equation for the correlation coefficient is given below:

$$r = \frac{\sum_{i=1}^{n}(x_i-\bar{x})(y_i-\bar{y})}{\sqrt{\sum_{i=1}^{n}(x_i-\bar{x})^2}\sqrt{\sum_{i=1}^{n}(y_i-\bar{y})^2}} \tag{2.31}$$

Here, x represents the simulated, and y the observed value of a variable. $\bar{x}$ and $\bar{y}$ are the averages of the simulated and observed values, respectively.

Wilks, (2011) stated two disadvantages of the Pearson correlation coefficient- 1) it is not robust, 2) not resistant. It is not robust because strong but nonlinear relationships between the variables may not be recognized. It is not resistant since it can be very sensitive to one or a few outliers.

The value of the coefficient ranges from -1 (for perfect negative correlation) to +1 (for perfect positive correlation). Thus, for any given sample size, the closer the coefficient is to +-1, the stronger the linear relationship. On the other hand, as the value approaches 0, the relationship between the variables become weaker.

Mc-Cuen et al. (1979) suggested not to use the correlation coefficient alone because it may sometimes give misleading results. When the total variation is relatively high, then both the numerator and error can be relatively high. This results in a high "r" but, at the same time, the average error might be quite large.

2.8.2 Root-mean-squared-error (RMSE)

The root-mean-square-error (RMSE) is another widely used criterion for model performance, which is often applied to hydrological and hydrodynamical models (e.g., Kim et al., 2012; Neal et al., 2012). It indicates the average error in the model predictions and is calculated as follows:

$$RMSE = \sqrt{\frac{\sum_{i=1}^{n}(x_i - y_i)^2}{n}} \tag{2.32}$$

While the RMSE indicates a model's overall performance, it says little about its ability to accurately simulate peak flows, which are an important indicator for floods.

RMSE is always non-negative, and a value of 0 (seldom achieved in practice) would indicate a perfect fit to the data. In general, a lower RMSE is better than a higher one. However, comparisons across different types of data would be invalid because the measure is dependent on the scale of the numbers used.

2.8.3 Relative error

The relative error is calculated as follows:

$$RE = \sum \left| \frac{(x_i - y_i)}{y_i} \right| \tag{2.33}$$

Here, x represents the simulated, and y the observed value of a variable. $\bar{x}$ and $\bar{y}$ are the averages of the simulated and observed values, respectively. n is the number of observations.

2.8.4 Nash-Sutcliffe coefficients

The Nash-Sutcliffe coefficient (NS), proposed by Nash & Sutcliffe (1970), compares the modeled output to the observed data. NS can be determined by computing the ratio of the sum of square error of observations and predictions, and variance of the observations. This ratio is subtracted from 1 to get the NS coefficient. NS is expressed in the following equation:

$$NS = 1 - \frac{\sum_{i=1}^{n}(x_i - y_i)^2}{\sqrt{\sum_{i=1}^{n}(y_i - \bar{y})^2}} \tag{2.34}$$

where x represents the simulated, and y the observed value of a variable. $\bar{x}$ and $\bar{y}$ are the averages of the simulated and observed values, respectively.

The range for NS can vary between -∞ and 1, where: $NS = 1$ corresponds to a perfect match between simulated and observed data; $NS = 0$ means that the model's predictions are as accurate as the mean of the observed data; and $NS < 0$ indicates that the mean value of the observed time series would have been a better predictor than the model, which indicates unacceptable performance (Wang et al. 2009). Though NS is widely used for evaluating model performance, however, there are limitations as pointed out by Legates and McCabe (1999). The limitations are because the differences between the observed and simulated values are calculated as squared values. As a result, there is an over-estimation of larger values in a time series, and lower values are neglected.

Lian et al. (2007) evaluated a model as "good" if the NS value is above 0.75 and "satisfactory" if the value lies between 0.36 and 0.75. Bredesen and Brown (2019) used intervels of NS as performance rating as follows; $0.75 < NS < 1$ is a "very good" performance rating, $0.65 < NS < 0.75$ is a "good" performance rating, $0.50 < NS < 0.65$ is a "satisfactory" performance rating, and $NS < 0.50$ is an "unsatisfactory" performance rating.

2.9 Performance assessment for inundation extent

Model skills can be evaluated by comparing simulated inundation extent with the observed by adopting several fit measures (Taylor, 1977 and Gallien et al. 2011). The measures used in this purpose are Agreement fit measures, Under-prediction measures, and Over-prediction measures. A brief description of the methods is given in the following paragraph.

2.9.1 Agreement fit measures

Agreement fit measures (F_A) represents the intersection of predicted and observed flood extents divided by the union of the predicted and observed flood extent. F_A is expressed by the following equation:

$$F_A = \frac{E_P \cap E_0}{E_P \cup E_0} \tag{2.35}$$

where E_O and E_P are the observed and predicted flood extents, respectively. $E_P \cap E_0$ is the intersection between E_O and E_P. $E_P \cup E_0$is the union between E_O and E_P. F_A values of zero and unity correspond to no agreement and complete agreement, respectively.

2.9.2 Under-prediction measures

Under-prediction measures (F_{UP}) the fraction of flooded area observed, but not predicted and is expressed as follows,

$$F_{UP} = \frac{E_0 - E_P \cap E_0}{E_P \cup E_0} \tag{2.35}$$

F_{UP} values of 0 and 1 correspond to no under-prediction and complete under-prediction, respectively.

2.9.3 Over-prediction measures

Over-prediction measures (F_{OP}) the fraction of flooded area predicted but not observed and expressed as follows:

$$F_{OP} = \frac{E_P - E_P \cap E_0}{E_P \cup E_0} \tag{2.36}$$

Where F_{OP} values of 0 and 1 correspond to no over-prediction and complete over-prediction, respectively.

Superior models will maximize the F_A while minimizing both F_{UP} and F_{OP}.

2.10 Concluding remarks of the literature review

There were several efforts (Dadson et al., 2010; Haag, 2015; Neal et al., 2012; Zsufa et al., 2013) to model the hydrodynamics of the IND. Among the studies, most notable is the study conducted by Neal et al. (2012). They applied LISFLOOD-FP for modeling the variables in IND. Although the model predicts discharge correctly, however, it was not able to simulate water level and inundation extent of the area with substantial accuracy. Although the author mentioned that the elevation data was the barrier to not to produce good prediction, another cause may be the finite difference method that was used to solve the shallow water equation with about 1.0km rectangular grid, that was too coarse for floodplain modeling.

A fine resolution, full 2D hydrodynamic model which can simulate the flow dynamics of the IND properly, is still absent. The present study is an endeavor to model the area with sophisticated modeling techniques. It is known that hydraulic model equipped with finite element solution in unstructured grid is less sensitive to terrain input and can account for the variation the geometry in the channel and over the floodplain (Cook and Merwade,2009). TELEMAC 2D is equipped with sophisticated numerical schemes, and it solvest the systems of equations with finite element methods in an unstructured grid. Sanyal et al. (2014) found that the TELEMAC-2D is more suitable than LISFLOOD-FP model for simulating extensive floodplain inundation in a data-scarce region.

Based on the fact that 2D models are appropriate for a flood plain modeling and process representation can better be done with finite element method with unstructured grid, we choose to apply TELEMAC 2D. No modeling was conducted in the study area with this model.

Ogilvie et al. (2015) conducted a flood mapping of the IND based on satellite images. They recommended using the satellite-based inundation extent maps for set up and calibration of hydrodynamic model. The study makes use of satellite-derived inundation maps to set up, calibration, and validation purposes.

Multimodeling techniques such as BMA will be applied to improve the simulation results. Georgakakos et al. (2004) stated that combining simulations from multiple models may better account for uncertainties in physical processes and model structure.

Pappenberger et al. (2006) mentioned that uncertainty could be generated from the boundary conditions, and the uncertainties in the boundary conditions are very often neglected. The study will also focus on improving the simulation by including loop rating curve.

Chapter 3

Study area and study material

3.1 Study area

The Inner Niger Delta, Mali, West Africa, has been selected as the study area of this research work. The IND is situated in a semi-arid region in the Sahelian zone (a broad semiarid belt, extending from the Atlantic Ocean to Sudan, averaging about 350 km wide). The Inner Niger delta is formed by the braiding channel system of the Niger River and its tributaries. The catchment of the IND is the Upper Niger Basin (UNB). Both the IND and UNB are part of the Niger River basin. The Niger River, the third-longest river (about 4200km long) in Africa, originates at the mountains in Guinea and Sierra Leone, flows towards UNB and IND, then heads south-east direction to Niger and Nigeria and finally flows into the Atlantic Ocean in coastal Nigeria. Two model domains are considered in this research work. The content of Chapter 5 and Chapter 6 are based on the model area corresponds to Fig. 3.1(c). In Chapter 7, the model domain that is considered is shown in Fig. 3.1(d), which has a larger area than the previous one.

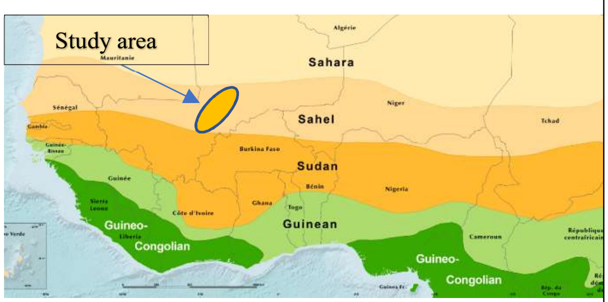

(a)

(b)

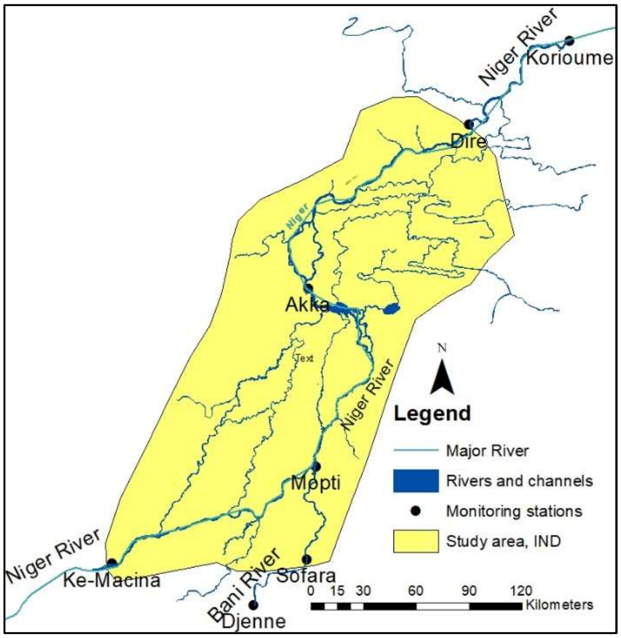

(c)

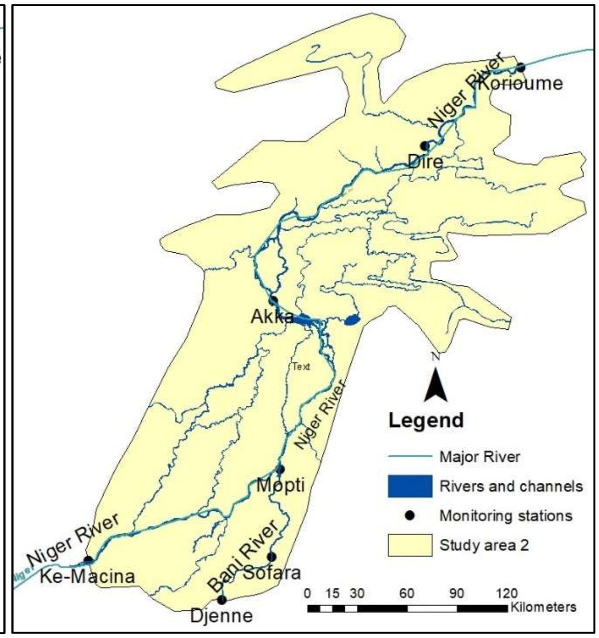

(d)

Fig. 3.1: (a) Study area in the context of Sahelian zone (source: CILSS, 2016); and (b) Study area within the countries in the West Africa; (c) model domain used in Chapter 5 and Chapter 6; (d) model domain used in Chapter 7.

3.2 Ecological importance of IND

The IND is a river-dependent ecosystem. The ecosystem service and natural resources depend on the magnitudes of the flow coming from upstream catchment through the Niger and the Bani Rivers. The river water is vital to the livelihoods of the surrounding riparian population, where individuals gain advantage for their economy from the flood caused by these rivers. These major economic activities include fishing, floating rice (Oryza glaberrima), rainfed millet on the fringes of the flooded fields, as well as Bourgou (Echinochloa stagnina) and other forage for which big seasonal migrations are carried out by livestock herders (Ogilvie et al., 2010). The IND has been designated as wetlands of International Importance (Ramsar Sites*)* in 2014 because of its important biodiversity.

3.3 Hydrology of IND

The Inner Niger Delta's primary source of water is the Niger and the Bani Rivers water flow, which in turn depends on the precipitation of the Upper Niger Basin. The July-August rainfall in this region is a useful measure of the Inner Niger Delta flooding in September-October. The Inner Niger Delta experiences flood dynamics between July and December. The water level may rise 4-6m during the rising flood and declines the same in receding flood. Most of the water flowing in IND comes from a very humid region in Guinea, which is situated in 600-900 km upstream. The headwater's annual rainfall can go up to 1750mm. However, in IND, the average annual rainfall varies between 200 mm per year at the downstream and 500mm per year at the upstream. Local rainfall is too limited to influence the flood height. The spatial repartition of annual rainfall in the upper Niger basin is shown in Fig. 3.2.

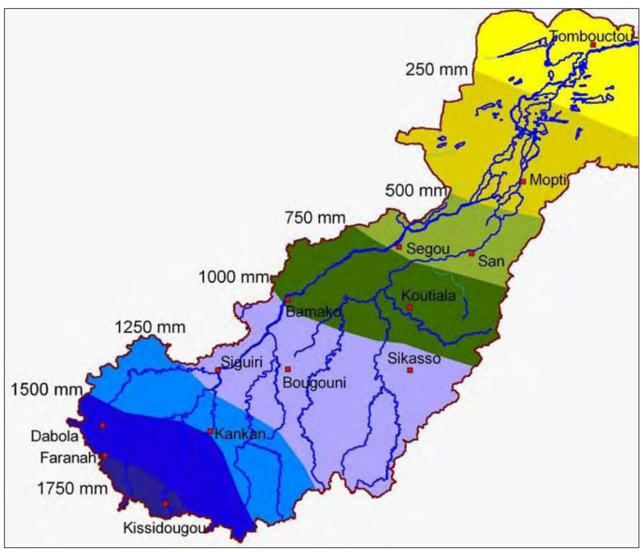

Fig. 3.2: Annual rainfall (mm per year) in the basin of the Upper Niger (Zwarts et al. 2005)

Evaporation has an immediate impact on the water balance of IND. The comparison between the inflow of the Niger and the Bani and the outflow into the Inner Niger Delta shows a large difference, which may be attributed to water loss due to evaporation (Mahé et al. 2009). Evaporation varies between 160 and 240 mm per month, depending on temperature and sunshine, with an average of 200 mm per month. Ogilvie et al. (2015) found evaporation rates between 4.0 mm per day and 7.0 mm per day over the year 2008–2009.

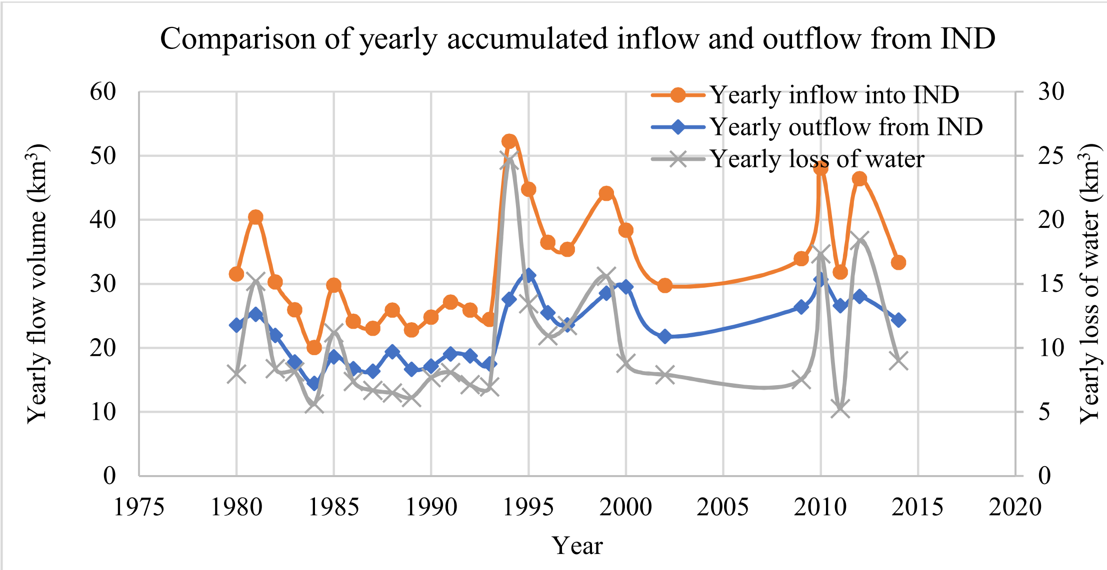

Fig. 3.3: Comparison of yearly accumulated inflow and outflow from IND

Yearly accumulated flow into IND resulting from the combined flow of the Niger and the Bani through KeMacina and Sofara is compared with the yearly outflow from IND through Dire in Fig. 3.3. The yearly average loss of water over the period 1980-2015 is about 10.14 km^3 out of average yearly inflow of 32.71 km^3, which corresponds to a loss of 31% of the total inflow. As can be seen in Fig. 3.3, the loss is not constant and varies over the years. The variation depends on the amount of water enters into IND through KeMacina and Sofara. The more water enters and spread into IND, the more the losses due to evaporation and infiltration. This amount of loss has a substantial impact on the water balance and should be accounted for during water resources analysis.

3.4 Available data

3.4.1 Discharge and water level data

Water level and discharge at Ké-Macina, Mopti, Akka, and Diré from 1990 to 2016, as well as a rating curve at Diré, were obtained from the Malian hydrometric services (Direction Nationale de l'Hydraulique, DNH). Fig. 3.4(a) shows the observed hydrographs at Ké-Macina, Mopti, Akka, and Diré from July 2001 to February 2002 and Fig. 3.4(b) shows a series of hydrographs at Dire representing driest (1984-85) to wettest year (1994-1995). Ke-Macina and Akka are located along the Niger River, while Mopti is at the confluence of the Niger and Bani rivers. The hydrographs at Ké-Macina and Mopti represent water entering the IND, while the hydrograph at Diré represents water leaving the IND.

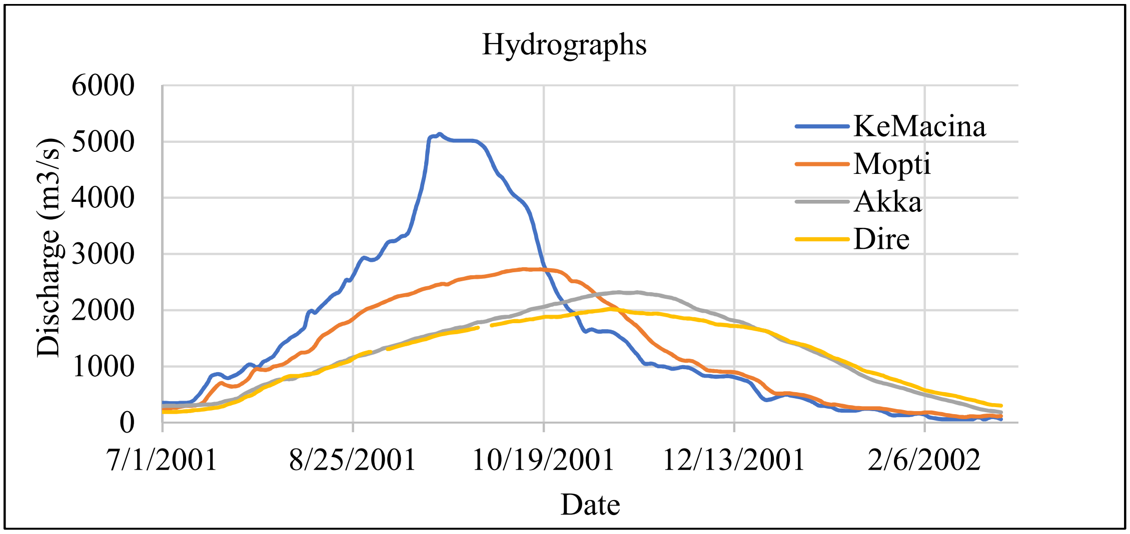

(a)

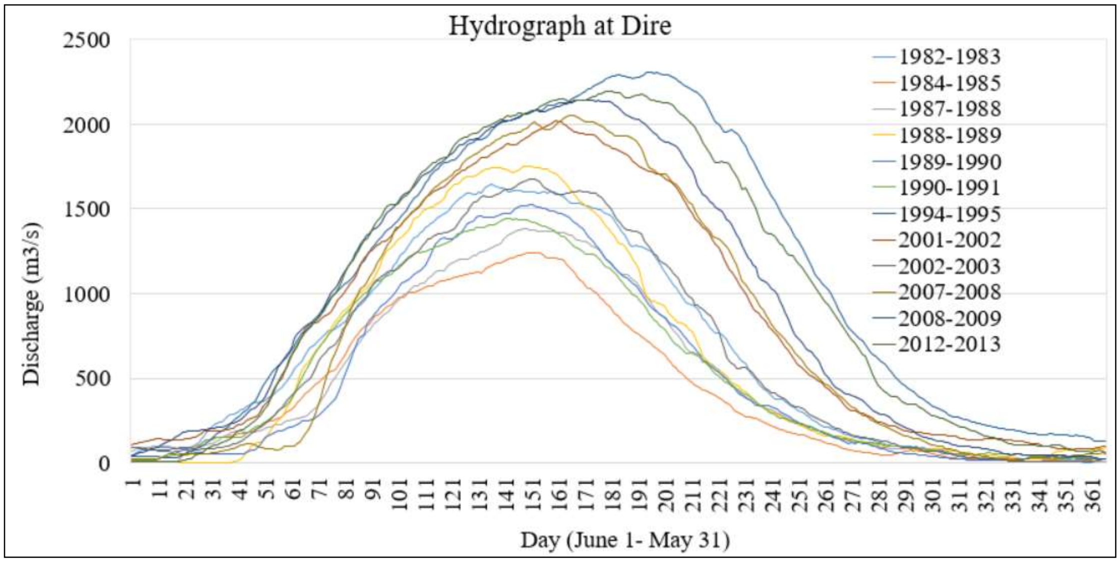

(b)

Fig. 3.4: (a) hydrographs at Ké-Macina, Mopti, Akka, and Diré from July 2001 to February 2002; (b) series of hydrograph showing driest (1984-85) to wettest year (1994-95).

3.4.2 Global digital elevation models

Two sets of global digital elevations were used for the study. One of them is the Shuttle Radar Topography Mission (SRTM) elevation data, which was downloaded from https://earthexplorer.usgs.gov/. SRTM data is available at a resolution of one arc-second (~30 m) for the study area. The other one is the DEM Multi-Error-Removed Improved-Terrain, MERIT DEM (Yamazaki et al., 2017), which is available at about 90m resolution and can be downloaded from http://hydro.iis.u-tokyo.ac.jp/~yamadai/MERIT_DEM/.

3.4.3 Available Satellite Imagery

In the absence of direct monitoring of inundation extent, remote sensing data is used to derive the flood situation of events. Landsat and MODIS images are the two sources from where data can be downloaded freely and processed to obtain water extent. Zwarts et al., (2005) processed Landsat 5 TM images captured on 24 different dates spanning from 1984 to 2003 and derive 24 water extent maps for the study area. Our study makes use of these water extent maps for model setup and calibration purposes and obtained from the Wetlands International, Mali Office. The images provide evidence of the minimal and maximal extents of inundation areas along with known water levels at Mopti, Akka, and Diré. Inundation extent obtained on July 28, 2001, and October 16, 2001 from the images are shown in Fig. 3.5.

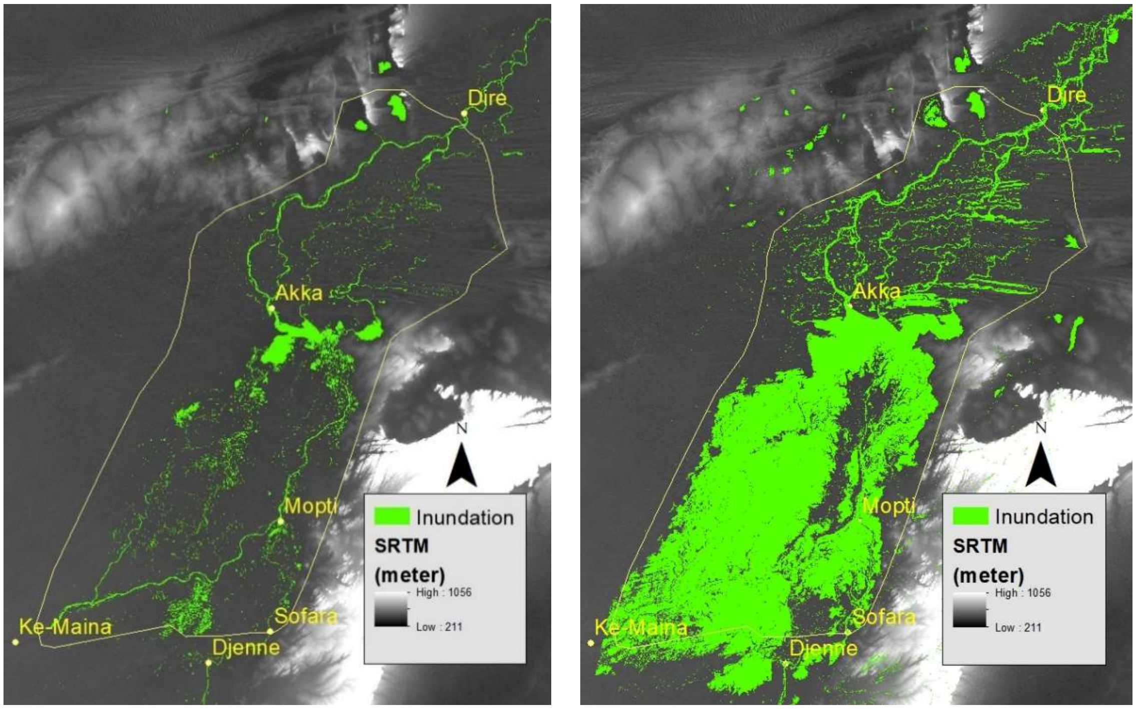

Fig. 3.5: Satellite Images of inundation extents of the Delta on July 28, 2001 (left) and October 16, 2001 (right) (Source: Zwarts, et al., 2005)

To validate the simulated inundation extent, a series of Landsat 7 ETM and MODIS images were processed to derive the inundation extent. A summary of satellite data usage is given in Table 3.1.

Table 3.1: Satellite images used for calibration and validation

Image source/ Name	Satellite	Path/row	Purpose	Date Captured	Resolution
Several images from Zwart et al. (2005)	Landsat 5 TM	197/49 and 197/50	Model setup, Calibration	1984 to 2003	30m
LE07_197049_20080901 LE07_197050_20080901 LE07_197049_20081104 LE07_197050_20081104 LE07_197049_20090224 LE07_197050_20090224	Landsat 7 ETM	197/49 and 197/50	Model validation	01 Sep 2008 04 Nov 2008 24 Feb 2009	30m

MOD09A1.A2008241 MOD09A1.A2008281 MOD09A1.A2009017	MODIS	-	Model validation	28 Aug 2008 07 Oct 2008 17 Jan 2009	500m
MOD09A1.A2010273 MOD09A1.A2010321 MOD09A1.A2010337 MOD09A1.A2010353 MOD09A1.A2011001 MOD09A1.A2011033 MOD09A1.A2011057 MOD09A1.A2005305 MOD09A1.A2005337 MOD09A1.A2005353 MOD09A1.A2006041	MODIS	-	Validation of Inundation curve	30 Sep 2010 17 Nov 2010 03 Dec 2010 19 Dec 2010 01 Jan 2011 02 Feb 2011 26 Feb 2011 01 Nov 2005 03 Dec 2005 19 Dec 2005 10 Feb 2006	500m

*The author processed the images described in 2^{nd}, 3^{rd} and 4^{th} rows

3.4.4 Rainfall-runoff modeling

A calibrated hydrological model, Soil Water Assessment Tools (SWAT), is used to generate lateral flows that end up in the IND and that are not captured by existing stream gauges. The SWAT model was run with observed climate data, and the discharge from surrounding watersheds was assumed to enter the area where the main channel crosses the boundary of the study area (Fig. 3.6).

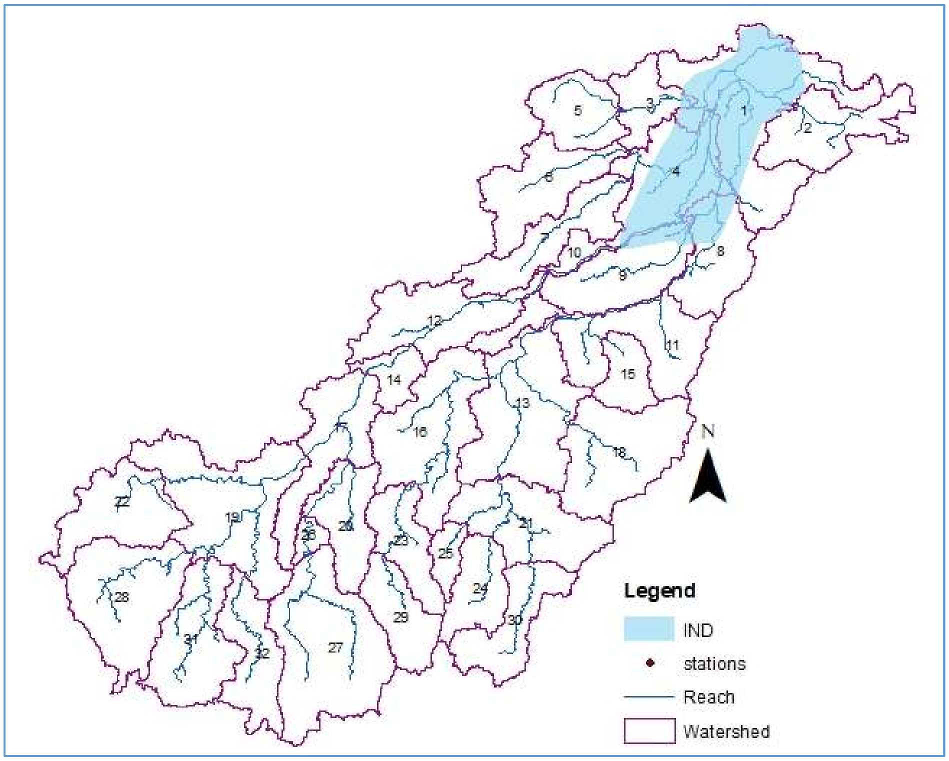

Fig. 3.6: Study area at the domain of the SWAT model (Source: Seidou, 2019)

3.4.5 USGS Land Use/ Land Cover data

The study used USGS Land Use/Land Cover data (Loveland et al., 2000) to get land use information of the study area, which was subsequently used to derive floodplain friction of the study area. The data was downloaded from https://earthexplorer.usgs.gov/. They are based primarily on the unsupervised classification of 1-km AVHRR (Advanced Very High-Resolution Radiometer) 10-day NDVI (Normalized Difference Vegetation Index) composites (Loveland et al. 2000). The area comprises 19 land classifications, which are linked to the Manning roughness coefficient as described by Asante et al. (2008). Fig. 3.7(a) displays the land use map of the study areas and Fig. 3.7(b) shows the distributed Manning's roughness coefficient at the IND's floodplain.

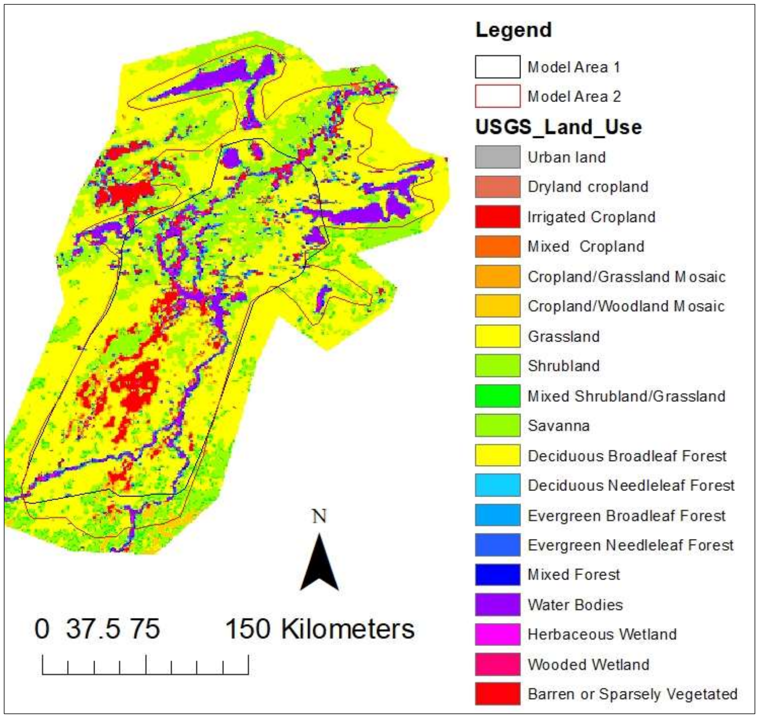

(a)

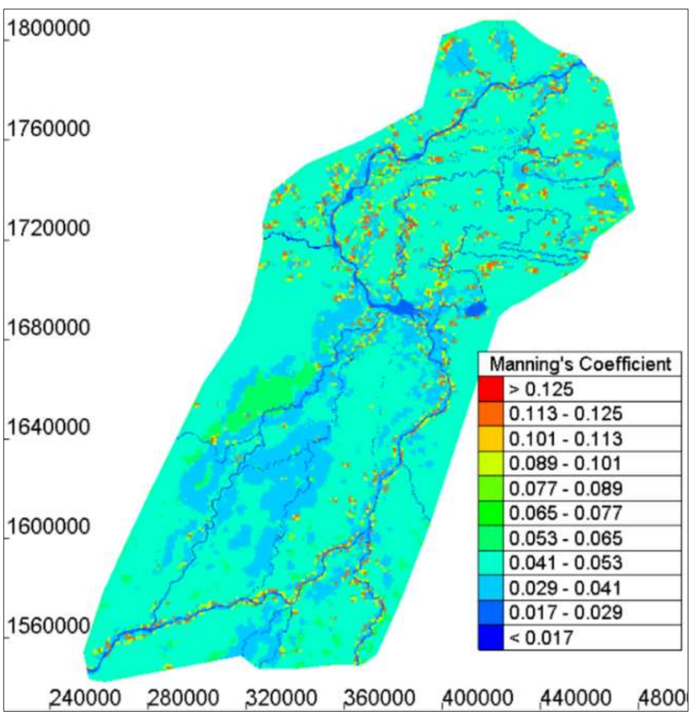

(b)

Fig. 3.7: The land use map of the study area (a); Manning’s coefficient at the floodplain (b).

Chapter 4

Improving the Accuracy of Hydrodynamic Simulations in Data Scarce Environments using Bayesian Model Averaging: a Case Study of the Inner Niger Delta, Mali, West Africa[1]

Abstract

The study area is the Inner Niger Delta, Mali, West Africa. The area is facing environmental challenges due to altered flow regimes resulting from climate change, increasing irrigation withdrawal, and dam operation on the main river reaches. An accurate understanding of spatial and temporal dynamics of inundation extent is needed to govern the water management choices of the area. The study aims to use 2D hydrodynamic modeling to simulate variables such as water level, depth, velocity, inundation extent. Three different digital elevations (SRTM, MERIT, and a DEM derived from satellite images) were used as source of elevation data for the model. Six different models were created with different sources of elevation data and different downstream boundary conditions. The simulation results were then combined through Bayesian Model Averaging (BMA) to have the best predictions of discharges and water levels. Despite data scarcity, the study develops a hydrodynamic model with 2D finite element TELEMAC-2D model, which can simulate the variables with reasonable accuracy. The accuracy of the simulation was further increased by combining model configurations using BMA. It was found no matter the source of elevation data, all models performed reasonably well (NS>0.8). It was also found that models built using MERIT DEM perform slightly better than SRTM in terms of NS coefficient in the simulations.

Keywords Inner Niger Delta, Uncertainty, TELEMAC 2D, Bayesian Model Averaging

[1] This part has been published as: Haque, M.M., Seidou, O., Mohammadian, A., Djibo, A.G., Liersch, S., Fournet, S., Karam, S., Perera, E.D.P., Kleynhans, M. (2019) Improving the Accuracy of Hydrodynamic Simulations in Data Scarce Environments Using Bayesian Model Averaging: A Case Study of the Inner Niger Delta, Mali, West Africa. *Water*, *11*, 1766. https://doi.org/10.3390/w11091766

4.1 Introduction

The Inner Niger Delta (IND) is the second-largest wetland in Africa, and its maximum inundated area can exceed 30,000 km^2 during wet years (Zwarts and Frerotte, 2012). Its main water sources are the Niger and Bani Rivers, which enter the study area at Ké-Macina and Sofara, respectively, flowing through the Delta over several hundred kilometers, before both exit at Diré (Fig. 4.1). The maximum inundation area shrinks to around 10,000 km^2 in dry years (Zwarts et al, 2005) under the combined impacts of climate variability, irrigation withdrawals, and dam operation. The IND faces many environmental challenges due to upstream water interventions on the river system, as well as high precipitation variability.

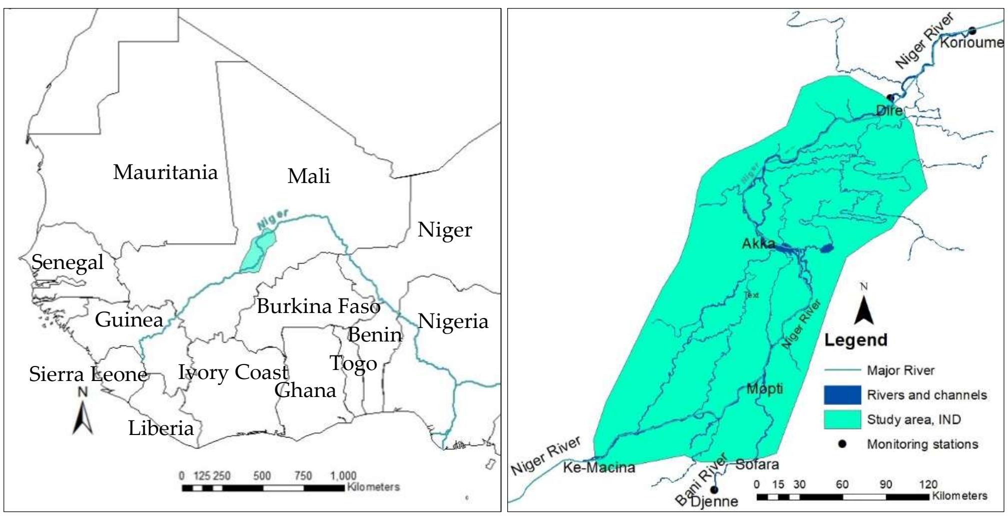

Fig. 4.1: Location map of the study area, the Inner Niger Delta, Mali, West Africa.

The IND is considered as a hub of human activities, including agriculture, fishing, transport, and tourism. The Delta plays an important role in promoting sustainable development for food security, water management, and the environment. Some upstream dams and irrigation structures are already in place, while more are at the planning stage. The infrastructures aim to increase economic development and food security. However, damming a river often implies a transfer of benefits from the downstream to the upstream regions. Thus, damming the main course or branches of the Niger River can impact on food security, ecology, and the environment as a whole by altering flow and inundation patterns. The operation of existing dams, such as Sélingué, Markala, and Talo has already modified flow patterns in the Delta, and planned dams, such as Fomi and Djenné, may exacerbate the changes. Fig. 4.2 shows the location of existing and planned dams/reservoirs upstream of IND. Zwarts and Frerotte (2012) have shown that on average, 9% of the total flood extent area has been lost due to the effects of the Selingue and Markala dams. Liersch et al. (2019) anticipated an average reduction of 24% flood extent compared to the natural condition due to the combined effect of existing and planned water infrastructures in the watershed. The situation may get worse due to increased evaporation as a result of global warming (CDKN, 2014). However, changes in precipitation are uncertain (USAID, undated) where some models project a wetter, and others a drier future in the Upper Niger basin (Liersch et al., 2019). A lower flow rate, in combination with a smaller flood plain, will most probably affect crop yields, fisheries, livestock, biodiversity, and environmental flow. To understand the possible impacts of these future changes on ecosystems and livelihoods, a realistic simulation of water levels, flow velocity, and inundations is required.

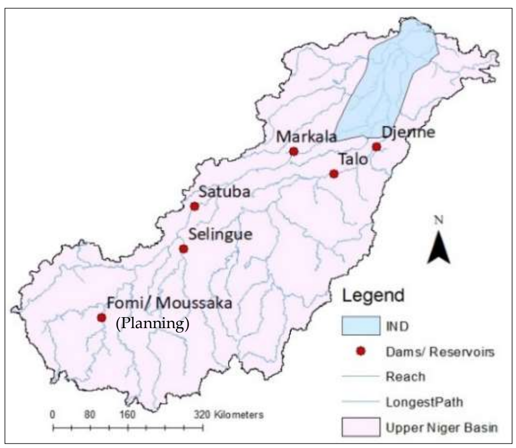

Fig. 4.2: Hydrodynamic model domain, along with dams and reservoirs in the Upper Niger basin.

Concerns about the hydrologic regime alterations in the watershed have triggered interest in ecosystem services and environmental health, especially in the IND area. The evaluation of ecosystem health requires the knowledge of relevant hydraulics parameters under altered flow scenarios. Such knowledge can only be achieved using hydrodynamic modeling. Unfortunately, previous attempts to develop a hydrodynamic model of the IND were only partially successful. For instance, Neal et al. (2012) applied LISFLOOD-FP (Bates and Rao, 2000), a raster-based sub-grid model, but model results were affected by the low-resolution (about 1 km) structured grid and simplified assumptions about the solution of the St. Venant equation. Dadson et al. (2010) applied a one-dimensional model with 25 km grids, and presented the inundation as a fraction of the cells which did not show the variability of inundation. Haag (2015) applied the D-Flow FM (Kemkamp et al, 2011, Deltares 2015), a shallow-water solver based on the finite-volume method on an unstructured grid to study the flood in the delta, and ended up having an imperfect simulation of water level, where inundation resulted from poor calibration efforts.

This study is an attempt to develop a working hydrodynamic model for the IND in support of ecosystems studies in the area. The modeling was done using TELEMAC 2D (Hervouet,2007), a finite-element computer program suite that solves shallow-water equations using the finite element method. Given the lack of accurate digital elevation models of the study area, two global digital elevation models were considered: the Shuttle Radar Topography Mission (SRTM) (NASA JPL, 2013), and the Multi-Error-Removed Improved-Terrain (MERIT DEM) (Yamazaki et al., 2017). However, the elevation accuracy of the DEMs makes their use in hydrodynamic modeling challenging. Rodriguez et al. (2006) reported an elevation error (standard deviation) of about 4.68 m of SRTM DEM in Africa. Yamazaki et al. (2017) reported a relative vertical height error of about 2 m of MERIT DEM for 58% of the land mapped by the DEM. A third DEM was therefore derived using the waterline method (Cracknell et al, 1987; Ramsay, 1995;Mason et al 1998).

Downstream boundary conditions were imposed by prescribing rating curves either in the form of discharge as a function of water level or water level as a function of discharge. Inflows in the domain were a combination of measurements and simulations using a Soil Water Assessment Tools (SWAT) hydrological model (Arnold et al. 1998) of the Upper Niger Basin. The combination of all available DEMs and downstream conditions led to a total of six models with different performances in simulating discharges, water levels, and inundation extents. Bayesian Model Averaging (BMA) (Hoeting et al, 1999) was used to combine the outputs of these six models to get improved results and identify the best individual models that could be used to simulate water levels and discharges with relatively high performance.

The paper is organized as follows: Section 1 contains the background and objective of the study; Section 2 presents the materials and methods, which includes available data, topographic data derivation, river network, bathymetric data, floodplain friction, adjustment of the elevation of SRTM and MERIT DEM, model setup, model calibration, and the theory of BMA; Section 3 deals with calibration results, BMA prediction, validation results, inundation extent, and performance of global DEMs; and finally, some concluding remarks complete the study.

4.2 Materials and Methods

4.2.1 Available Data

4.2.1.1 Discharge and Water Level

Water levels and discharge at Ké-Macina, Sofara, Mopti, Akka, and Diré, as well as a rating curve at Diré were obtained from the Malian hydrometric services (Direction Nationale de l'Hydraulique, DNH). Water level data have been referenced to Institut national de l'information's (IGN) datum. Water entered into the study area at KeMacina and Sofara through the Niger and Bani rivers, respectively. Mopti is located downstream of the confluence of the Bani and Niger rivers. Akka is situated almost at the middle of the study area, along the Niger River. Water drains the system at Dire station.

4.2.1.2 Topographic Data Sources

The SRTM DEM has been available at a resolution of one arc-second (about 30 m) since 2014. It is a widely used DEM: Biancamaria et al. (2009), Neal et al. (2012) and Schumann et al. (2014) used SRTM gridded data for hydraulic modeling of the Ob in western Siberia, the Scioto River in the eastern U.S., and the Niger River (Inner Niger Delta) in Mali, respectively. The SRTM elevation data used in this study were downloaded from https://earthexplorer.usgs.gov/.

The MERIT DEM is available at three arc-sec resolutions (about 90 m), and was derived from SRTM and AW3D-30 m (JAXA, 2018) by removing multiple error components, such as absolute bias, stripe noise, speckle noise, and tree height bias (Yamazaki et al., 2017). The MERIT DEM was used by Hawker et al. (2018) and Archer et al. (2018) for the flood modeling study of the Ba catchment, Fiji. The MERIT DEM was downloaded from http://hydro.iis.u-tokyo.ac.jp/~yamadai/MERIT_DEM/.

4.2.1.3 DEM Derivation Using the Waterline Method

An additional DEM was developed using the waterline method from the combined uses of the water extent map derived from Landsat satellite images by Zwart et al. (2005) and water level data collected on particular dates. The waterline method involves determining the horizontal position of the land–water boundary from a time series of remotely sensed images taken during different periods, and then superimposing on this boundary the heights relative to a datum.

The procedure is as follows:

- Seven inundation extent polygons derived from Landsat satellite images by Zwarts et al. (2005) for dates 5 July 1985, 10 June 2001, 8 August 1984, 28 July 2001, 25 October 1984, 16 October 2001, and 28 November 1999 were selected to represent the range of possible water elevations in the Inner Delta.
- For each of the seven flood inundation maps, water levels at Ké-Macina, Mopti, Akka, and Diré were used to calculate the slope of the water surface along principal flow paths between Ké-Macina and Akka, between Mopti and Akka, and between Akka and Diré. In the absence of additional information, it was further assumed that the water level variation between any two stations is linear.
- A series of orthogonal lines were drawn at 30 m intervals along principal flow paths.
- It was assumed that water levels along these lines are constant. Therefore, an elevation value could be set at the intersection points between water extent polygon and the orthogonal lines.
- At the end of the process, an altitude was estimated for each point within the flood extent polygons.
- Areas outside the larger polygon were populated using SRTM elevation data.
- GIS was used to interpolate (with Inverse Distance Weighting, IDW) the elevation data inside the study area.

The mean elevation of the Waterline DEM, SRTM, and MERIT DEM were 264.86 m, 267.06 m, and 266.77 m, respectively (Fig. 4.3).

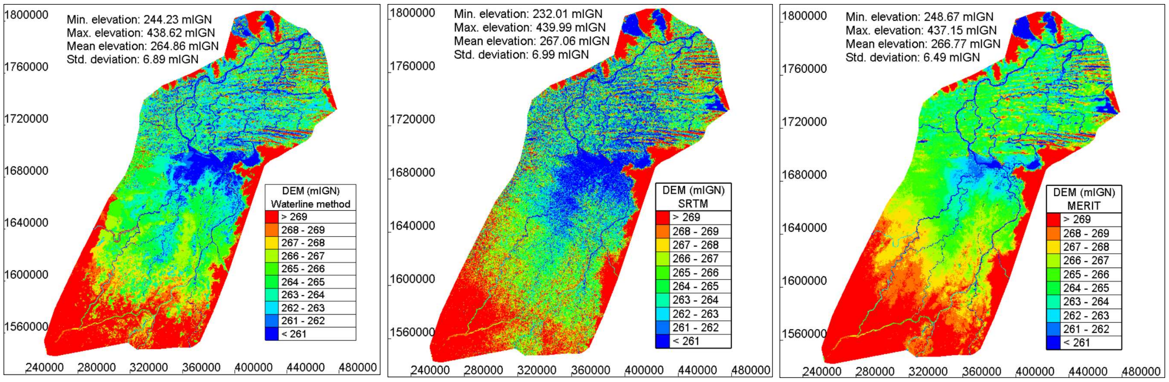

Fig. 4.3: Digital elevation model derived from the waterline method (left), Shuttle Radar Topography Mission (SRTM) (middle), and Multi-Error-Removed Improved-Terrain (MERIT DEM) (right).

Difference of DEM are calculated and presented in Fig. 4.4. MERIT exhibits lower elevation at the northern part (d/s) of the area than Waterline and SRTM. It also shows lower elevation at the most south-western and south-eastern part than compared to Waterline and SRTM respectively. The white color represents that the DEM represent same or small variations in the elevation (-0.5 to-0.5m).

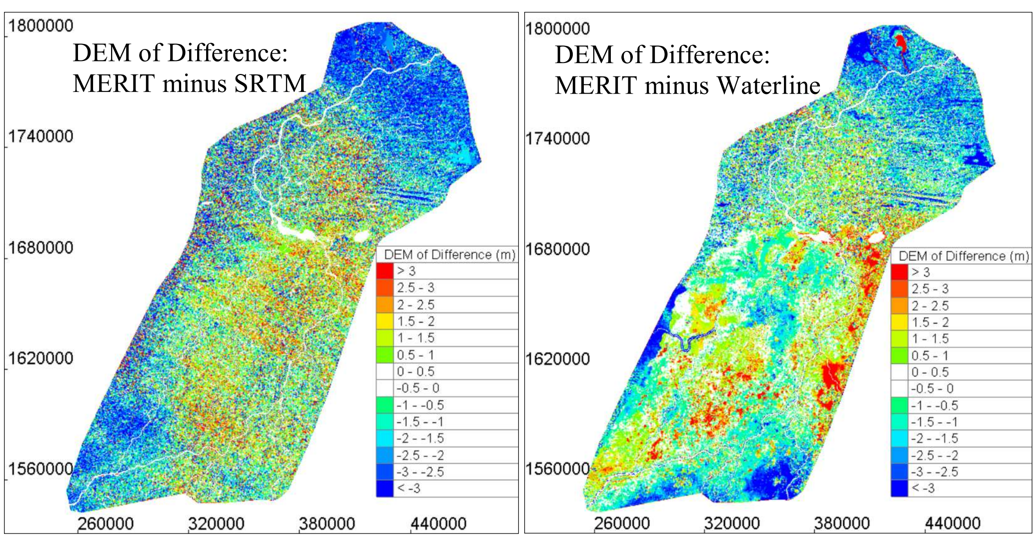

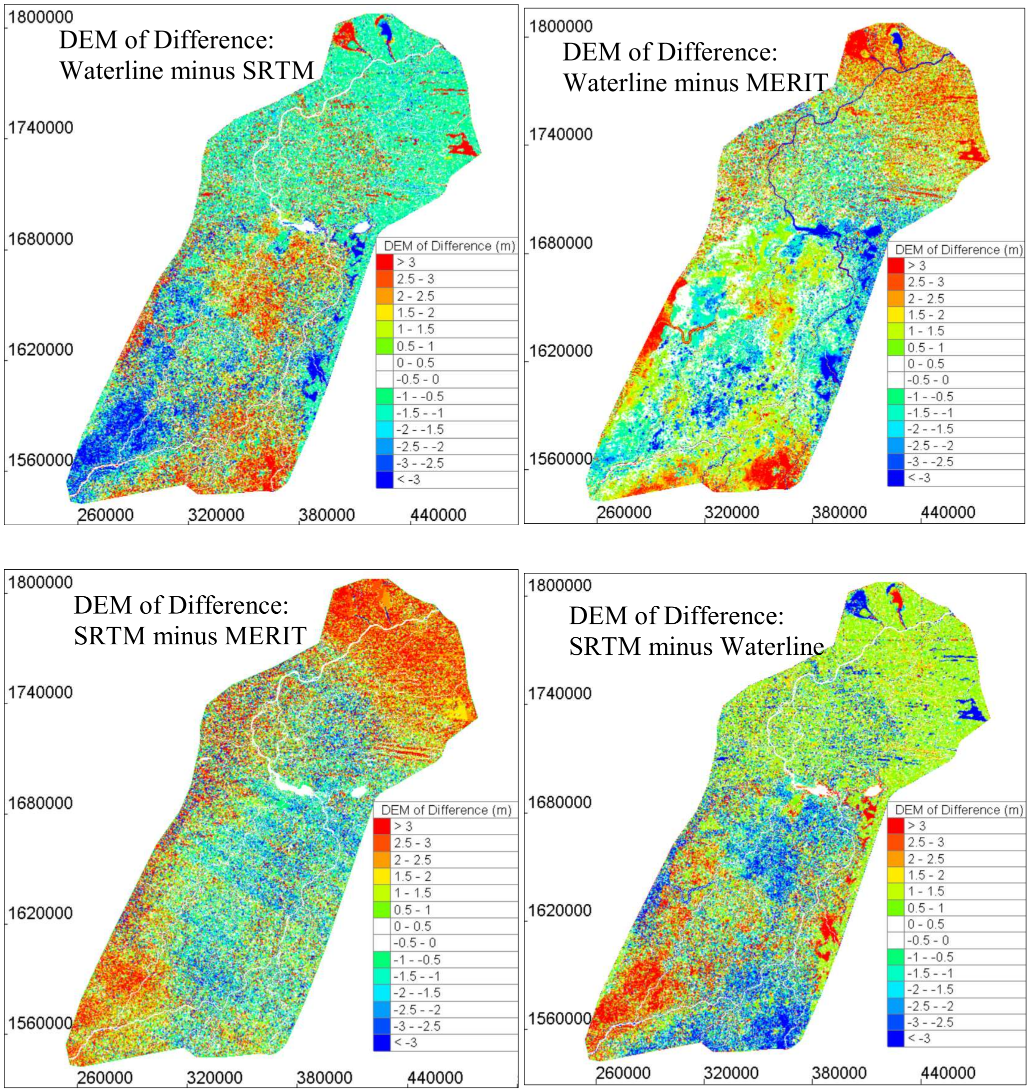

Fig. 4.4:: Difference of DEMs between MERIT, SRTM, and Waterline DEM's

4.2.1.4 Satellite Imagery

This study makes use of the water extent maps derived from Landsat images by Zwarts et al. (2005). Zwarts et al. (2005) processed Landsat 5 TM images captured on 24 different dates spanning from 1984 to 2003, and derived 24 water extent maps for the study area. The images provide evidence of the water extents of inundation areas, along with known water levels at Mopti, Akka, and Diré. The inundation extent obtained from the images on 28 July 2001 and 16 October 2001 are shown in Fig. 4.5.

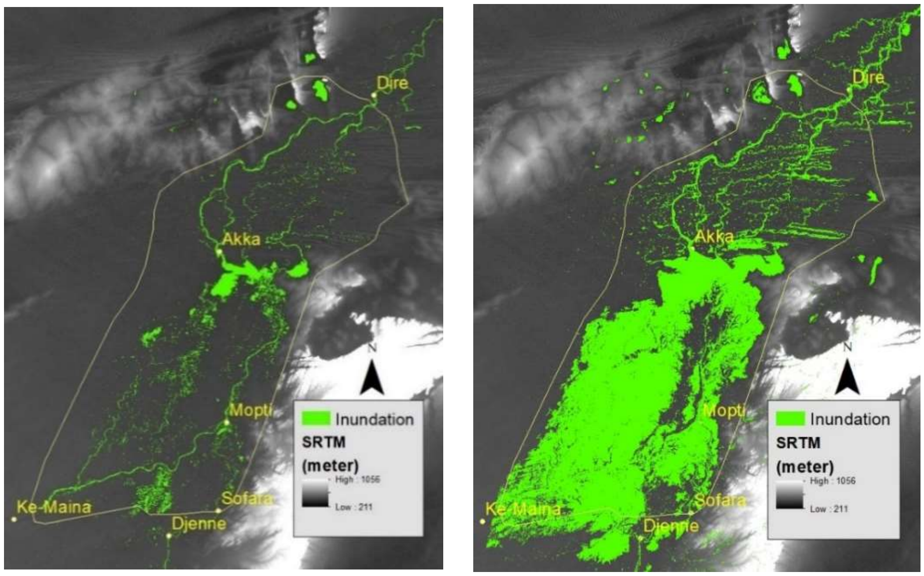

Fig. 4.5: Satellite Images of inundation extents of the Delta on 28 July 2001 (left) and 16 October 2001 (right) (Source: Zwarts, et al., 2005).

To validate the simulated inundation, a series of Moderate Resolution Imaging Spectroradiometer (MODIS) images were processed to derive the inundation extent. A summary of the satellite data usage is given in Table 4.1.

Table 4.1: Satellite images used in the study.

Image Source/Name	Satellite	Path/Row	Purpose	Date Captured	Resolution
Several images from Zwart et al. [0]	Landsat 5 TM	197/49 and 197/50	Model setup, Calibration	1984 to 2001	30 m
MOD09A1.A2008241 MOD09A1.A2008281 MOD09A1.A2009017	MODIS	-	Model validation	28 August 2008 7 October 2008 17 January 2009	500 m

We used two spectral indices to separate water pixels from non-water pixels. The indices are the Modified Normalized Difference Water Index (MNDWI) (Zu, 2006) and the Normalized Difference Moisture Index (NDMI) (Wilson and Sader, 2002).

MNDWI and NDMI indexes are expressed as follows:

$$\text{MNDWI} = \frac{\text{Green} - \text{MIR}}{\text{Green} + \text{MIR}} \tag{4.1}$$

$$\mathrm{NDMI} = \frac{\mathrm{NIR} - \mathrm{MIR}}{\mathrm{NIR} + \mathrm{MIR}} \tag{1.2}$$

For MODIS images, Green, NIR, and MIR represent reflectance from Band 4 (545 nm–565 nm), Band 2 (841 nm to 876 nm), and Band 6 (1628 nm to 1652 nm), respectively. The study makes use of the finding by Ogilvie et al. (2015) on the threshold value of NDMI and MNDWI. They analyzed MODIS images to study the spatial and temporal dynamics of floods across the Niger Inner Delta over the period of 2000–2011. Water was classified when the pixel had a threshold value of 0.15 for NDMI, and for the MNDWI, classifying pixels above the threshold of −0.34 was considered a flooded area.

4.2.2 River Network

The river network was derived from the inundation extent map derived from a Landsat image on 8 July 1985 by Zwarts et al. (2005). Only major rivers and channels were extracted. Small channels, especially at the northern part of the delta, could not be taken into consideration due to their haphazard geometry and complex meandering. Fig. 4.6 shows the delineated river network used in the model.

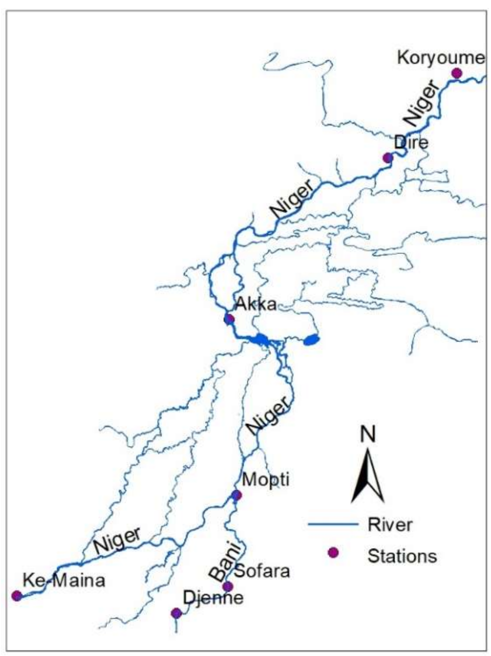

Fig. 4.6: River network for the model.

4.2.3 Channel Geometry

The bed elevation of river sections at Ké-Macina, Mopti, Akka, and Diré was approximated using hydraulic geometry equations proposed by Leopold and Maddock (1953). Hydraulic geometry relationships are a series of power laws that relate river width (w), depth (d), and velocity (v) to discharge. These functions are:

$$w = aQ^b \tag{4.3}$$

$$d = cQ^f \tag{4.4}$$

$$v = kQ^m \tag{4.5}$$

Here, a, c, and k are coefficients, and b, f, and m are exponents with $b + f + m = 1$, and

$$a * c * k = 1.$$

Empirical values of the hydraulic geometry coefficients and exponents derived by Hey and Thorne (1986) for Gravel-Bed Rivers in Britain were used in this study. Hey and Thorne (1986) found that a = 3.67, b = 0.45, c = 0.33, and f = 0.35 were a fair representation of hydraulic geometry. The same coefficients were used by Neal et al. (2012) in the IND.

Leopold (1994) suggested taking the bankfull discharge for the analysis, as it is related to channel morphology. The bankfull discharge is often assumed to be the discharge, with a return period of about 1.5 years. Table 4.2 shows the river bed elevation at KeMacina, Mopti, Akka, and Dire. Elevations of other points in between the sections were calculated assuming a linear variation along the longitudinal direction. It is to be noted here that the coefficients values proposed by Hey and Thorne (1986) were used only to get an approximation of the river bed. The bathymetry of tributary channels is approximated form the confluence of the channels and Niger river, as the elevation of that point is already known, by interpolating the elevation moving upstream along the length of the tributary. This derived set of bathymetry data is used for setup the model. The bathymetry data of the Niger River was adjusted during calibration and the data of the tributaries were changed accordingly.

Table 4.2: Bed elevation of the Niger River at Ke-Macina, Mopti, Akka, and Dire.

Monitoring Stations	Bankfull Discharge (m^3/s)	Bankfull Stage (mIGN)	Bankfull Depth (m)	Bed Elevation (mIGN)
KeMacina	3518.00	274.31	5.81	268.50
Mopti	2340.00	266.42	5.04	261.38
Akka	1816.00	262.81	4.61	258.20
Dire	1760.00	261.45	4.56	256.89

4.2.4 Estimation of Inflow at Ungauged Inlets

Observed streamflow time series were available only at two inlets of the hydrodynamic model domain, namely Ke-Macina and Sofara. Streamflow at the seven other inlets was generated by local precipitation that generate ephemeral streams which ultimately end up in the IND. These ungauged inflows were estimated using a SWAT model of the upper Niger and Bani Rivers basins developed in a previous project (Seidou, 2019). SWAT is a process-based and spatially semi-distributed hydrological model. In the SWAT model, the whole watershed is divided into multiple sub-basins, and each sub-basin is divided into several Hydrological Responsible Units (HRUs) that consist of unique homogeneous combinations of soil, land use, and topographic features in each sub-basin (Arnold et al, 2012). The hydrological cycle simulated by the SWAT model is based on the water balance equation (Neitsch et al. 2005):

$$SW_t = SW_0 + \sum_{i=1}^{i=0} \left(R_{day} - Q_{surf} - E_a - W_{perc} - Q_{gw} \right) \tag{4.6}$$

where SW_t, SW_0 are the final and initial soil water content (mm/d), respectively; t is the time (day); R_{day} is the precipitation(mm/d); Q_{surf} is the runoff (mm/d); E_a is the evapotranspiration (mm/d); W_{perc} is the percolation (mm/d); and Q_{gw} is the return flow (mm/d). The SWAT model implements multiple options for the description of hydrological processes, such as the Soil Conservation Service (SCS) curve number method (USDA, 1972) for runoff calculation and the Penman-Monteith (Monteith, 1965) method for the estimation of potential evapotranspiration. The details on SWAT modeling tools can be found from Arnold et al., (1988), Arnold et al. (2012), and Neitsch et al. (2005).

The SWAT model of the UNB contains 32 sub-watersheds (Fig. 4.7a). The model was calibrated and validated using streamflow from 14 hydrometric stations listed in Table 4.3, along with the calibration and validation performance. The performance criteria used in the calibration and validation process is NS. Sensitivity analysis was performed to select the parameters to use for calibration: CN2 (SCS runoff curve number for moisture condition II), RCHRG_DP (Deep aquifer percolation fraction), and RES_K (Hydraulic conductivity of the reservoir bottom, mm/hr) which were tuned during calibration. The Sequential Uncertainty Fitting program, SUFI-2 (Abbaspour, 2007) was used for calibration purposes. A detailed description of the model used in this study can be found in Seidou (2019) and Maiga (2019).

Table 4.3: Calibration and validation performance of the Soil Water Assessment Tools (SWAT) model.

Monitoring Station	**Latitude**	**Longitude**	**NS at Calibration**	**NS at Validation**
Kankan	10.38	−9.31	0.65	0.8
Baro	10.51	−9.72	0.68	0.73
Kouroussa	10.64	−9.88	0.68	0.78
Banankoro	11.68	−8.67	0.86	0.9
Sélingué	11.64	−8.24	0.45	0.64
Koulikoro	12.85	−7.56	0.87	0.93
Kirango	13.69	−6.08	0.86	0.82
Ké-Macina	13.95	−5.36	0.9	0.91
Bougouni	11.39	−7.45	0.77	0.78
Pankourou	11.44	−6.58	0.74	0.6
Douna	13.21	−5.9	0.79	0.9
Mopti	14.49	−4.21	0.8	0.78
Akka	15.4	−4.24	0.87	0.84
Diré	16.27	−3.39	0.9	0.75

The calibrated SWAT model was forced with observed climate data, and the discharge from surrounding watersheds was assumed to enter the area where the main channel crosses the boundary of the study area (red dots in Fig. 4.7b). Yellow dots in Fig. 4.7b indicates observed discharge stations. The formulas used to calculate inflows into the hydrodynamic model domain from the SWAT model outputs are provided in Table 4.4.

Table 4.4: Inflows into the hydrodynamic model domain from the SWAT model outputs.

Inlet Point Location	SWAT Model Subbasin(s)	Remarks
Inlet boundary 1 (Inlet B. 1)	Watershed 9	60% of the outflow of watershed 9
Inlet boundary 2 (Inlet B. 2)	Watershed 9	40% of the outflow of watershed 9
Inlet boundary 4 (Inlet B. 4)	Watershed 1	0.2126 * (Inflow of watershed 1-Outflow of watershed 1)
Inlet boundary 5 (Inlet B. 5)	Watershed 2	Outflow of watershed 2
Inlet boundary 6 (Inlet B. 6)	Watershed 1	0.125 * (Inflow of watershed 1-Outflow of watershed 1)
Inlet boundary 7 (Inlet B. 7)	Watershed 3	Outflow of watershed 3
Inlet boundary 8 (Inlet B. 8)	Watershed 6 and watershed 7	Outflow of watershed 6 + Outflow of watershed 7

* 0.2126 and 0.125 are the fractions of watershed 1 that lie outside the study area in each case.

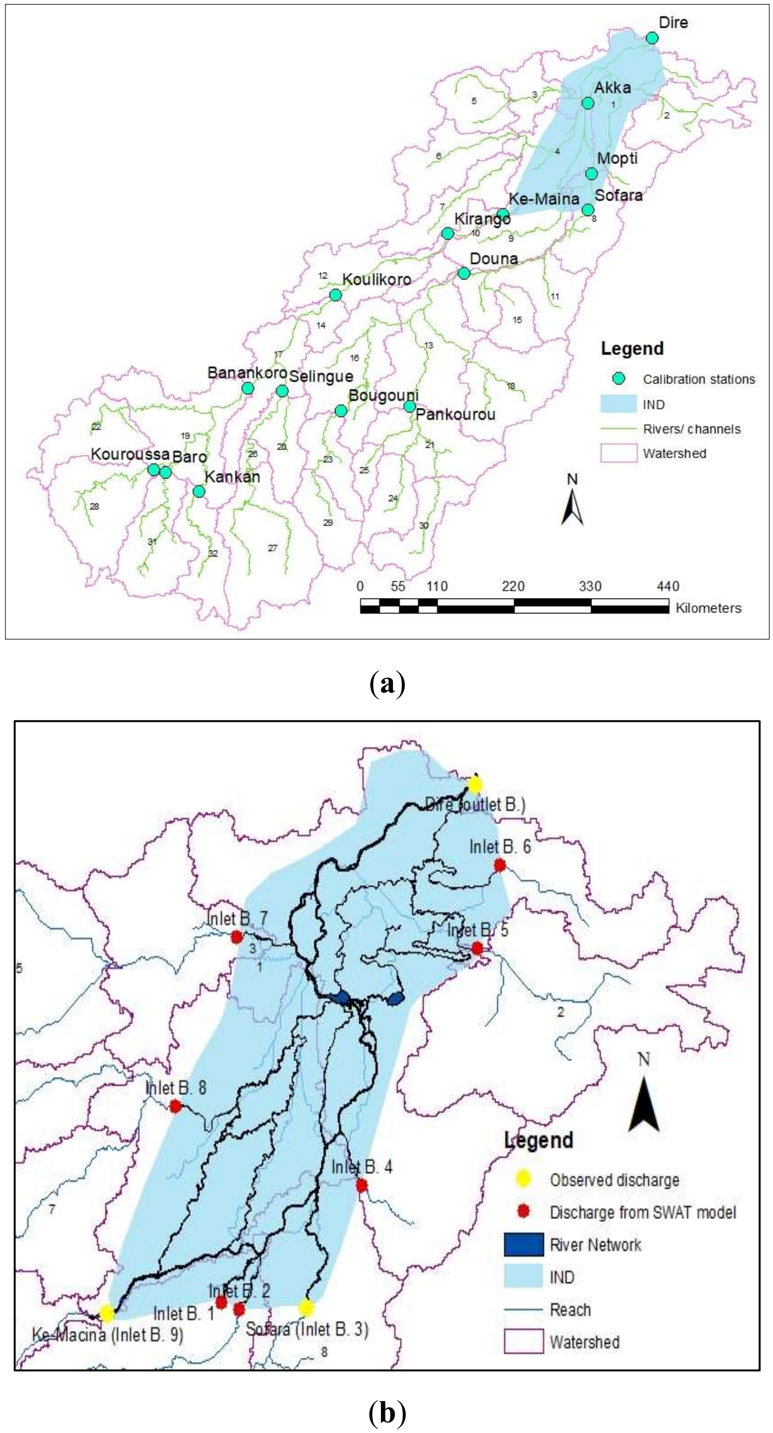

Fig. 4.7: (**a**) Extent of the SWAT model with calibration stations (Source: Seidou, 2019) and (**b**) locations of the liquid boundaries in the hydrodynamic model.

4.2.5 Floodplain Friction

The Manning roughness coefficient was derived from the USGS Global Land Cover Characterization (Loveland et al., 2000) database following Asante et al. (2008). Fig. 4.8 shows the distributed Manning's roughness coefficient at the IND.

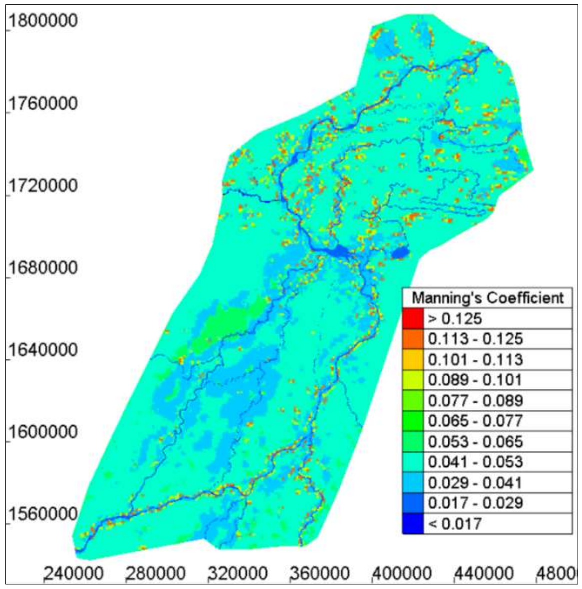

Fig. 4.8: Manning's coefficient at the floodplain of Inner Niger Delta (IND).

4.2.6 Hydrodynamic Model Setup

The hydrodynamic modeling was performed using TELEMAC 2D, a hydrodynamic model used worldwide. TELEMAC-2D solves the depth-integrated Shallow Water Equations (SWEs) using the finite element method on an irregular mesh.

In TELEMAC 2D, the SWE's are solved using a fractional step method (Marchuk, 1975), whose main principle is that the hyperbolic and parabolic parts of the SWE's should be treated separately. The solution comprises two steps: a solution of advection terms, and the solution of the propagation, diffusion, and source terms. Several schemes are available for the advection step, where the Method of Characteristics has been applied to solve the advection of u and v. The Streamline Upwind Petrov-Galerkin (SPUG) method (Brookes and Hughes, 1982) has been applied to solve the advection of h in the continuity equation. Variational formulations and space discretization transform the continuous equations into a linear triangular element, where the dependent variables u, v, and h are expanded using equal order interpolation functions. In the second step, the propagation, diffusion, and source terms are coupled through an implicit time scheme, and the resulting linear system is solved with a variant of the conjugate gradient method (Bates et al, 1997).

4.2.6.1 Mesh Generation

The entire domain was discretized using a system of irregular triangular elements. In the channel mesher, the rivers and channels were discretized separately, and in the combined mesher, the river and flood plain were joined together to form a combined mesh. The combined mesh has 220,289 nodes and 438,716 elements. The smallest length of the elements is about 50 m, and maximum length is about 844 m.

4.2.6.2 Model Boundary Conditions

The model has ten liquid boundaries. Nine of the liquid boundaries are inlets, while the last one is an outlet boundary. The location of liquid boundaries is shown in Fig. 4.7b. Time-varying discharges were used to prescribe flows at the inlet boundaries. Among the nine inlets, two are fed with the measurement, and seven comes from the output of a SWAT model. The downstream boundary is prescribed with two types of rating (stage-discharge) curves, where the Type (1) rating curve is in the form of water level as a function of discharge, and the Type (2) rating curve is in the form of discharge as a function of water level. We used a relaxation parameter to the Type 1 rating curve to possibly obtain a stable simulation of water level and discharge free from oscillation, as suggested by Hervouet (2017). Relaxation to the rating curve gives rise to the possibility of a smoothly varying boundary condition, which may otherwise trigger instabilities (Hervouet, 2017).

Rainfall was not included in the hydrodynamic model, because local rainfall has some effect on IND flood magnitude. The IND is in a semi-arid area, and most of the water flowing in it comes from a very humid region in Guinea, 600–900 km upstream. The headwaters' annual rainfall can go up to 1750 mm. However, in IND, average annual rainfall varies between 200 mm/yr at the downstream and 500 mm/yr at the upstream (Zwarts et al., 2005). We did account for precipitation and evaporation on the watershed through the SWAT model, but chose not to include precipitation directly on the water body. Zwarts (2010) found that local rainfall was too limited to influence the flood height in IND.

Evaporation was considered constant during the simulation. The authors acknowledge that constant evaporation has a lot of limitations, but the estimation of evaporation in the IND is an ongoing debate, with multiple papers published on the topic, and rather diverging estimates. Evaporation varies between 160 and 240 mm per month, with an average of 200 mm per month (Zwarts et al. 2005). Ogilvie et al. (2015) found evaporation rates were between 4 mm/day and 7 mm/day over the years 2008–2009.

Given the huge uncertainty in the estimated evaporation and the fact that our main purpose was flood wave propagation, we believe that the choice of constant evaporation had little impact on the results. The authors are considering the inclusion of dynamic precipitation and evaporation in the model that involves modifications of the TELEMAC 2D routines.

4.2.6.3 Initial Conditions

An introductory simulation was performed with prescribed constant discharges at each inlet, as well as a constant prescribed elevation at the outlet boundary to obtain the initial condition for subsequent runs. The simulation time step was set as 60 sec. It was selected in such a way so that it would not produce any instability on the simulation. It is to be noted that the courant number gives the impression of the stability of the model to perform the calculation. The Courant number of the simulation was kept below 4. Manning’s friction coefficient, as discussed in the previous section, was assigned to the nodes. The Manning coefficient at the floodplain was constant during simulation. However, the Manning’s coefficient at the river channel was considered variable, and tuned during calibration.

4.2.6.4 Model Configurations

Given that three elevation data sets were available and that there were two possibilities for downstream boundary conditions to be set (by prescribing a rating curve in one of the following forms: discharge as a function of water level—type 1 or water level as a function of discharge—

type 2), we obtained total of six different hydrodynamic models (Table 4.5). Prescribing Type 1 boundary conditions often leads to resonances or uncontrollable oscillations because of the feedback of the level on the local discharge. To address the issue, the developers of TELEMAC 2D estimated water levels at time t as a weighted average of the water level, corresponding to the discharge prescribed at time t and the water level corresponding to the discharge prescribed at time $t-1$. The weight of the water levels corresponding to the prescribed discharge at time t is called the relaxation coefficient (R). The developers of TELEMAC 2D recommend a value of R between 0.01 and 1.0 to smoothly prescribe discharges. In this paper, the value of R has been set to its default value of 0.02.

Table 4.5: Configuration of the six models.

Model Number	Elevation Data	Downstream Boundary Condition
Model 1	Merit DEM	Rating curve in the form of water level as a function of discharge, R = 0.02
Model 2	Merit DEM	Rating curve in the form of discharge as a function of water level
Model 3	SRTM DEM	Rating curve in the form of water level as a function of discharge, R = 0.02
Model 4	SRTM DEM	Rating curve in the form of discharge as a function of water level
Model 5	Waterline DEM	Rating curve in the form of water level as a function of discharge, R = 0.02
Model 6	Waterline DEM	Rating curve in the form of discharge as a function of water level

Ogilvie et al. (2015) found that the years 2001–2002 and 2008–2009 experienced relatively few clouds. Our study used these two periods as the calibration and validation period, respectively. MODIS and Landsat images during the months of September–February were considered for extracting water extent, as these months showed fewer clouds than the other months (Ogilvie et al., 2015). The periods between 1 July 2001 to 28 February 2002, and from 1 July 2008 to 28 February 2009 were thus chosen for calibration and validation, respectively.

4.2.7 Calibration

In flood modeling, the roughness coefficient is typically used as a calibration parameter (Woodhead et al. 2007). It is commonly recognized that friction varies in space, and that the precision of simulation can be improved through calibration and the use of effective friction coefficients (Aronica et al. 1998; Woodhead et al. 2007). The model was calibrated by changing the Manning coefficients in the reaches of the Niger river: KeMacina to Mopti (slope = 0.052 m/km), Mopti to Akka (slope = 0.029 m/km), and Akka to Dire (slope = 0.007 m/km). The Manning coefficient in the other reaches was assumed to be constant (0.02). As discussed before, the Manning coefficient of the floodplain was derived from GLCC. The calibration period of the model was chosen as July 2001–February 2002. The simulation results were evaluated by Pearson's correlation coefficient (r) and Nash-Sutcliffe coefficients (NS) at Akka and Mopti. Pearson's correlation coefficient (r) and Nash-Sutcliffe coefficients (NS) are described in the following equations:

$$r = \frac{\sum_{i=1}^{n}(x_i - \bar{x})(y_i - \bar{y})}{\sqrt{\sum_{i=1}^{n}(x_i - \bar{x})^2}\sqrt{\sum_{i=1}^{n}(y_i - \bar{y})^2}} \tag{4.7}$$

$$NS = 1 - \frac{\sum_{i=1}^{n}(x_i - y_i)^2}{\sqrt{\sum_{i=1}^{n}(y_i - \bar{y})^2}} \tag{4.8}$$

Here, x represents the simulated, and y the observed value of a variable. $\bar{x}$ and $\bar{y}$ are the averages of the simulated and observed values, respectively.

Models 1, 3, and 5 (Table 4.5) were calibrated for discharge and water level, and the calibration parameters were used for Models 2, 4, and 6, respectively.

After having a good calibration of the models against discharge and water level, we moved to further adjust the waterline DEM with respect to the inundated area. Adjustment was made on the elevation data to match the observed inundation area. Inundation extent maps by Zwarts et al. [0] on 28 July 2001, 25 October 1984, and 16 October 2001, which represent small, medium, and high flooded areas corresponding to 166 cm, 331 cm, and 432 cm water heights at Akka, respectively, were chosen for this purpose. The model was run for 1984–1985 with same parameter and Manning's coefficient. Underprediction, agreement, and overprediction areas were calculated by comparing simulated and observed inundation. Over- and under-predicted areas were those areas that were not supposed to submerge or dry in real cases. Simulated water depth at the overpredicted and underpredicted areas were extracted from the simulation result. The topography of the areas where inundation was overpredicted was adjusted by adding the water depth with the elevation at the grid points, and vice versa. This process continued until a good match was obtained between observed and simulated inundation.

4.2.8 Bayesian Model Averaging

Bayesian model averaging (BMA) is a statistical procedure used to infer a consensus prediction by weighing individual predictions based on their probabilistic likelihood measures. A BMA which assesses the performance of a model using its likelihood of predicting the observation is called the model's marginal likelihood, or Bayesian Model Evidence (BME) (Schöniger et al. 2014). The BME is often normalized and transformed into model weights. The better the model, the higher its evidence, hence its weight. A BMA's outcomes has more skill and reliability than the original ensemble members generated by competing models (Madigan et al. 1996; Raftery et al. 2005). Several authors (Duan et al. 2007; Zhu et al. 2013) applied BMA to combine hydrological simulations. For instance, Zhu et al. (2013) applied BMA for flood prediction and uncertainty estimation of flood event predictions. Beckers et al. (2008) applied BMA to a set of water-level forecast models used in the Flood Forecasting and Warning System for Rhine and Meuse rivers.

In this study, we applied BMA to the predicted water level and discharge by the six models developed in this paper, with the expectation that these models' outputs will be combined into a robust prediction. BMA was applied at each location (Akka and Mopti) and for each variable. Therefore, the combined model would be different according to the location and variable of interest. A brief description of the methodology is given below, as per Hoeting et al. (1999)

If Δ is the quantity of interest, then its posterior distribution, given data D, is

$$\mathrm{pr}(\Delta|D) = \sum_{k=1}^{K} \mathrm{pr}(\Delta|M_k, D)\mathrm{pr}(M_k|D) \tag{4.9}$$

This is an average of the posterior distributions under each of the models considered, weighted by their posterior model probability. In Equation (4.9), $M_1, \ldots \ldots \ldots, M_k$ are the models considered. The posterior probability for model M_k is given by:

$$\mathrm{pr}(M_k|D) = \frac{\mathrm{pr}(D|M_k)\mathrm{pr}(M_k)}{\sum_{l=1}^{K} \mathrm{pr}(D|M_l)\,\mathrm{pr}(M_l)} \tag{4.10}$$

where

$$\mathrm{pr}(D|M_k) = \int \mathrm{pr}(\,(D|\theta_k, M_k)\mathrm{Pr}((\theta_k|M_k)d\theta_k \tag{4.11}$$

$\mathrm{pr}(D|M_k)$ is the integrated likelihood of model M_k, θ_k is the vector of parameters of model M_k (e.g., for regression $\theta = (\beta, \sigma^2)$), $\mathrm{Pr}(\theta_k|M_k)$ is the prior density of θ_k under model M_k, $\mathrm{pr}(D|\theta_k, M_k)$ is the likelihood, and $\mathrm{pr}(M_k)$ is the prior probability that M_k is the true model. $\mathrm{pr}(M_k|D)$ is also known as the BMA weight w_k, and the sum of w_k is equal to 1, that is, $\sum_{k=1}^{K} w_k = 1$.

The Bayesian Model Evidence (BME) is defined as:

$$BME_k = \mathrm{pr}(D|M_k)\mathrm{pr}(M_k) \tag{4.12}$$

The posterior mean and variance of Δ are calculated as follows:

Mean:

$$E[\Delta|D] = \sum_{k=0}^{K} \hat{\Delta}_k \mathrm{pr}(M_k|D) \tag{4.13}$$

Variance:

$$Var[\Delta|D] = \sum_{k=0}^{K}\left(Var[\Delta|D, M_k] + \hat{\Delta}^2{}_k\right) \mathrm{pr}(M_k|D) - E[\Delta|D]^2 \tag{4.14}$$

Where (Raftery, 1993; Draper, 1995)

$$\hat{\Delta}_k = E[\Delta|D, M_k]. \tag{4.15}$$

The successful implementation of the BMA requires estimates of the weights, w_k and standard deviationsof the conditional probability density function (pdfs) of the ensemble members. Their values can be estimated through the maximum likelihood method (Raftery et al. 2005).

Let

$$\theta = \{w_k, \sigma_k, k = 1, \ldots K\}. \tag{4.16}$$

The logarithmic likelihood function can be approximated as follows:

$$l(\theta) = \sum_{t=1}^{T} log\left(\sum_{k=1}^{K} w_k \ \mathrm{pr}_k(\Delta|M_k, D)\right) \tag{4.17}$$

Equation (4.17) cannot be solved analytically for θ. The BMA weights can be calculated by two approaches, such as the Markov Chain Monte Carlo (MCMC) (Vrugt et al. 2008) algorithm and Expectation-Maximization (EM) (McLachlan and Krishnan, 1997) algorithm. We applied the EM algorithm, as recommended by Raftery et al. (2005), to get the optimum value of θ.

4.3 Results and Discussion

4.3.1 Calibration Results

The calibration performance of all models is shown in Table 4.6.

Table 4.6: Correlation (r) and Nash-Sutcliffe (NS) coefficients for simulated discharge and water level at the calibration.

Models	Discharge				Water Level			
	Mopti		Akka		Mopti		Akka	
	NS	r	NS	R	NS	r	NS	r
Model 1	0.975	0.996	0.879	0.944	0.984	0.992	0.946	0.988
Model 2	0.975	0.995	0.863	0.983	0.984	0.999	0.941	0.992
Model 3	0.954	0.995	0.908	0.983	0.951	0.999	0.907	0.992
Model 4	0.954	0.995	0.871	0.974	0.954	0.999	0.915	0.986
Model 5	0.956	0.994	0.958	0.986	0.981	0.997	0.871	0.998
Model 6	0.956	0.994	0.945	0.983	0.981	0.997	0.838	0.994

The results in

Table 4.6 show that the downstream boundary condition affects model performance. Although the NS of discharge and water level at Mopti has no variation, the model performance varies in Akka in the simulating discharge and water level. Models 1, 3, and 5 generally performed better than Models 2, 4, and 6 in terms of NS. Results suggest that prescribing the downstream boundary condition, ‘water levels as a function of discharge (Type 1)’, leads to better simulations than prescribing the boundary, ‘discharge as a function of water level (Type 2)’. The authors speculate that providing a Type 1 boundary condition leads to better results. The reason seems to the use of the relaxation coefficient (R), as described in Section 2.6.4, which smooths out the solution, but introduces some errors in the algorithm.

Models have been ranked in order of decreasing performance when simulating discharge (resp. water levels) in Table 4.7 (resp. Table 4.8). While models built on MERIT DEM generally performed well, the order of the models can change according to the boundary condition, the location (Akka or Mopti), the performance measure (r or NS), and finally, the variable under investigation. The results are in line with the findings of Pappenberger et al. (2006) that the boundary condition is a source of uncertainty.

Table 4.7: Model ranking based on performance (NS and r) for discharge at Mopti and Akka.

Hydrometric Station	MOPTI				AKKA			
Variable	**Discharge**				**Discharge**			
d/s Boundary Condition	**Type 1 [a]**	**Type 1**	**Type 2 [b]**	**Type 2**	**Type 1**	**Type 1**	**Type 2**	**Type 2**
Performance Criteria	**NS**	**r**	**NS**	**r**	**NS**	**r**	**NS**	**r**
Best models/associated DEM	MERIT [d] (M1 [c])	MERIT (M1)	MERIT (M2)	MERIT (M2) and SRTM(M4)	Waterline (M5)	Waterline (M5)	Waterline (M6)	Waterline (M6) and MERIT(M2)
Second model/corresponding DEM	Waterline (M5)	SRTM (M3)	Waterline (M6)	-	SRTM (M5)	SRTM (M3)	SRTM (M4)	-
Third model/Corresponding DEM	SRTM (M3)	Waterline (M5)	SRTM (4)	Waterline (M6)	MERIT (M1)	MERIT (M1)	MERIT (M2)	SRTM (M4)

[a] Type 1: d/s Boundary condition—water level as a function of discharge; [b] Type 2: d/s Boundary condition—discharge as a function of water level; [c] M1, M2…: Model 1 and Model 2 and so on; [d] MERIT DEM.

Table 4.8: Model ranking based on performance (NS and r) for water level at Mopti and Akka.

Hydrometric Station	MOPTI				AKKA			
Variable	**Water Level**				**Water Level**			
Boundary Condition	**Type 1 [a]**	**Type 1**	**Type 2 [b]**	**Type 2**	**Type 1**	**Type 1**	**Type 2**	**Type 2**
Performance Criteria	**NS**	**r**	**NS**	**r**	**NS**	**r**	**NS**	**r**
Best model/associated DEM	MERIT [d] (M1 [c])	SRTM (M3)	MERIT (M2)	MERIT (M2) and SRTM (M4)	MERIT (M1)	Waterline (M5)	MERIT (M2)	Waterline (M6)
Second model/correspondin g DEM	Waterline (M5)	Waterline (M5)	Waterline (M6)	Waterline (M6)	SRTM (M3)	SRTM (M3)	SRTM (M4)	MERIT (M2)

Third model/Corresponding DEM	SRTM (M3)	MERIT (M1)	SRTM (M4)		Waterline (M5)	MERIT (M1)	Waterline (M6)	SRTM (M4)

[a] Type 1: d/s Boundary condition—water level as a function of discharge; [b] Type 2: d/s Boundary condition—discharge as a function of water level; [c] M1, M2...: Model 1 and Model 2 and so on, [d] MERIT DEM.

4.3.1.1 BMA Weights

The BMA weights calculated in the calibration period (2001–2002) for each of the six models are given in Table 4.9.

Table 4.9: Bayesian Model Averaging (BMA) weights of the models.

Model	BMA Weight to Obtain Discharge		BMA Weight to Obtain Water Level	
	Mopti	**Akka**	**Mopti**	**Akka**
Model 1	0.0002	0.1177	0.3650	0.9602
Model 2	0.7931	0.0000	0.1820	0.0000
Model 3	0.1417	0.0000	0.0001	0.0000
Model 4	0.0000	0.0000	0.0000	0.0398
Model 5	0.0614	0.8823	0.3320	0.0000
Model 6	0.0017	0.0000	0.1200	0.0000

The fact that the best-performing model depends on several factors was an incentive to use Bayesian Model Averaging (BMA) at each location for each variable to get a location-specific combination of models exploiting the relative strength of the available models. For instance, the combined BMA simulation of discharge at Akka relies on Model 1 (weight = 0.1177) and Model 5 (0.8823), and almost completely ignores Models 2, 3, 4, and 6 (wight = 0.0000 each); the combined BMA simulation of water level at the same location relies more on Model 1 (weight = 0.9602) and Model 4 (0.0398) than on Models 2, 3, 5, and 6 (wight = 0.0000 each). BMA allows the end-user to have a robust estimate of key parameters by varying the weight according to location and variable of interest. If one location and one variable are more important for the end-user and resources are not available to run six models in parallel, the BMA weights will help them identify which model to maintain.

One of the assumptions in the BMA approach is that BMA weights should reflect relative model skill. BMA weights were highly correlated with model performance statistics (Duan et al. 2007). Model weights and BME are probabilistic model performance measures, and both are typically associated in the context of BMA (Guthke et al. 2017), as shown in Equation (4.12). On the other hand, NS, "r", daily root mean square error (DRMS), and daily absolute error (DABS) are used for deterministic model performance measurements. Previous authors (Duan et al. 2007; Zhu et al. 2013) used performance statistics such as Nash-Sutcliffe (NS), DRMS, or DABS to examine the consistency of the BMA predictions in terms of their weight. In this exercise, we compared model performance in term of NS and "r" with their BMA weight.

If we compare the highest NS values in Table 4.6 with the highest BMA weight in Table 4.9, we can see that the highest NS value corresponds to the highest BMA weight, though the "r" values give a mixed picture. The high correlation between NS statistics and BMA weight confirms one of the central assumptions of the BMA scheme, that better-performing models receive higher weights (Duan et al. 2012). BMA weights provide an additional means to assess the relative credibility of the six models. If we take NS statistics and BMA weight together, Model 1 was found to perform well in simulating water levels at Mopti and Akka, and Model 2 is better in simulating discharge at Mopti. Finally, Model 5 outperformed the others in simulating discharge at Akka. Thus, we considered Models 1, 2, and 5 to be the best three among the six models.

4.3.1.2 BMA Estimates of Water Levels and Discharge in the Calibration Period

The models were combined based on their respective weight values, as shown in Table 4.9. The maximum weights of the value of the individual model was found to contribute more to the resultant forecast. For instance, the BMA forecast of discharge at Mopti mainly comes from the combination of Model 2 and Model 3 with 79.31% and 14.17%, respectively, from their simulated discharge. A comparison of the discharge and water level from the best individual models, as well as the BMA prediction at the stations, are given in Fig. 4.9.

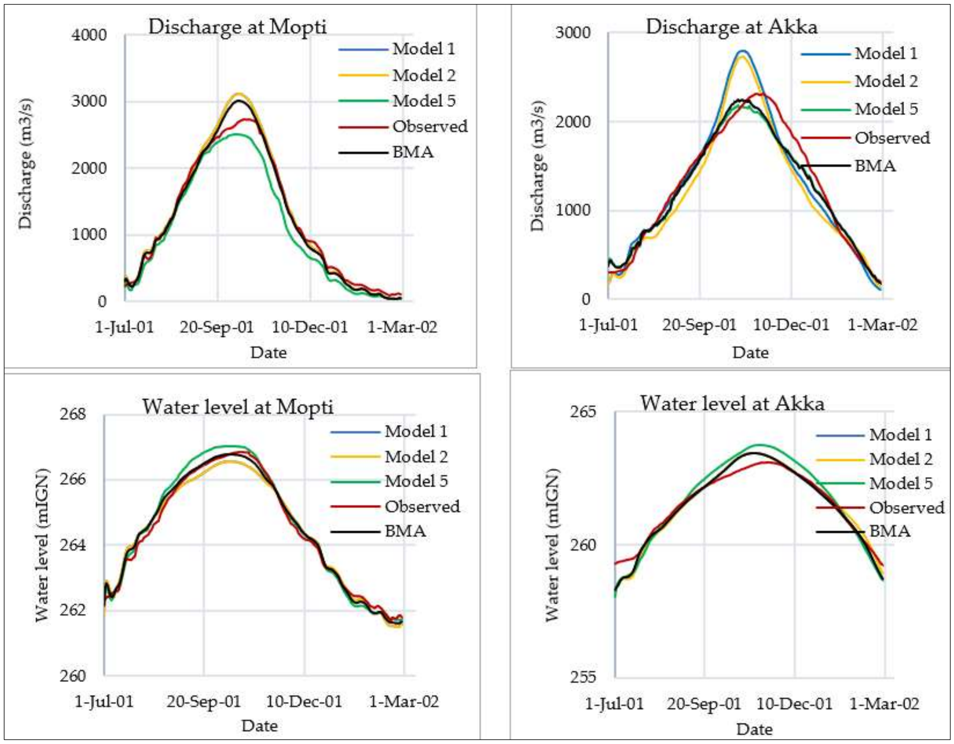

Fig. 4.9: Comparison of discharge (top) and water level (bottom) of the best models and BMA.

The BMA estimate of discharge and water level at the monitoring stations is shown in Fig. 4.9, where there seems to be a good match between observed values (red) and BMA predictions (black). The highest NS values (Fig. 4.10) confirms that BMA outperforms each best individual model.

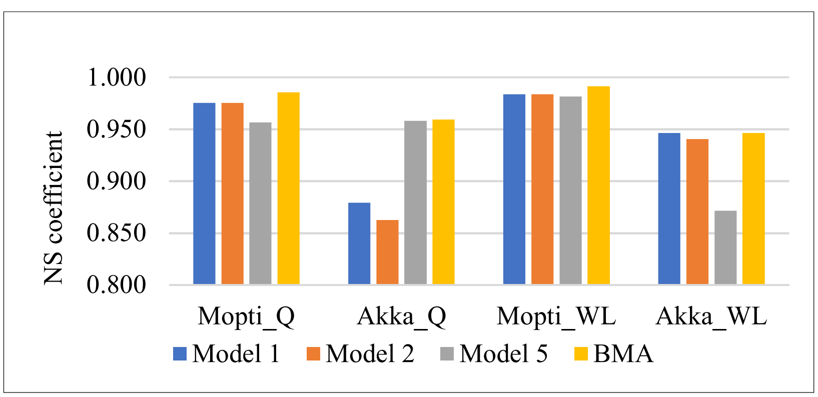

Fig. 4.10: Comparison of the Nash-Sutcliffe (NS) coefficient of BMA and the three best individual models.

4.3.2 Hydrodynamic Models Validation

The model results were validated using the 2008–2009 discharge, water levels, and water extent. Each of the models was run with inflows of 2008–2009 at the model inlets keeping the same parameters as obtained at the calibration. Table 4.10 summarizes the NS and "r" statistics of the model simulations.

Table 4.10: Correlation (r) and NS coefficients for simulated discharge and water level in the validation period.

Models	Discharge				Water Level			
	Mopti		Akka		Mopti		Akka	
	NS	r	NS	R	NS	r	NS	r
Model 1	0.982	0.995	0.836	0.918	0.962	0.984	0.940	0.992
Model 2	0.982	0.995	0.803	0.979	0.964	0.997	0.975	0.994
Model 3	0.939	0.995	0.830	0.979	0.933	0.997	0.917	0.994
Model 4	0.939	0.995	0.800	0.975	0.939	0.997	0.953	0.996
Model 5	0.935	0.990	0.882	0.976	0.973	0.993	0.876	0.988
Model 6	0.935	0.990	0.857	0.975	0.974	0.993	0.881	0.995
BMA	0.972	0.995	0.887	0.972	0.978	0.990	0.940	0.983

4.3.3 BMA Validation

The weights obtained from the calibration periods were used to compute BMA predictions for the validation period. The performance statistics, including NS and "r", were again employed to examine the consistency of the BMA predictions. A comparison of NS statistics between BMA and each of the models 1, 2, and 5 are shown in Fig. 4.11.

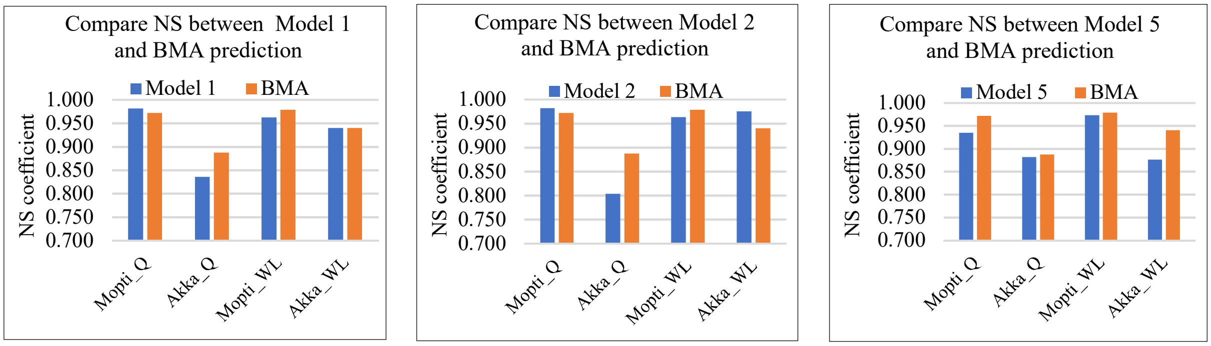

Fig. 4.11: Comparison of NS coefficient of BMA to each of Models 1,2, and 5.

Discharge and water levels simulated by Models 1, 2, and 5 have been compared to BMA estimates in Fig. 4.12. The figure shows a good match between observed values (red) and BMA predictions (black).

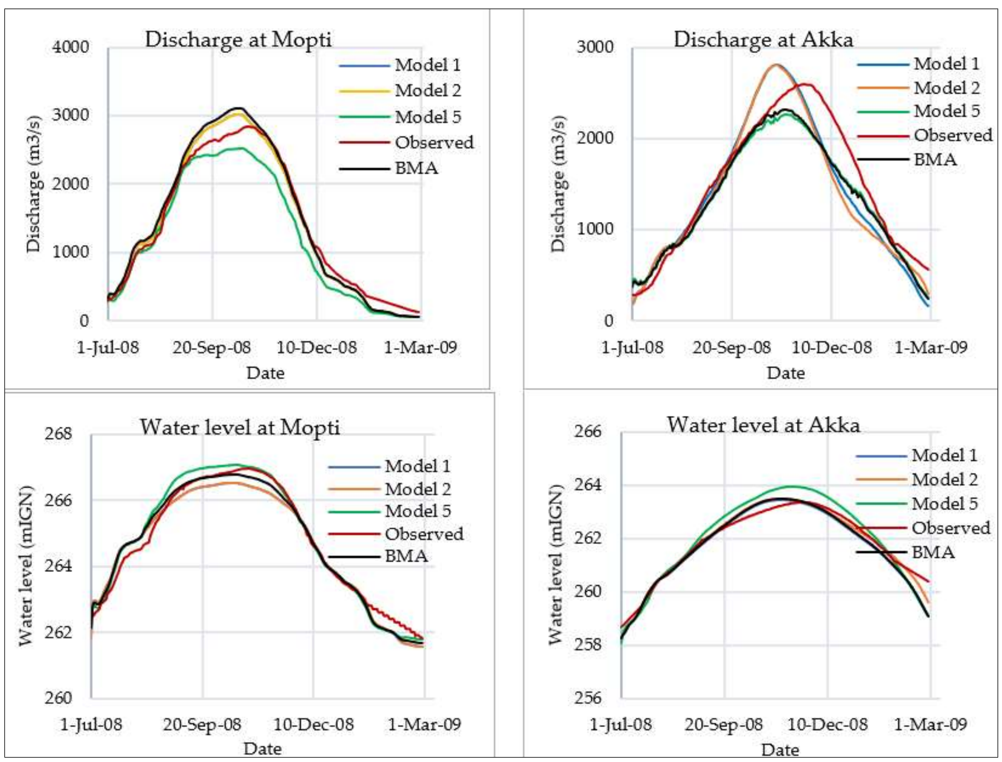

Fig. 4.12: Comparison of discharge (top) and water level (bottom) from the best individual models and BMA prediction at the validation.

It can be seen that the BMA predictions perform better than the best individual in most of the cases. Minor degradation of NS statistics also took place; for instance, BMA performance in the validation is slightly worse than that of Models 1 and 2 in predicting discharge at Mopti and the water level at Akka, respectively. Although there is some minor degradation in the performance when the BMA result is compared with the best individual models, BMA is generally superior to that of the individual models, which is consistent with previous studies (Duan et al. 2007; Vrugt and Robinson, 2007). The improvement due to BMA is relatively low when NS is close to 1, as there is then little room for improvement. When the NS is low, like in the simulation of discharge at Akka (Figures 9 and 10), the improved accuracy is much more obvious. The use of BMA for estimating both variables is, therefore, preferable to the use of individual model simulations. This feature of BMA is particularly interesting in data-scarce environments, such as Mali, where the only available information often comes from global sources with rather coarse resolutions.

4.3.4 Simulated Inundation Extent from Best Individual Models

This section provides a brief comparison between simulated and satellite-derived inundation extents for 2008–2009. Only the best individual models (Models 1, 2, and 5), as obtained from Section 4.3.1, are considered in the comparison. The reference inundation extents were derived from MODIS imagery for three days, representing the rising, peak, and recession limb of the 2008–2009 hydrograph. These images were taken on 28 August 2008, 7 October 2008, and 17 January 2009. The inundation extent simulated with Models 1, 2, and 5 along with the satellite-derived inundation extent is shown in Fig. 4.13. The simulated inundation in the central part of the study area, containing Lakes Walado, Debo, and Korientze, shows better agreement with the observed inundation for Model 5 for almost all the three days. The flood extent between KeMacina and Akka on 28 August was better simulated by Model 5 than Models 1 and 2. The inundation pattern simulated by Model 5 also closely matched with the observed inundation on 7 October.

It was also found that, while Model 5 performed well in reproducing the inundation extent of 28 August 2008 and 7 October 2008, it performed poorly in reproducing the inundation extent of 17 January 2009 (receding flood), especially in the area between Ke-Macina and Akka. The simulations show water in interconnecting channels that seem to be dry in the satellite images. This, however, has to be interpreted with care, as the coarse resolution of the MODIS images (500 m) does not allow the detection of narrow channels.

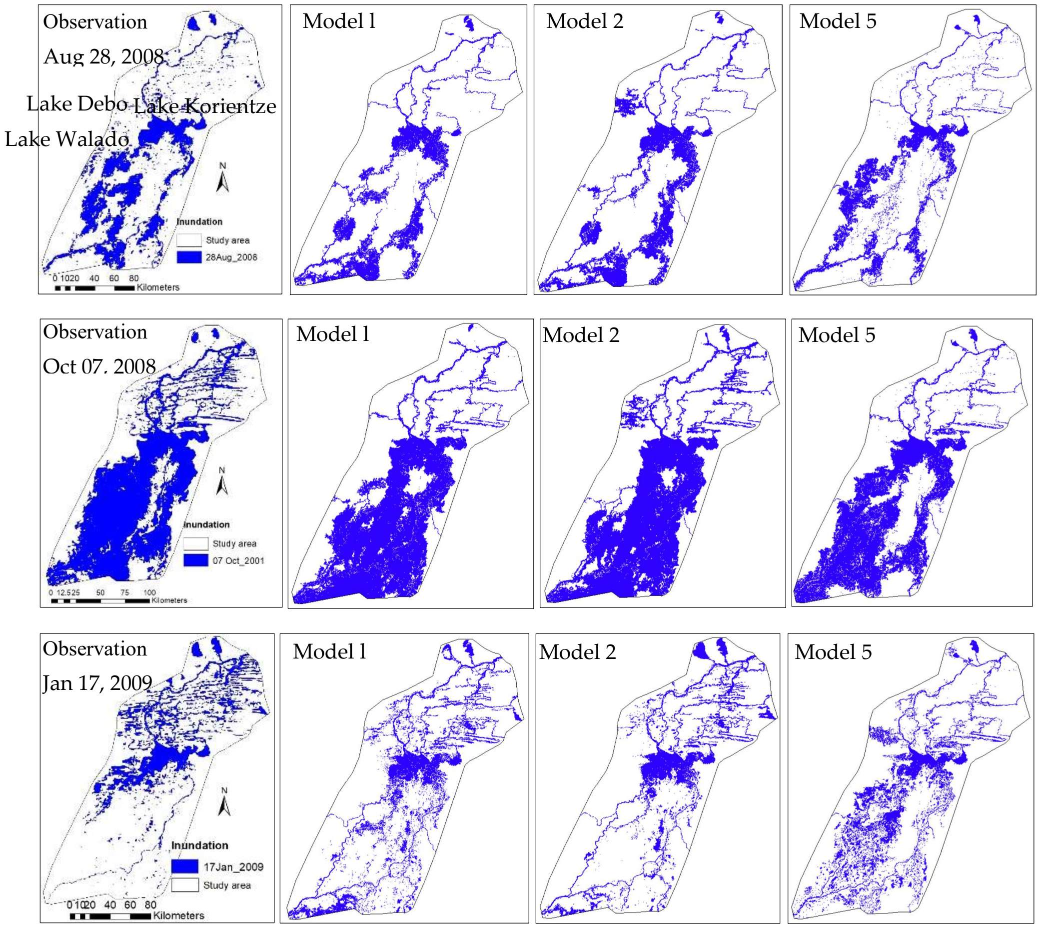

Fig. 4.13: Inundation extent on 28 August 2008 (left panel), 7 October 2008 (middle), and 17 January 2009 (right panel).

Based on the above facts, we can consider Model 5 to be the best in terms of simulating inundation. It is worth mentioning here that among the individual models, Model 5 was calibrated against inundation obtained from Landsat images captured in the 2001–2002 season. This probably makes this particular model the best among the participating models in simulating inundation extent.

Agreement, over prediction and under prediction area were calculated by comparing observed and simulated inundation extents and presented in Fig 4.13. It is seen that the agreement is better for Model 5 during rising flood because the inundation matches about 54% and 67% with the observed on August 28, 2008 and October 07, 2008 respectively. Nevertheless, the model (Model 5) slightly degrade in simulating the inundation extent on January 17, 2009 because it shows less agreement with respect to Model 1 and Model 2.

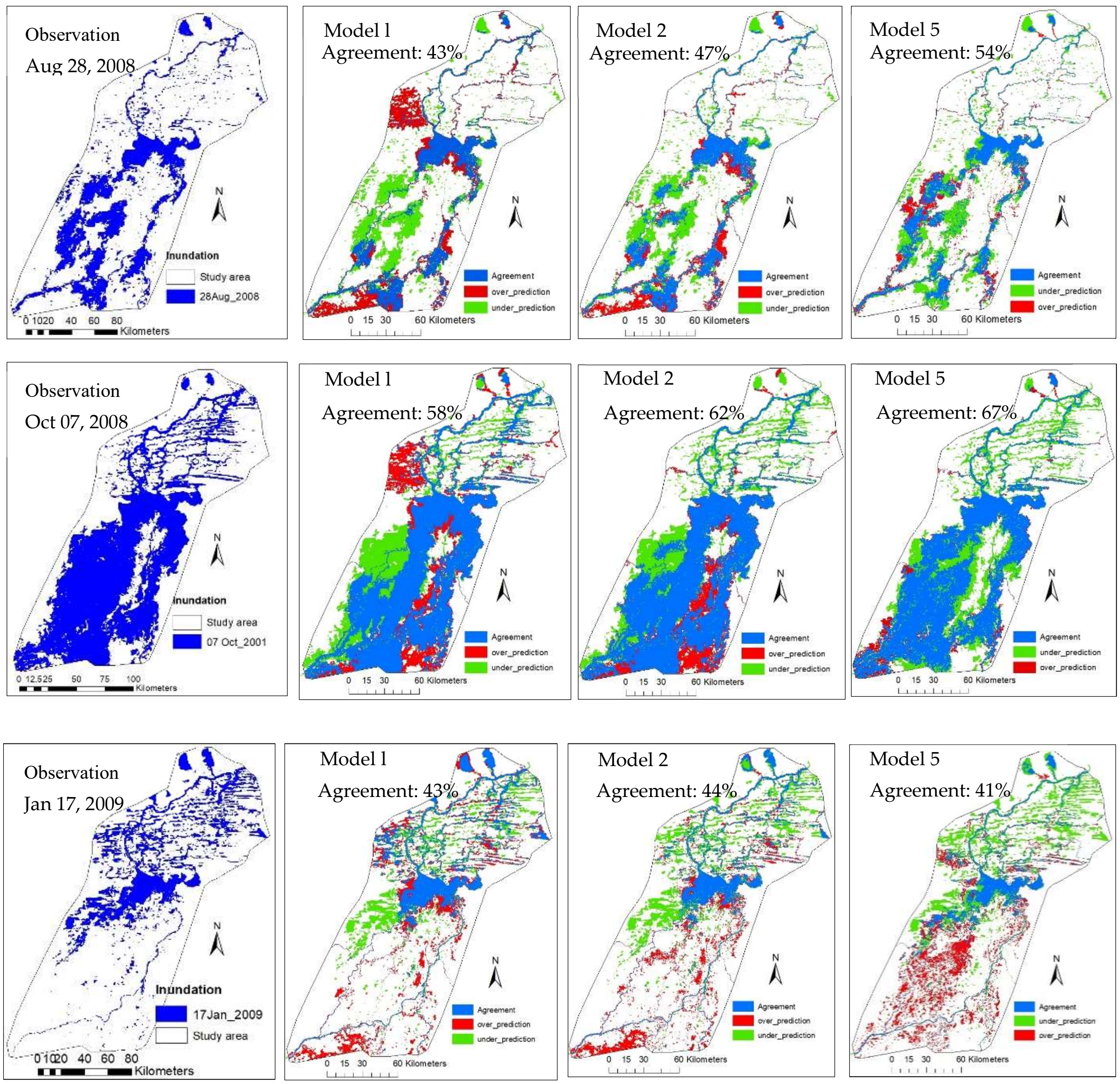

Fig. 4.14: Comparison of agreement, over prediction and under prediction areas

It is to be noted that the values of agreements found in this study are relatively low compared to previous studies where authors used high-resolution topography (e.g. Bates and De Roo, 2000; Horritt and Bates, 2001), who found an agreement of 81.9%. but the agreement percentage in this study is relatively high compared to the results from other data-sparse areas such as Amarnath et al. (2015) who found 38% and Sayama et al. (2012) who found 61% for agreement. It is noteworthy to mention here that the authors evaluated the agreement for the studies during the flood period. The agreement percentage found in this study is about 67% (on Oct 07, 2008) which, is quite high compared to the findings of the other authors in data scarce region. Visual inspection shows that the disagreements between the observed and simulated inundation extents are large in the northern part where the channels could not be represented properly with the current resolution of the DEM. Another source of discrepancy is the observed inundation map on January 17, 2009 that were derived from MODIS, which has a resolution 500m. The derived inundation map shows the existence of uncertainty in the image itself because it does not show the river and channels at the u/s part which were not dried at that time. The comparison with such a map, obviously, will lead to errors in the result. High-resolution satellite imagery such as Sentinel-2 and high-resolution mesh at the d/s part should improve the quality of the inundation map simulation.

4.3.5 Potential Usages of the Developed Model

The IND is a complex floodplain that is used by 1.5 million people, where there is little information about floodplain dynamics. Simple empirical equations are used to link water levels at key stations to inundation extents, and flood forecasting is done using linear regressions (OPIDIN, undated). A hydrodynamic model, even if not perfect, provides more insight into the flood dynamics, and will be more useful for decision making. The model developed here will be later used to replace or improve the empirical relationships currently used by local authorities, and to develop a process-based flood forecasting model.

4.4 Conclusions

In this study, six different hydrodynamic models of the Inner Niger Delta (IND) in Mali were developed using three different DEMs and two different downstream boundary conditions. The elevation data came from two global DEMS (SRTM and MERIT), as well as a DEM derived from satellite imagery and water level observations using waterline methods. Given the data scarcity in the area, a considerable amount of input data, such as bathymetry, the river network, friction coefficient, and inundation extent were derived from secondary sources, leading to a high level of uncertainty in the simulations. The six models which were developed showed unequal performances in simulating water levels, discharges, and floodplain extent, with none of them outperforming the others in all fronts. It was found that specifying the boundary condition (water levels as a function of discharge) led to better results. The reason for this seems to the use of the relaxation coefficient in the algorithm of the stage-discharge curve. Overall, the MERIT DEM was the best DEM among the ones considered in this paper, as it is a processed DEM by removing errors from SRTM. Bayesian Model Averaging (BMA) was used to produce a more robust estimate of water levels and discharges. BMA also helped to identify which individual models had the highest value for an end-user who is more interested in a particular location in the IND and a particular hydraulic variable.

Chapter 5

Effect of rating curve hysteresis on flood extent simulation with a 2D hydrodynamic model: a case study of the Inner Niger Delta, Mali, West Africa[2]

Abstract: The Inner Niger Delta (IND) is a complex hydraulic system where the flood dynamics and connectivity between water bodies is the main driver for ecosystem services and economic activities. Therefore, it is of pivotal importance that hydraulic models used to assess ecosystem services and socio-economic usages in the IND are capable of capturing both the inundation and connectivity dynamics. A particularity of the IND is that a strong hysteresis effect can be observed in the stage-discharge relationships at all hydrometric stations in the area. However, existing hydrodynamic models of the IND typically use a static stage-discharge relationship as the downstream boundary condition during both the rise and recession of the flood, which leads to potential inaccuracies when trying to predict the flood extent. This paper explores how the simulation results of the flood and connectivity dynamics in the IND can be improved by using a looped rating curve at the downstream model boundary. Two different methods are explored to integrate the hysteresis into the rating curve: one is based on dimensionless discharges and water levels (DLRC) while the second is based on the modified Jones formula. The results show that while the hysteresis effect is better represented using the DLRC approach, either approach was capable to improve the accuracy of predicting floodplain extent and connectivity dynamics between the Niger river system and an important lake in the IND. The improvement in water level predictions decreased steadily with the distance from the downstream boundary of the modelled area.

Keywords Inner Niger Delta, floodplain inundation, hydrodynamic model, hysteresis

[2] Haque, M. M., Seidou, O., Mohammadian, A. (2019) Effect of rating curve hysteresis on flood extent simulation with a 2D hydrodynamic model: a case study of the Inner Niger Delta, Mali, West Africa. *Journal of African Earth Sciences* (Revised)

5.1 Introduction

Floodplains play a vital role in preserving biodiversity and providing environmental services to human populations (Di Baldassarre, 2012). The Inner Niger Delta (IND), Mali, West Africa (Fig. 5.1), is one of the biggest floodplains in the world and represents a vast natural resource that continues to attract many people to live in and around the delta (Liersch et al. 2012, Zwarts et al. 2005). The IND is considered a hub of human activities that include agriculture, fishing, transport, and tourism.

The IND receives flow mainly from the Niger and Bani rivers at KeMacina and Sofara, respectively. The delta extends for several hundred kilometers before terminating at Dire. When water level is increasing during the rising stage of water, the main rivers and important lakes such as Lake Fati and Lake Horo become interconnected and turn into important habitats for fish and birds, while providing a feeding ground for local cattle. During the dry seasons, the channels connecting the lakes and rivers fall dry. In our study we focus on Lake Fati (Fig. 5.1), situated in the northernmost (downstream) part of the study area, to examine the seasonal connection and disconnection dynamics between the local water bodies.

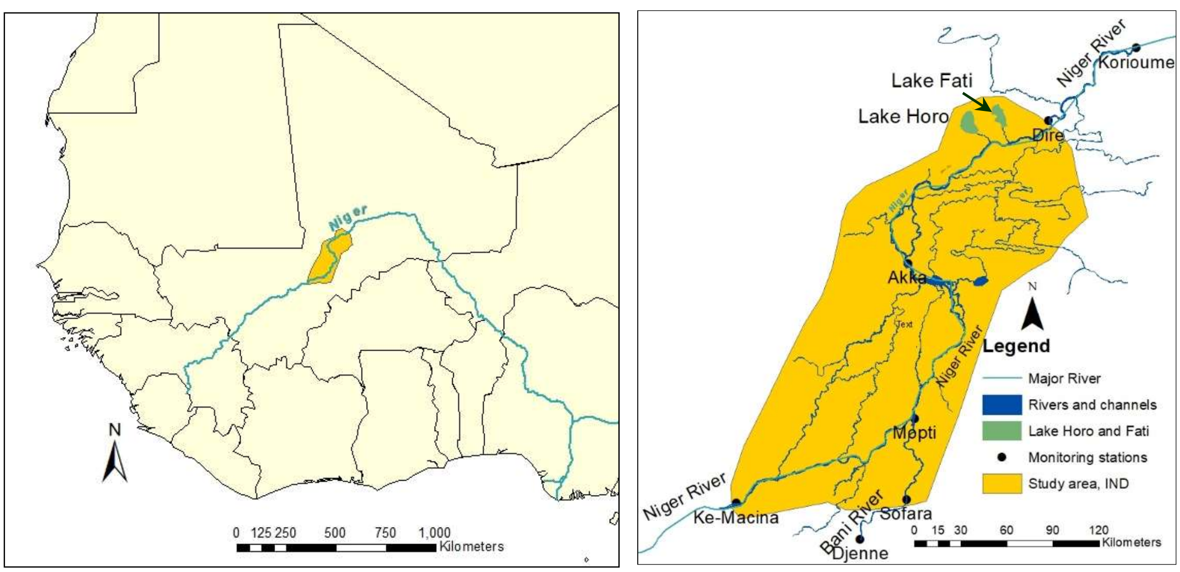

Fig. 5.1: Location map of the Inner Niger Delta, Mali, West Africa.

The IND plays an important role in promoting its sustainable development for food security, water management, and the environment. Given the economic importance of the inundation areas, there have been several studies examining the dynamics of the flooded areas. The techniques used include the generation of time series of inundation maps using satellite imagery (Zwarts et al., 2005; Mariko, 2003; Ogilvie et al., 2015), the development of empirical functions that linked the water level at key stations to the inundation extent (Zwarts et al, 2005; Mariko,2003; 2015; Mahe et al., 2011), and numerical simulations using hydrodynamic models (Neal et al., 2012; Haque et al. 2019). Other studies focused on the flood modeling of the IND (Haque et al., 2019; Neal et al., 2012; Dadson et al., 2010; Haag, 2015).

A special feature of the IND is that a strong hysteresis effect can be observed in the stage-discharge relationships at all hydrometric stations in the area. Horritt (2000) found that the hysteresis phenomenon may influence the accuracy of the simulations near the downstream boundary. He also mentioned that the impact of the downstream boundary condition for dynamic circumstances may extend further upstream.

Rating curves estimated on the basis of a single-valued rating curve assumption become inaccurate if the stage-discharge relationship is significantly affected by unsteadiness (Petersen-Øverleir, 2006). If the flow is characterised by hysteretic phenomena i.e. a given stage value corresponds to two discharge values, simulation should be done with this condition. This phenomenon is also referred to as unsteadiness or looping in the rating curve. Unsteadiness arises due to irregular cross section, presence of water infrastructures such as bridges, dams, hydroelectric plant in the stream channels, changing channel, backwater effect, unsteadiness of the river flow, variable channel storage, aquatic vegetation, and freezing and breaking of ice. Their presence could create backwater effects affecting water stage at the gauge (Wu and Yang, 2008, Boyer,1964). The flood wave passes through several channels and overflows huge floodplain until it reaches at downstream. The flow in the IND become unstable and looped once it enters into the area. It is found that stage discharge curve at IND is characterised by unsteadiness.

However, no previous study at IND considered the hysteresis effect that can be observed at the downstream boundary of the study area (Fig. 5.2). While Haque et al. (2019) considered a non-looped (single) rating curve at Diré station (the downstream boundary of the study area) *in situ* observations at Diré hydrometric station show a clear hysteresis (Fig. 5.2).

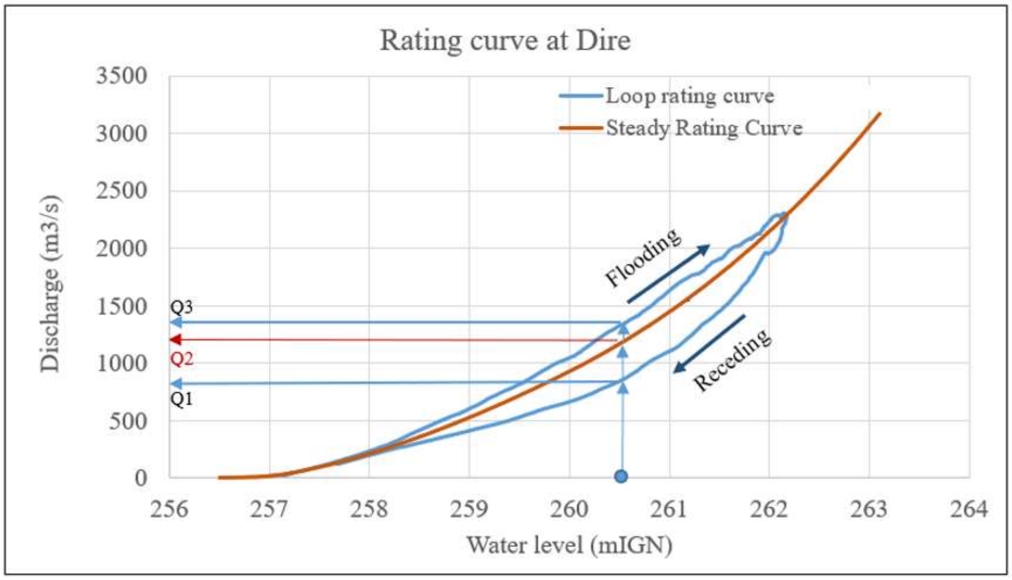

Fig. 5.2: The looped rating curve observed *in situ* at Diré station from 2001-2002 versus the non-looped (single/ steady) rating curve used in the model by Haque et al. (2019).

In this paper, we examine whether the use of a looped instead of a steady or single rating curve boundary condition leads to significant improvements in the modelled predictions of flow, water level, connectivity, and inundation extent in the IND. For this purpose, we adapt the hydrodynamic model developed in Haque et al. (2019) to include a hysteresis at the downstream boundary and compare the results from the single and looped rating curve boundary conditions to *in situ* observations.

This paper is organized as follows: Section 2 presents the materials and methods used and introduces the study area; Section 3 presents and discusses the results of the hydrodynamic simulation using the looped and non- looped rating curve. Some concluding remarks complete the study.

5.2 Materials and Methods

5.2.1 Hydrological Data

Observed water level and discharge data for the period 1980 - 2016 were obtained from the Mali Hydrometric Service (Direction Nationale de l'Hydraulique, DNH) at Mopti, Akka, and Diré hydrometric stations. In addition, the study uses Landsat 5 images from between 1984 and 2002 (Zwarts et al. 2005).

5.2.2 Hydrodynamic model of the IND

The hydrodynamic model used in this paper was developed by Haque et al. (2019) and is based on the TELEMAC 2D hydrodynamic model (Hervouet, 2007). TELEMAC-2D solves the depth-integrated shallow water equations (SWEs) using the finite-element method on an irregular grid.

5.2.3 Elevation data

In this paper, we use the digital elevation data from Haque et al. (2019) who derived the data using the waterline method (Cracknell et al. 1987; Ramsey, 1995; Mason et al. 1998). The depth of the river bed at Ké-Macina, Mopti, Akka, and Diré was approximated using the hydraulic geometry equations proposed by Leopold and Maddock (1953), while the bathymetry of the other points along the river was estimated assuming a linear variation of the water slope between stations. In this study, we use the same Manning coefficients for the river and floodplain and also the same general setup, elevation, bathymetry and friction data as in Haque et al. (2019).

5.2.4 Domain discretization

The model domain was discretized using a system of irregular triangles yielding a mesh consisting of 220,289 nodes and 438,716 elements. The smallest and largest distances between nodes are about 50 m and 844 m, respectively. More details on the model can be found in Haque et al. (2019). The model liquid boundaries consist of nine inlets and one outlet (Fig. 5.3).

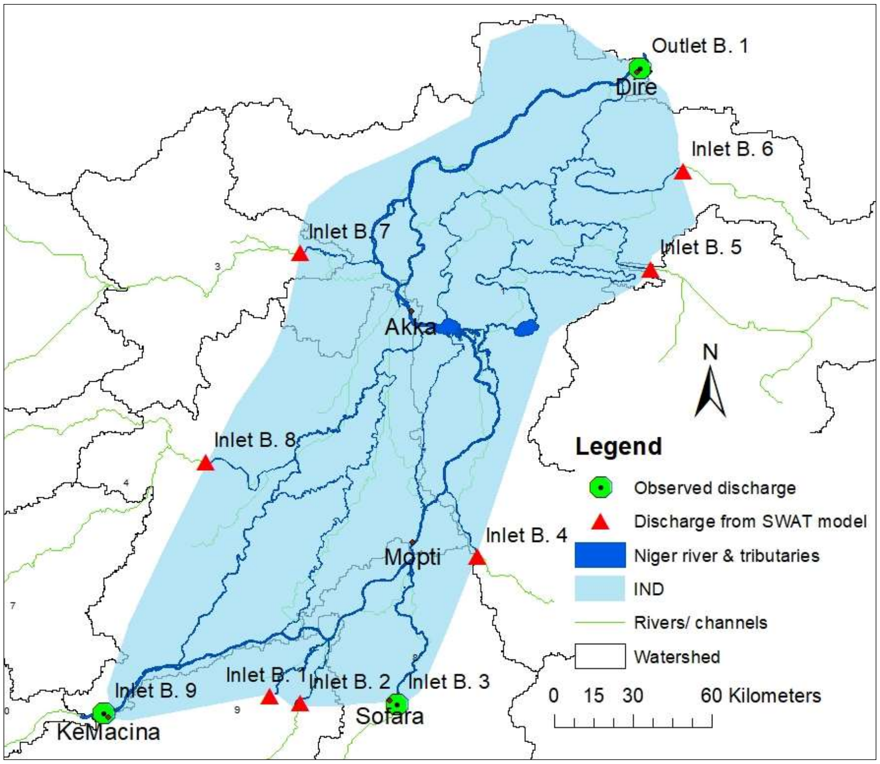

Fig. 5.3: Locations of the 10 liquid boundaries (B) in the hydrodynamic model, specified as inlets and outlets.

5.2.5 Boundary condition

Time-varying (daily) observed discharges were prescribed at the inlet boundaries. Ungauged discharge at the inlet boundaries were estimated using a hydrological model, Soil Water Assessment Tools (SWAT) (Arnold et al. 1998) of the upper Niger and Bani Rivers basins developed in a previous project (Seidou, 2019). Three types of rating (stage-discharge) curves were applied to the downstream (outlet) boundary: (1) a single non-looping rating curve, (2) a looped rating curve derived from dimensionless discharge and water level observations, and (3) a looped rating curve derived from the modified Jones Equation (Petersen-Øverleir, 2006). The TELEMAC 2D source code was modified to include the possibility of using a looped rating curve in the simulation satisfying the Courant criteria and related stabilities

5.2.6 Calibration and validation

We used the same model calibration that had already been used successfully in Haque et al. (2019), based on streamflow data and water levels of the 2001-2002. The model had been validated using streamflow data, water levels, and inundation extent of the 2008-2009. The quality of the simulated discharge and water levels were evaluated with Pearson's correlation coefficient and Nash-Sutcliffe coefficients (Table 5.1).

Table 5.1: Pearson's correlation coefficients (r) and Nash-Sutcliffe coefficients (NS) for the model calibration and validation of the simulated discharges and water levels.

Model	Discharge				Water Level			
	Mopti		Akka		Mopti		Akka	
	NS	r	NS	r	NS	r	NS	r
Calibration	0.956	0.994	0.958	0.986	0.981	0.997	0.871	0.998
Validation	0.935	0.99	0.882	0.976	0.973	0.993	0.876	0.988

5.2.7 Derivation of a looped rating curve for the Diré station

Two methods were used to generate the rating curve at Diré; one is based on the dimensionless forms of the discharge (Q) and the water level (WL) (Mishra and Seth,1998) while the second is based on the modified Jones Equation (Jones, 1916).

5.2.8 Deriving the dimensionless forms of Q and WL

Mishra and Seth (1998) postulated that hysteresis can be represented by dimensionless quantities derived from stage and discharge values. To this purpose, we normalized the observed water level for each year using the following formulae:

$$(H_{sc})_i = \frac{H_i - H_{min}}{H_{max} - H_{min}} \tag{5.1}$$

where H_{sc} is the normalized water level; H is the observed water level; H_{min} and H_{max} are the annual minimum and maximum water level, respectively; i is the i^{th} observation in the hydrologic year.

Similarly, the discharge is normalized using:

$$(Q_{sc})_i = \frac{Q_i - Q_s}{Q_{max}} \tag{5.2}$$

where Q_{sc} is the scaled discharge, Q is the observed discharge, Q_{max} is the annual maximum discharge, i is the i^{th} observation of the hydrological year, and Q_s is the discharge obtained from the single (non-looping) rating curve.

These scaled values can be used to obtain the looping rating curve:

$$WL_{loop} = (H_{sc})_i * (H_{max} - H_{min}) + H_{min} \tag{5.3}$$

$$Q_{loop} = (Q_{sc})_i * Q_{max} + Q_s \tag{5.4}$$

where Q_{loop} and WL_{loop} are the discharge and water level, respectively, for the looping rating curve.

Once the scaled values have been calculated for each year, the dimensionless curves are obtained by plotting Q_{sc} as function of H_{sc}. Two polynomials are used to represent the relationship between H_{sc} and Q_{sc} with one equation being fitted to the upper part ($Q_{sc} > 0$), which represents the rising flood, and the second equation being fitted to the lower part ($Q_{sc} < 0$) which represents the receding flood.

5.2.9 Jones formula

The Jones formula (Jones, 1916) is the best-known method to derive a looped rating curve. Jones (1916) used the following equation:

$$Q_L = Q_s\left[1 + \frac{1}{S_0 c}\frac{\partial h}{\partial t}\right]^{1/2} \tag{5.5}$$

where Q_s is the single rating discharge which can be obtained from the single rating curve, S_0, the mean slope of the stream and the kinematic wave speed c. $\partial h/\partial t$ is the rate of change of the river stage.

Q_s can be approximated by the following power-law function (Herschy, 1995; ISO 1998; Kennedy, 1984; Rantz et al., 1982b):

$$Q_s = a(h\text{-}b)^c \tag{5.6}$$

Petersen-Øverleir (2006) modified the Jones equation (hereafter Modified Jones Method) in the following way:

$$Q_L = a(h\text{-}b)^c\left[1 + \theta(h\text{-}b)^{\text{-}M}\frac{\partial h}{\partial t}\right]^{1/2} \tag{5.7}$$

where $\theta = \frac{(1+N)^{M+1}}{KS_0^{\frac{3}{2}}(M+N+1)}$

K is the conveyance factor, M the friction law exponent *(~2/3),* and N the channel-shape parameter *(~0-1).* a and c are rating curve constants while b is the water level that corresponds to zero discharge. The coefficients a and c are obtained from the relationship between discharge and water level. The value for θ is optimized for each year and averaged over the years. $\partial h/\partial t$ is the rate of change of the river stage over the previous six days which was fixed after several trials.

5.2.10 Evaluating Model Performance

The model results are evaluated using the relative error (RE), the Nash-Sutcliffe coefficient (NS), and the root-mean-square-error (RMSE). The equations for NS, RMSE, and RE are given bellow:

$$NS = 1 - \frac{\sum_{i=1}^{n}(x_i - y_i)^2}{\sqrt{\sum_{i=1}^{n}(y_i - \bar{y})^2}} \tag{5.8}$$

$$RMSE = \sqrt{\frac{\sum_{i=1}^{n}(x_i - y_i)^2}{n}} \tag{5.9}$$

$$\mathrm{RE} = \sum \left| \frac{(\mathrm{x_i} - \mathrm{y_i})}{\mathrm{y_i}} \right| \tag{5.10}$$

where *x* represents the simulated, and *y* the observed value of a variable. $\bar{x}$ and $\bar{y}$ are the averages of the simulated and observed values, respectively. *n* is the number of observations.

5.2.11 Estimation of the connectivity and water level threshold for Lake Fati

Inundation extents (Zwarts et al. 2005) derived from Landsat images were analyzed to examine the connectivity dynamics between Lake Fati and the Niger river (Fig. 5.4). A series of images were placed on top of each other to find out the connection and disconnection scenarios.

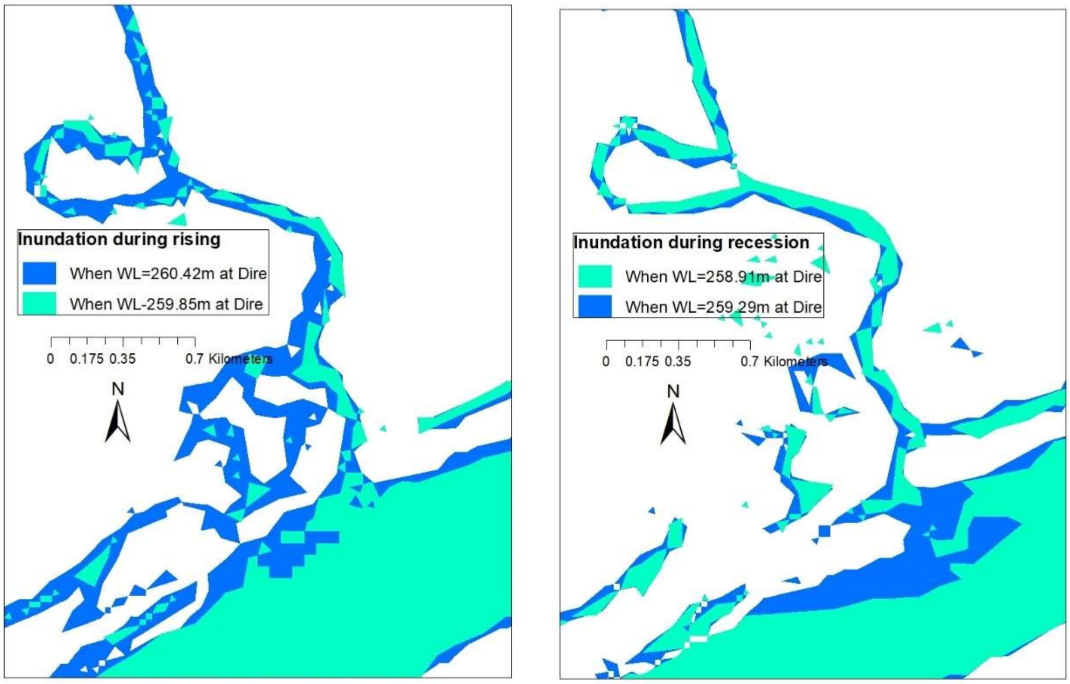

Fig. 5.4: Two consecutive inundation extent maps are superimposed to show the switch from the disconnected to the connected state (between Lake Fati channel with Niger river) during rising water levels (left) and the reverse during receding water levels (right).

A connection between the Niger River and Lake Fati is established once the water level at Diré reaches about 260.42 mIGN during rising water levels. Conversely, this connection is severed when the water level falls below 258.91 mIGN during receding waters.

5.2.12 Simulation of the connectivity between the Niger River and Lakes Fati

Given that Lake Fati is close to Diré station, we decided to link the connectivity between the lakes to the water levels at Diré. In combination with satellite imagery, we established an approximate threshold that separates the connected from the disconnected states. This threshold is used on the entire water level time series at Diré (either simulated and observed) to decide whether Lake Fati is connected to the Niger River or not.

5.3 Results and Discussion

5.3.1 Rating curve derived from the dimensionless forms of Q and WL at Diré

A discharge time series containing 12 hydrological years (June 1 to May 30) from between 1980 and 2016 at Diré are shown in Fig. 5.5. The selected 12 years contain both the wettest and the driest years from the 36 year period and also evenly cover anything in between (Fig. 5.5).

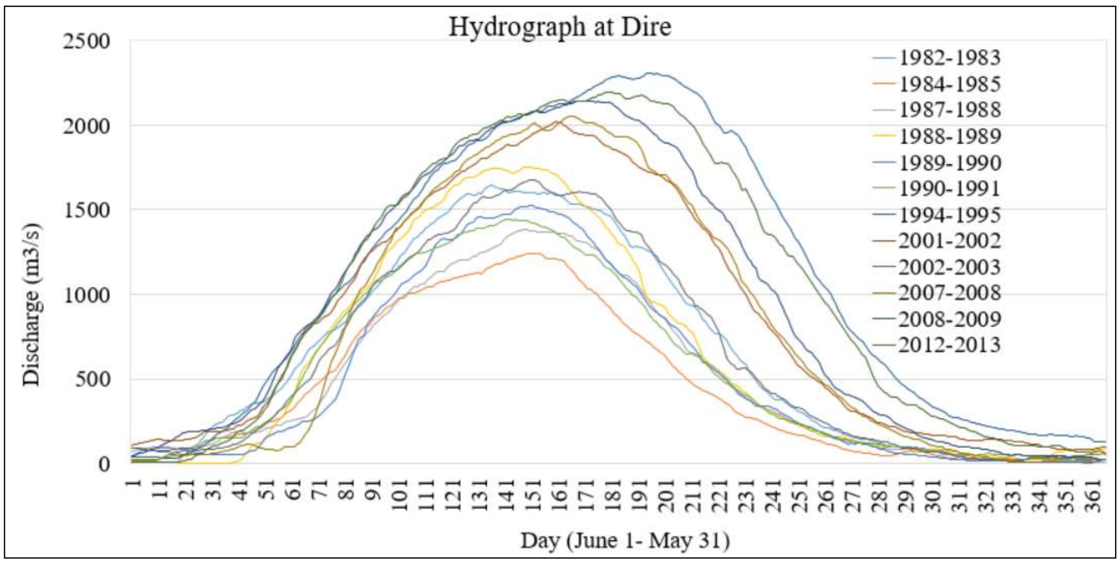

Fig. 5.5: Hydrographic data for 12 selected hydrological years between 1980 and 2016.

The dimensionless discharges and water levels were calculated from above data using equation 5.1 and 5.2 and plotted on Fig. 5.6. 8th order polynomial was used to fit the curves as it gave the highest R^2 value. Fitted 8th order polynomial equation for upper and lower parts are given in equation 5.11 and 5.12:

Upper part:

$$f(x) = -50.87x^8 + 193.3x^7 - 300.5x^6 + 246.4x^5 - 114.6x^4 + 29.74x^3 - 3.637x^2 + 0.1928x - 0.001341 \quad (5.11)$$

Lower part:

$$f(x) = 14.85x^8 - 38.7x^7 + 32.91x^6 - 6.81x^5 - 2.821x^4 + 0.7256x^3 - 0.1647x^2 + 0.00001401x - 0.0003196 \tag{5.12}$$

where, *f(x)* is the scaled discharge and *x* is the scaled water level.

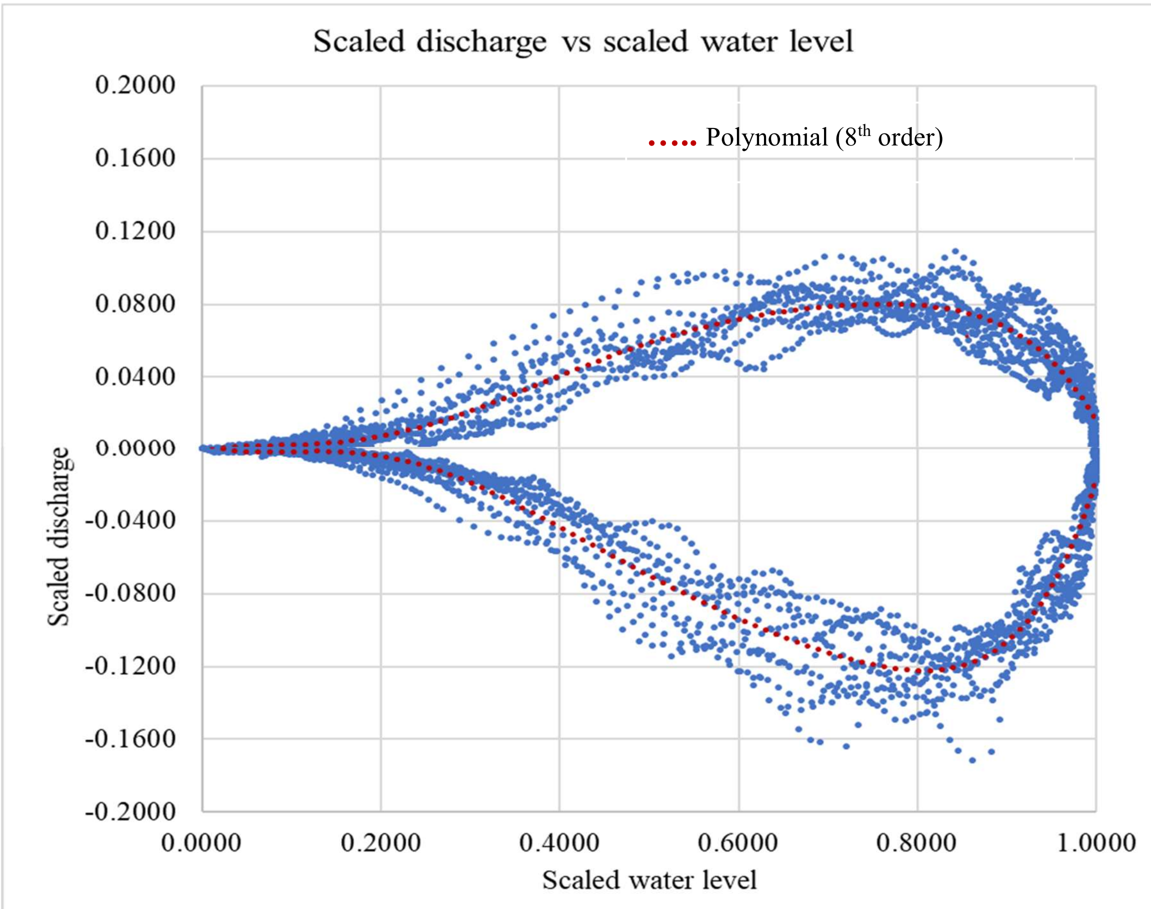

Fig. 5.6: Scaled discharge and water levels

5.3.2 Rating curve derived from Modified Jones method

A new stage-discharge (Q-H) relationship (Eq. 14) at Diré station is obtained from the implementation of Equation 5.7 to estimate the discharge based on the water level:

$$Q_L = (66.804H^2 - 34243H + 4388140.24)\left(1 + 7.7947\frac{dh}{dt}\right)^{0.5} \tag{5.13}$$

The first part of the right side of the equation 5.13 corresponds to the single (non-looping) rating curve and the second part is the correction to account for the hysteresis.

5.3.3 Performance of the looped rating curves

We used dimensionless discharges and levels and the modified Jones Equation to obtain the loop rating curve at Diré. Let us denote the above rating curves as DLRC and MJRC respectively. The years 1994-1995 and 2001-2002 were used for the calibration while the validation was performed for the years 1996-1997 and 2005-2006 (Table 5.2 and Table 5.3).

Table 5.2: Model performance during calibration showing the root-mean-square-error (RMSE), the relative error (RE), and the Nash-Sutcliffe coefficient (NS).

Year	Single rating			DLRC			MJRC		
	RMSE	*RE*	*NS*	*RMSE*	*RE*	*NS*	*RMSE*	*RE*	*NS*
2001-2002	143.94	12.74	0.942	36.32	3.751	0.996	46.47	4.11	0.994
1994-1995	171.88	12.11	0.928	41.54	3.13	0.996	56.81	4.37	0.992

DLRC outperforms MJRC for both 2001-2002 and 1994-1995 which can also be seen in the graphical representation of both methods where the looped rating curve obtained from either method closely matches the observed rating curve (Fig. 5.7).

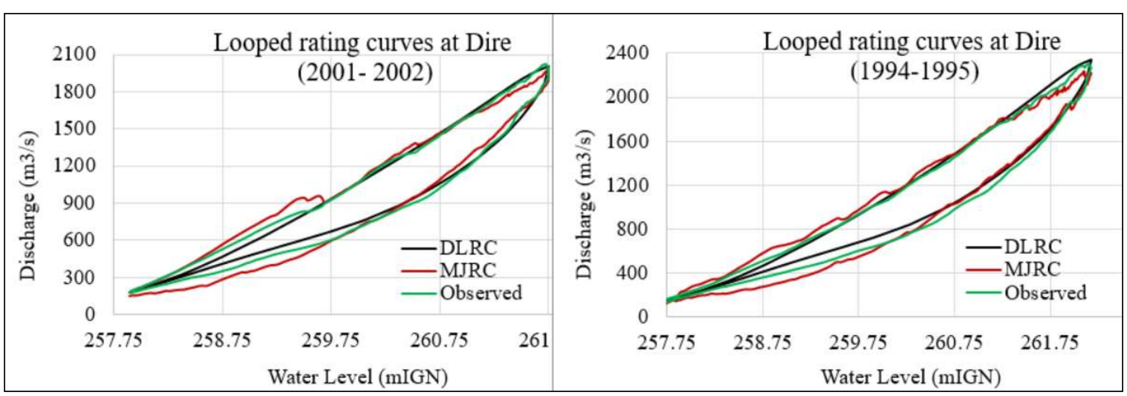

Fig. 5.7: Comparison of the rating curves at Diré.

Table 5.3: Performance of the methods during validation showing the root-mean-square-error (RMSE), the relative error (RE), and the Nash-Sutcliffe coefficient (NS).

Year	Single rating			DLRC			MJRC		
	RMSE	*RE*	*NS*	*RMSE*	*RE*	*NS*	*RMSE*	*RE*	*NS*
2005-2006	145.84	30.16	0.928	32.25	9.54	0.996	34.18	7.49	0.996
1996-1997	205.69	31.70	0.937	47.52	7.34	0.996	50.63	7.44	0.996

For the validation period, both rating curves exhibit similar performances in terms of NS, while DLRC outperforms MJRC in terms of RMSE. The RE statistics show a mixed picture with MJRC having a better RE in 1996-1997 but a slightly worse one in 2005-2006 (see also Fig. 5.8). Both DLRC and MJRC are significantly better than the single rating curve during calibration and validation.

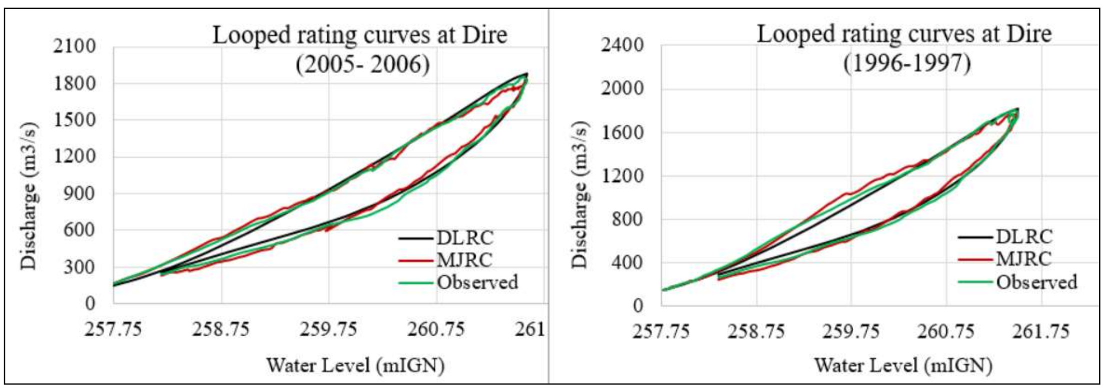

Fig. 5.8: Comparison of the rating curves at Diré during validation.

5.3.4 Impact of a looped rating curve on the simulation of discharge and water level

Table 5.4 shows the models ability to simulate discharge and water level as measured by RMSE and NS.

Table 5.4: Performance of simulated discharge and water levels at Mopti, Akka, and Diré for 2001-2002 in terms of root-mean-square-error (RMSE) and Nash-Sutcliffe coefficient (NS).

Stations	Downstream boundary condition	Discharge		Water level	
		RMSE	NS	RMSE	NS
Mopti	MJRC	165	0.96	0.17	0.98
	DLRC	166	0.96	0.17	0.98
	single rating curve	166	0.96	0.17	0.98
Akka	MJRC	127	0.97	0.41	0.89
	DLRC	134	0.96	0.41	0.89
	single rating curve	116	0.96	0.44	0.87
Diré	MJRC	94	0.97	0.21	0.97
	DLRC	104	0.97	0.18	0.98
	single rating curve	111	0.96	0.23	0.96

These results clearly show that using a looped rating curve (MJRC and DLRC) resulted in an improvement of the predicted discharge and water level at Diré. At Akka, the use of a looped rating improves the discharge and water level simulation in term of NS; however, the RMSE turns to be better for water level and slightly worse for discharge. At Mopti there is essentially no difference between the looped and single rating curves.

Simulated water surface profile from downstream boundary at Diré to upstream at Akka is plotted in Fig. 5.9 on two dates during rising and recession time of flood.

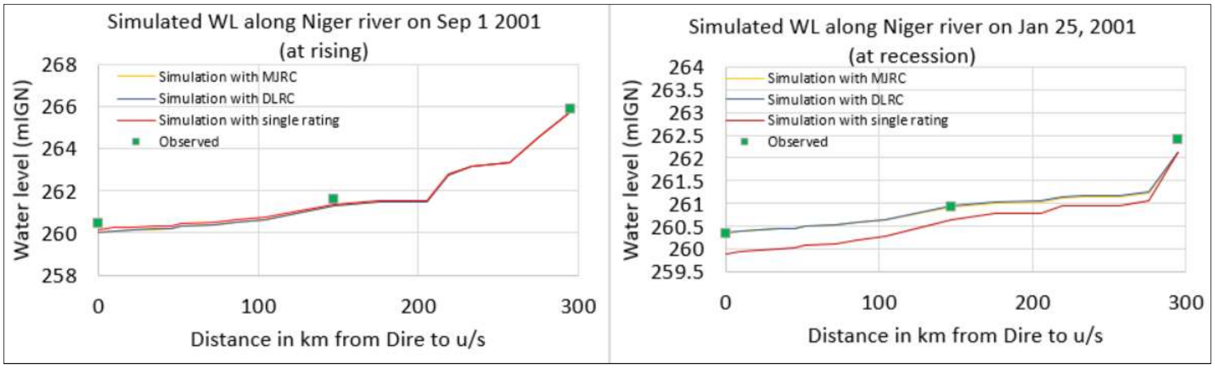

Fig. 5.9: Simulated water level along Niger River from Diré to Mopti during rising water levels on Sep 1 2001 (left) and during receding water levels on Jan 25 2002 (right).

The effect of the looped raing curve is most important at Diré (downstream), and diminishes we move further upstream (Fig. 5.9). Use of the looped raing curve predicts slightly lower water levels during rising waters and higher water levels during receding waters.

5.3.5 Effect of a looped rating curve on predicting the inundated area

Comparing the simulated inundation areas for the single and looped rating curves we find that the looped rating curve yields smaller inundated areas compared to the single rating curve when the hydrograph is rising (Fig. 5.10). During receding water the opposite is true.

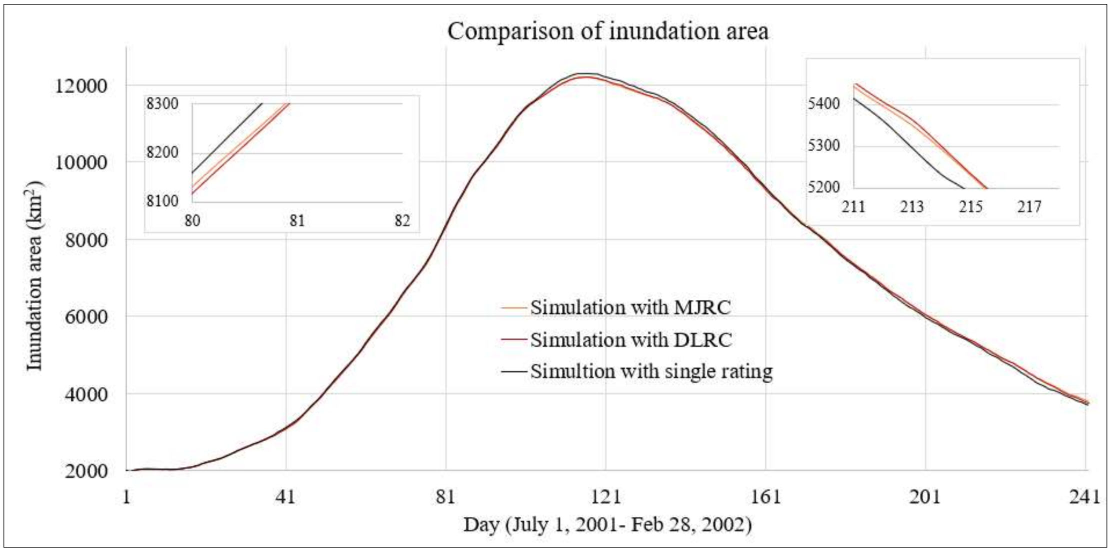

Fig. 5.10: Predicted inundation area with the looped and single rating curves at the downstream boundary. The insets show enlargements of the rising/receding waters on Sept 01 2001/Jan 25 2002.

Predicted inundation areas on Sept 01, 2001 and Jan 25, 2002 obtained with the looped and single rating curves is shown in Table 5.5.

Table 5.5: Comparison of simulated inundation areas for the looped (DLRC and MJRC) and single rating curves.

Boundary condition	Inundation area (km^2)	
	Rising	Recession
	(Sept 01, 2001)	(Jan 25, 2002)
DLRC	5555.8	5560.9
MJRC	5586.3	5569.8
Single rating	5605.6	5510.0

Inundation pattern of the area adjacent to the downstream boundary is shown in Fig. 5.11 . For brevity, inundation at recession time of flood on Jan 25, 2002 is considered.

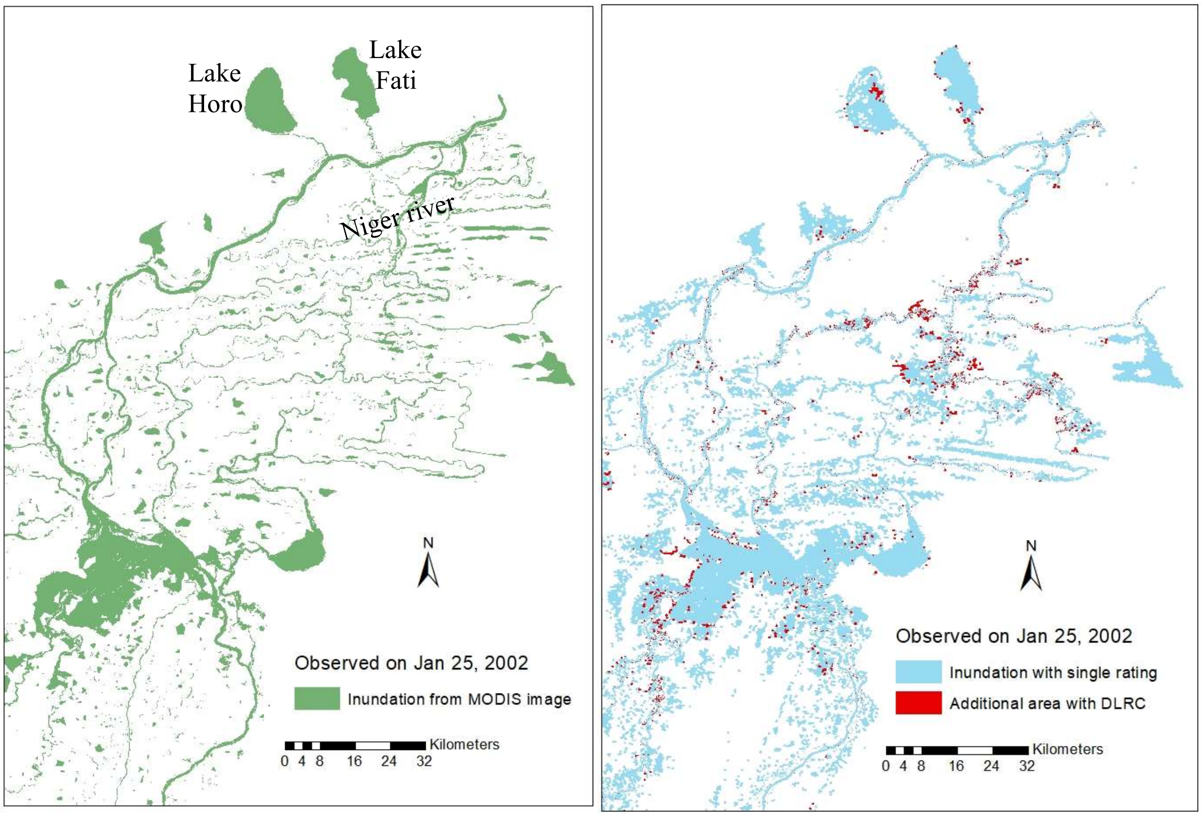

Fig. 5.11: Comparison between observed (left) and simulated (with DLRC, right) inundation areas in the downstream part of the study area on Jan 25, 2002.

The observed (from MODIS) and simulated inundation maps for January 25, 2002 (receding waters) show that simulations with looped rating curves yield larger flooded areas (excess shown in red). Especially around Lake Horo and Lake Fati, as well as along the Niger river and other channels there are more inundated areas with the looped rating curves which also seems a better match with observations. While these improvements may seem minor in terms of absolute inundated area, they can be significant in an ecological context as these slight differences may cause a change in connectivity between water bodies which can affect the migration of aquatic species in the water system.

5.3.6 Estimating the connection and disconnection dates for Lake Fati

The water level at Diré during rising (260.42 mIGN) and receding waters (258.91 mIGN) are considered as thresholds that separate the connected from the disconnected periods of the channel. In other words, using the Diré water level time series of a particular year, we can estimate the connectivity dynamics of Lake Fati. Using simulated water levels with DLRC, MJRC, and the single rating curve, we obtain the connectivity durations and presented in Table 5.6.

Table 5.6: Connectivity periods and durations for Lake Fati from observations and simulated water level data at Diré station (see main text for thresholds).

Data source for water levels	Connectivity period based on water level thresholds	Days connected
In situ observations	Sep 02, 2001 to Feb 20, 2002	167
Model with MJRC	Sep13, 2001 to Feb 26, 2002	167
Model with DLRC	Sep 12, 2001 to Feb 21, 2002	163
Model with single rating curve	Sep 09, 2001 to Feb 15, 2002	161

The simulated connectivity period is longer when using either of the looped rating curves (MJRC or DLRC). The best match with regard to the onset and breakdown of the connectivity is provided by DLRC while the MJRC approach yielded the best match for duration. These results can be further improved by using a finer mesh in the channels in combination of high-quality elevation data and high-resolution radar satellite images such as Sentinel-2 (resolutions of about 10m to 20m) to gauge the inundation. While the connectivity is not directly simulated by the hydrodynamic model, the results of this study can be used to assess changes in water management or climate change and their impact on the ecological dynamics in the IND.

5.4 Conclusion

Despite a significant hysteresis being present at all hydrometric stations of the Inner Niger Delta (IND), existing hydrodynamic models of the area do not account for it. In this study, the effect of including the hysteresis in the rating curve at the downstream model boundary on the inundation and connection dynamics of different water bodies in the IND have been investigated. We employed two different methods to reproduce the hysteresis effect at the downstream boundary; one was based on dimensionless discharges and water levels and the second was based on the modified Jones formula. The quality of the simulation results was evaluated using root-mean-square-error (RMSE), the relative error (RE), and the Nash-Sutcliffe coefficient (NS). We found that accounting for hysteresis improved the simulation results, particularly the predictions for water level, discharge, and inundation extent in the downstream part of our study area. By including hysteresis, we could also make better predictions of the connectivity between different water bodies such as Lakes Fati, which are of great ecological and economic importance to the IND. The observed improvements in the model predictions suggest that if an area is subjected to hysteresis, hydrodynamic simulations must be performed with looped rating curves in order to obtain a better match with observations.

Chapter 6

Development of an improved relationship between water levels and flooded areas in the Inner Niger Delta, Mali, West Africa[3]

Abstract: The Inner Niger Delta (IND) is a vast floodplain with abundant natural resources that supports the livelihood of millions of people. Accurate knowledge of the extent to which flooding occurs is crucial for the proper management of natural resources in the IND. Previous studies have developed empirical relationships between water levels at key stations in the IND and the area flooded in an attempt to provide a simple tool to link hydraulic parameters to the performance of socio-economic activities in the IND. However, simulations from an IND hydrodynamic model show that the relationship between water level and the extent of inundation varies greatly from year to year and that this relationship cannot be adequately captured by static formulas. In this study we first demonstrate that if the maximum water level is known in advance, an accurate relationship between water level and inundation extent can be derived. Secondly, we use stepwise regression to develop a function that forecasts maximum water levels at Mopti using observed streamflow and precipitation upstream of the Delta. The combination of the two results allows for a real-time estimation of the inundated area in the IND using observed water levels, precipitation, and streamflow.

Keywords: Inundation extent, forecasting, hydrodynamic model, Inner Niger Delta

[3] Haque, M. M., Seidou, O., Mohammadian, A. Djibo, A. G., (2019) Development of an improved relationship between water levels and flooded areas in the Inner Niger Delta, Mali, West Africa, *Journal of Hydrology: Regional Studies* (Revised)

6.1 Introduction

Floodplains are dynamic systems that are periodically flooded, creating distinctive habitats through the exchange of water, sediment, and organisms (Tockner and Stanford 2002, Opperman et al. 2010). Flood dynamics provide numerous advantages that help the development of aquatic ecosystems and benefit human communities (RRP, 2016). The Inner Niger Delta (IND) in Mali, West Africa is one of the largest floodplains in the world and is a vast natural resource that attracts many people to live in and around it (Zwarts et al. 2005).

Methods for estimating the inundation area can be roughly divided into three types: methods based on Digital Elevation Models (DEMs), methods based on hydrodynamic model simulations, and remote sensing methods (Chen et al. 2019). DEM methods work for small and still water bodies for which high-resolution bathymetry is available. They cannot be applied to moving water or large lakes where the water surface cannot be assumed to be horizontal. Methods based on hydrodynamic simulations have several advantages, but require the availability of a calibrated hydrodynamic model, and the input data to run it. Despite the availability of a few hydrodynamic models for the IND (e.g., Neal et al., 2012; Haag, 2015), these methods were not used here because the models were developed and operated by institutions outside of Mali, and expertise in IND hydrodynamic modeling has not yet been transferred to local institutions. Remote sensing is a widely used technique for inundation extent estimation (Bates, 2012; Bates et al. 1997). It is extremely useful in remote regions and in developing countries (Domeneghetti et al. 2019) where data collection is challenging. Several studies have used remote sensing to derive inundation extents and build a relationship between water level and the area flooded, such as Ogilvie et al. (2015), Mahe et al. (2011), Zwarts et al. (2005) and Mariko (2003). Ogilvie et al. (2015) used a total of 526 Moderate Resolution Imaging Spectroradiometer (MODIS) images from July 2000 to December 2011 to derive a relationship between inundation and water level in Mopti, Mali. Mahe et al. (2011) used NOAA/AVHRR images from 1990 to 2000 to map the flooded areas and link them to water heights at Mopti's gauge station. Zwarts et al. (2005) derived a correlation between flooded areas and Akka's water stage level by analyzing 24 Landsat images spread over several years. Mariko (2003) derived inundation extent using NOAA AVHRR images. An inundation function (a relationship between water levels and flooded areas) was developed using the average water height at Mopti and Akka gauges. However, the use of remote sensing is subject to constraints such as unavailable or poor quality images, the presence of clouds, noisy images, and spectral confusion between water and non-water surfaces. Bates et al. (1997) found that the extrapolation of satellite-derived inundation extents to estimate the area of inundation during high floods was problematic. Extrapolating the empirical equations derived by Zwarts et al. (2005) and Mariko (2003) during peak water levels resulted in a poor estimate of the inundation area. Another major limitation in the existing relationship between water levels at a reference station and the inundation area is that these equations are not able to accurately describe hysteresis behavior. Mahe et al. (2011), Zwarts et al. (2005), and Mariko (2003) stressed this matter in their studies but were not able to provide a solution to this problem due to an insufficient amount data on inundation extent. The above mentioned issues highlighted in previously published studies, suggest that relationships between water levels and inundation extent in the IND are highly imprecise.

The main objectives of this paper were to develop a relationship between water levels at one reference station and predict the inundation extent in the IND that can a) have year-to-year variations and b) be used in real-time. Simulated timeseries of water levels and inundation extents were generated using a two-dimensional hydrodynamic model of the IND that was set up, calibrated, and validated for discharge, water level, and inundation extent. The simulated timeseries of water levels and inundated area were used to build a relationship between water levels and inundation area, given the maximum water level and maximum flooded area. Finally, stepwise regression was used to develop a relationship that forecasts maximum water levels and maximum inundation in the IND using observed streamflow and precipitation.

6.2 Materials and Methods

6.2.1 Overview of the methodology

The methodology adopted in this paper has three main parts:

4. The development, calibration, and validation of a hydrodynamic model and the development of a relationship between simulated water levels at Mopti and inundation

extent in the IND, conditioned on the knowledge of yearly maximum water levels $H_{\max}$ and yearly maximum inundation extents $I_{\max}$;

5. The development, calibration, and validation of a linear model that can forecast $I_{\max}$ and $H_{\max}$ given precipitation and streamflow measured on the upper Niger river basin (UNB) before the flood season;
6. The combination of the relationships developed in points 1 and 2 to obtain a relationship between water levels at Mopti and inundation extent in the IND that changes from year to year. The inundation extent predicted by the new relationship is then compared to the predicted relationships developed by other studies, and with the inundation extent obtained from MODIS satellite imagery.

An overview of the methodology is presented in Fig. 6.1:

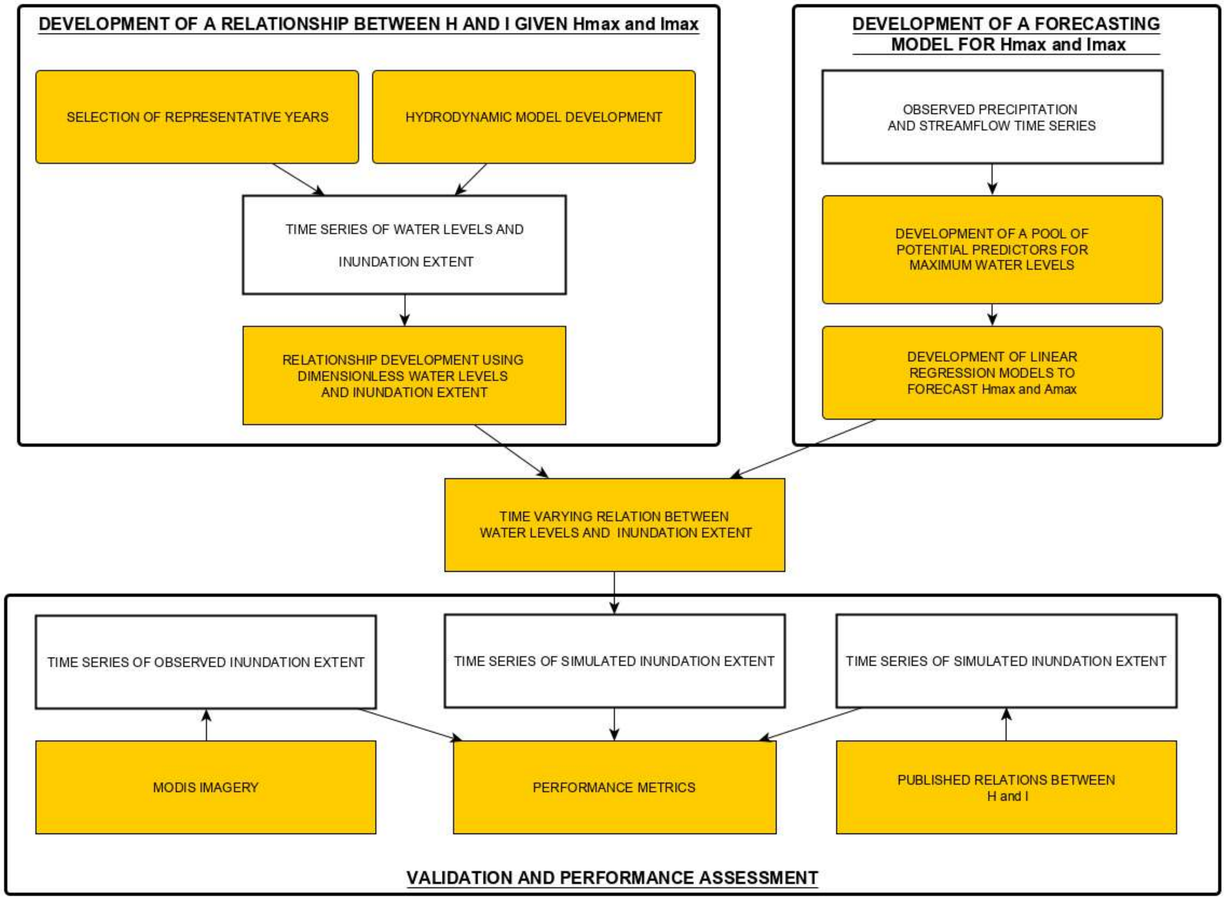

Fig. 6.1: Overview of the methodology

6.2.2 Study area

The study area is the Inner Niger Delta (IND), in Mali, West Africa. The IND has relatively flat topography (approximately 0.036 m/km) with a network of tributaries, channels, swamps, and lakes providing vital habitats for fish, agriculture and livestock, and is home to many ethnic communities such as the Fulani herders, the Bozo and Somono, and the Marka, Bambara, and Sonrai. In the literature, the area of the Inner Delta varies from 36,000 km^2 to 80,000 km^2 (Liersch et al. 2012). In our study, the area spans from KeMacina and Djenne in the upstream reaches to Korioume in the downstream reaches, with an area of approximately 45,521 km^2. We delineate the area in such a way that it encompasses all water bodies in the IND during high flood conditions. The study area is shown in Fig. 6.2.

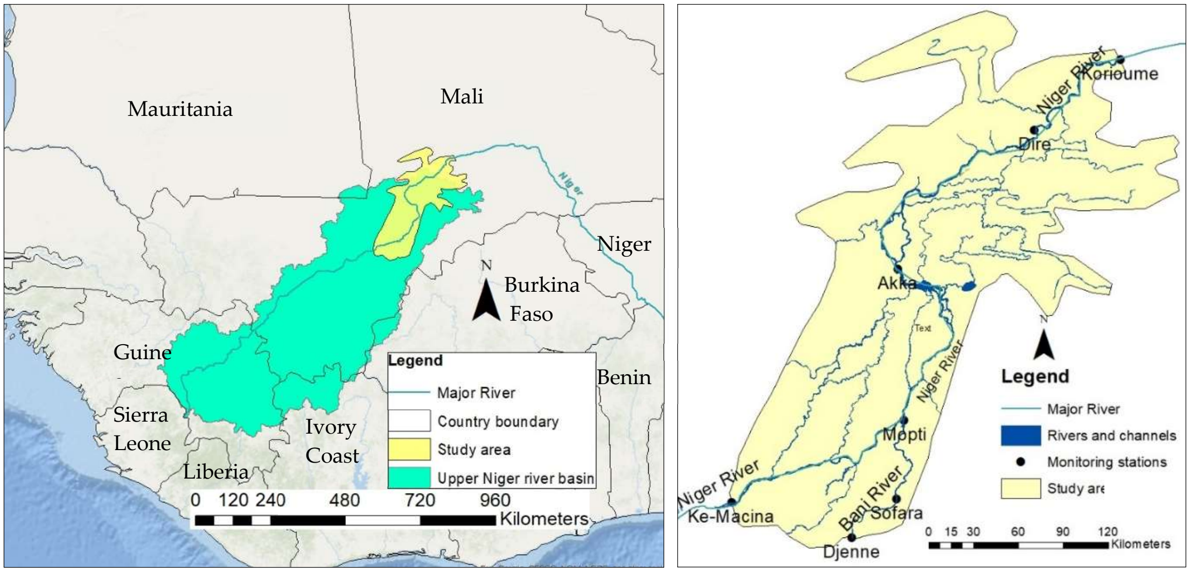

Fig. 6.2: Study area of the Inner Niger Delta in Mali, West Africa within the Upper Niger river basin

6.2.3 Development of a relationship between water levels and inundation extent

6.2.3.1 Hydrodynamic model development

The hydrodynamic model used in this study is similar to that of Haque (2019) except that the modeled area was extended to match that of Mariko (2003), Zwarts et al. (2005), Mahe et al. (2011) and Ogilvie et al (2015). The modeled domain is shown in Fig. 6.3.

The study uses elevation data from MERIT DEM (Yamazaki et al. 2017). MERIT DEM is available at a resolution of three arc-sec (approximately 90 m) and was derived from SRTM (NASA JPL, 2013) and AW3D-30 m (JAXA, 2018) by removing multiple error components such as absolute bias, stripe noise, speckle noise, and tree height bias (Yamazaki et al. 2017). The bathymetry of Niger and the Bani river was approximated using hydraulic geometry equations proposed by Leopold and Maddock (1953). The procedure to derive the data can be found in Haque et al. (2019).

The hydrodynamic model (TELEMAC 2D) (Hervouet, J.M. 2007) has a mesh with 347,324 nodes. The time step was 120 sec for all simulations. The hydrodynamic model has eight open boundaries, seven of which are inlets, while one is an outlet (Fig. 6.3). The inlet boundaries were fed with discharge timeseries data for each of the selected years. The downstream boundary condition is the rating curve at Korioume. As in Haque et al. (2019), inflow at two of the inlet boundaries is the observed streamflow at KeMacina and Sofara. Inflows at the other boundaries were simulated with Soil Water Assessment Tools (SWAT) and were used to provide flow at the inlet boundaries which were not gauged. The model was developed by Seidou (2019) for the upper Niger and Bani River basins.

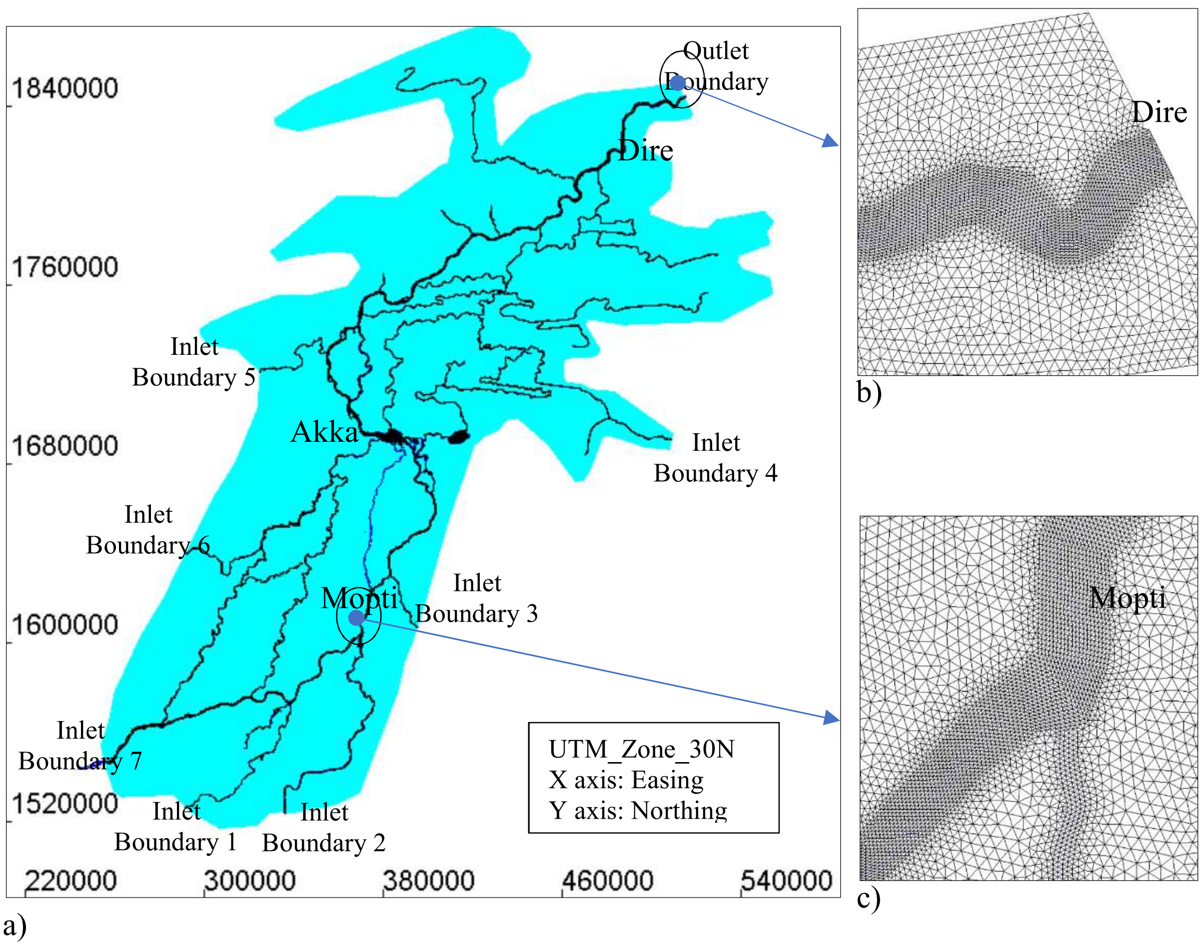

Fig. 6.3: Discretization of the study area including the inlet and outlet boundaries (a); a closeup view of the meshes near Dire (b) and Mopti (c)

6.2.3.2 Hydrodynamic model calibration and validation

The 2001-2002 hydrological year was chosen for calibration of the hydrodynamic model, while the 2008-2009 hydrological year was chosen for validation. Discharge and water levels at Mopti, Akka, and Dire were compared using Pearson's correlation coefficient (r) and Nash-Sutcliffe's coefficient (NS) and are described in the following equations:

$$r = \frac{\sum_{i=1}^{n}(x_i - \bar{x})(y_i - \bar{y})}{\sqrt{\sum_{i=1}^{n}(x_i - \bar{x})^2}\sqrt{\sum_{i=1}^{n}(y_i - \bar{y})^2}} \tag{6.1}$$

$$NS = 1 - \frac{\sum_{i=1}^{n}(x_i - y_i)^2}{\sqrt{\sum_{i=1}^{n}(y_i - \bar{y})^2}} \tag{6.2}$$

where x represents a simulated value of a variable and y the observed value. $\bar{x}$ and $\bar{y}$ are the averages of the simulated and observed values, respectively.

6.2.3.3 Performance assessment for inundation extent

Performance of simulated inundation extents was evaluated with agreement fit measures, under-prediction measures and over-prediction measures (Taylor, 1977 and Gallien et al. 2014) and are given in the following equations:

Agreement fit measures (F_A):

$$F_A = \frac{E_P \cap E_0}{E_P \cup E_0} \tag{6.3}$$

where E_O and E_P are the observed and predicted flood extents, respectively. $E_P \cap E_0$ is the intersection between E_O and E_P. $E_P \cup E_0$is the union between E_O and E_P. F_A values of zero and unity correspond to no agreement and complete agreement, respectively.

Under-prediction measures (F_{UP}):

$$F_{UP} = \frac{E_0 - E_P \cap E_0}{E_P \cup E_0} \tag{6.4}$$

F_{UP} values of 0 and 1 correspond to no under-prediction and complete under-prediction, respectively.

Over-prediction measures (F_{OP}):

$$F_{OP} = \frac{E_P - E_P \cap E_0}{E_P \cup E_0} \tag{6.5}$$

Where F_{OP} values of 0 and 1 correspond to no over-prediction and complete over-prediction, respectively.

Once a satisfactory calibration was obtained, the simulated inundation extent was validated using reference inundation extents derived from images captured by NASA's MODIS. Two spectral indices were used to separate water pixels from non-water pixels. The indices are the Modified Normalized Difference Water Index (MNDWI) (Xu, 2006) and the Normalized Difference Moisture Index (NDMI) (Wilson et al. 2002).

6.2.3.4 Simulation of water level and inundation extent timeseries

Simulations were carried out using a wide range of hydrological years that span from extremely dry years to extremely wet years. The hydrological years selected to represent flooding from lowest to highest are: 1984-1985, 1990-1991, 2002-2003, 2001-2002, 2008-2009, 1994-1995 and span from1980-2012. The peak discharge of the chosen years at Mopti and Dire is given in

Table 6.1, where peak discharge is presented chronologically from the lowest peak (1984-1985) to the highest peak (1994-1995).

Table 6.1: Peak discharge at Mopti and Dire.

Year	Maximum discharge (m^3/s)	
	Mopti	Dire
1984-1985	1414	1241
1990-1991	1866	1443
2002-2003	2072	1680
2001-2002	2730	2022
2008-2009	2832	2146
1994-1995	3027	2307

6.2.3.5 Choosing a reference station for water levels in the IND

Mopti was chosen as the reference station in this paper. The hysteresis phenomenon can be well described at this station. Previously, the Mopti gauging station was used to model annual floods in the IND (Mahé et al., 2011; Mariko, 2003). Ogilvie et al. (2015) found a coherence between seasonal flood dynamics in the IND and the Mopti flow regime while analyzing the behavior with satellite images.

6.2.3.6 Derivation of the relationship between water levels at the reference station and the inundation extent

The method followed here is inspired by the dimensionless rating curve method introduced by Mishra and Seth (1998) and used in Haque et al. (2019b). The timeseries of simulated inundation area and water level areas were transformed into their dimensionless form. Observed water levels for each year have been normalized using the following formula:

$$(H_{sc})_i = \frac{H_i - H_{min}}{H_{max} - H_{min}} \tag{6.6}$$

where H_{sc} is the normalized water level, H is the observed water level, H_{min} is the minimum and H_{max} is the maximum water level, and i is the i^{th} data of the respective year.

Inundation for each year has been normalized using the following formula:

$$(I_{sc})_i = \frac{I_i - I_{min}}{I_{max} - I_{min}} \tag{6.7}$$

where I_{sc} is the normalized inundation, I is the simulated inundation, I_{max} is the maximum inundation, and i is the i^{th} data of the respective year.

These normalized values can be used to obtain a timeseries of inundation extent with corresponding water levels by using the following equations:

$$I = (I_{sc})_i * (I_{max} - I_{min}) + I_{min} \tag{6.8}$$

$$H = (H_{sc})_i * (H_{max} - H_{min}) + H_{min} \tag{6.9}$$

where I and H are inundation and water level, respectively.

6.2.4 Development of a forecasting model for maximum water levels and inundation extent

Prior to applying Equations 6.8 and 6.9, the yearly maximum water level and the maximum inundation extent must be known. In this paper, the maximum water level was forecasted using stepwise regression analysis with monthly discharge, monthly maximum discharge, and monthly average precipitation data at selected locations in the Upper Niger Basin. These data were used as predictors. Stepwise regression was used to screen the data (Sittichok et al. 2014, Gado Djibo et al. 2015) in each set of the predictors that closely match with the predictand. Then a linear model was established by regressing observed maximum water levels over the qualifying data obtained from the stepwise method.

6.2.4.1 Selection of the pools of potential predictors

Three types of potential predictors, namely monthly average discharge, monthly maximum discharge, and monthly precipitation in the Upper Niger Basin (UNB) were chosen for the analysis. Monthly average discharge from January to September at Kouroussa, Baro, Kankan, Koulikoro, and KeMacina for the period from 1990-2009 were used as the first pool of potential predictors. Maximum monthly discharge at the same stations and for the same years formed the second pool of predictors. Monthly average precipitation at each of the 32 sub-basins of the SWAT model, as shown in Fig. 6.4 formed the third pool of predictors. Three pools of predictors are selected because of their location within the UNB and influence on the IND water level. However, other data situated at remote location such as sea surface temperature (SST) (SST in equatorial Atlantic, equatorial Indian, eastern equatorial Pacific, southern tropical Indian oceans, Atlantic and the Pacific Ocean), southern oscillation index, sea level pressure, relative humidity, air temperature etc. can be considered as predictors.

Only months between January and September from 1979-2009 were used for this analysis as floods in the IND region start in September. These pools of predictors are denoted as:

1. Pool 1: $\overline{Q}_M^S$ where $M \in \{Jan, Feb, Mar, ..., Sep\}$ and
   $S \in \{\text{Kouroussa}, \text{Baro}, \text{Kankan}, \text{Koulikoro}, \text{KeMacina}\}$
2. Pool 1: $Q\text{max}_M^S$ where $M \in \{Jan, Feb, Mar, ..., Sep\}$ and
   $S \in \{\text{Kouroussa}, \text{Baro}, \text{Kankan}, \text{Koulikoro}, \text{KeMacina}\}$
3. Pool 1: PCP_M^{Sub} where $M \in \{Jan, Feb, Mar, ..., Sep\}$ and
   $Sub \in \{1,2,...,32\}$

   for example,

   at Kankun, $\overline{Q}_M^S \rightarrow \bar{Q}_{Aug}^{Kankan}$: Average discharge during August at Kankan

   at Koulikoro, $Q\text{max}_M^S \rightarrow Qmax_{Sep}^{Koulikoro}$: Max. discharge during Sept at Koulikoro

   at watershed 31, $PCP_M^{Sub} \rightarrow PCP_{Apr}^{31}$: Average precipitation during April in watershed 31

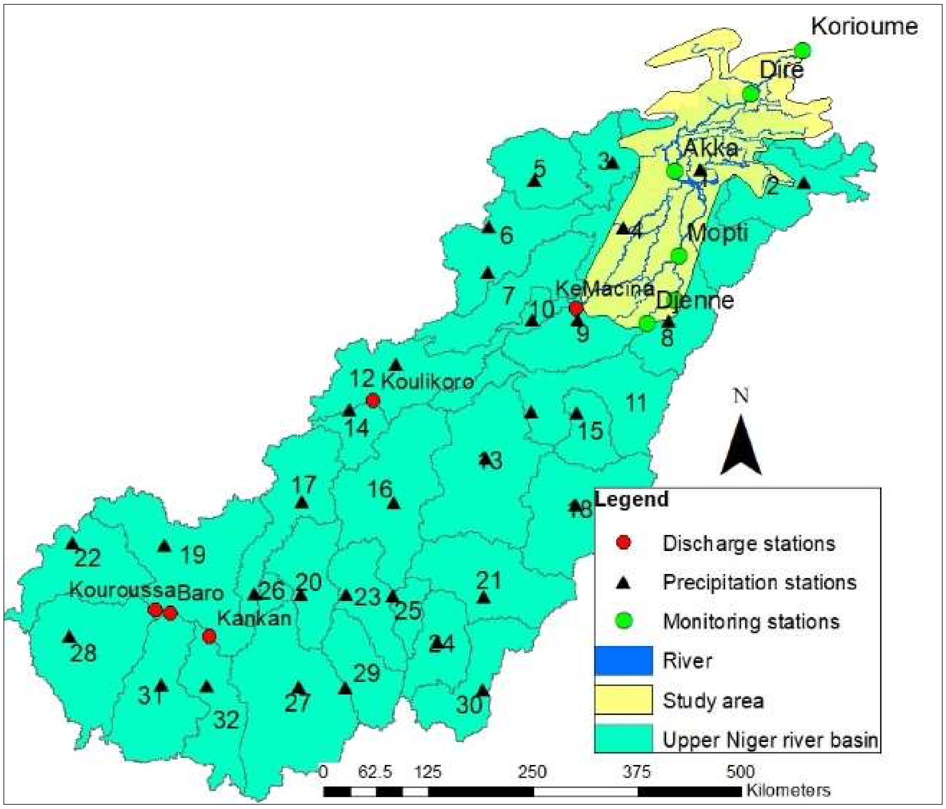

Fig. 6.4: Upper Niger river basin (SWAT model boundary). The regions outlined in black color represent sub-basins (a total of 32 sub-basins) of the model

6.2.4.2 Stepwise regression

Stepwise regression is a statistical procedure used to identify the best independent variables from several possible variables and provide the best model. This approach is likely the best way to pick the correct predictors for the simulation (Wang et al., 2009) in this study. There are two main types of stepwise regression: forward and backward selections. Forward stepwise regression starts with no independent variables. Then it adds variables one at a time, and the new model is evaluated according to values with a specific criterion. Backward stepwise regression begins with all the independent variables in the model. It then deletes one variable at a time using the same criteria as defined by the user. In this paper, both forward and backward stepwise regression are used to select the predictors. The periods 1990-2001 and 2002-2009 were selected for the calibration and validation of Pool 1 and Pool 2 datasets, respectively. In Pool 3, the periods 1979-1998 and 1999-

2009 were chosen as the calibration and validation periods, respectively. Stepwise regression was applied to each of the three pools of predictors to get an equation for H_{max}; the outputs of the three equations were then combined in one single linear equation and used in the forecasting model for determining H_{max}.

6.2.5 Performance evaluation

The performance of the developed relationship between water level and inundation extent is compared to predictions using the formulas developed by Zwarts et al. (2005), Mariko (2003) and Mahe et al. (2011), as described below. Zwarts et al. (2005) developed the following formula:

$$I = \begin{cases} 0.0005x^3 - 0.215x^2 + 28.807x + 194.36 \text{ (rising part)} \\ 0.0002x^3 - 0.0687x^2 + 25.121x + 656.14 \text{ (recession part)} \end{cases} \tag{6.10}$$

where x is the water level gauge height (cm) at Akka station (for water level <511cm), and I is the inundation area in km^2.

The formula developed by Mariko (2003) is presented below:

$$I = \begin{cases} 234.07e^{0.0075x} \text{(rising part)} \\ 7523\ln(x) - 32640 \text{ (recession part)} \end{cases} \tag{6.11}$$

where x is the average water level gauge height (cm) of Mopti and Akka station, and I is the inundation area in km^2.

The equation developed by Mahe et al. (2011) is given below:

$$I = 225.45e^{0.0064} \tag{6.12}$$

where x is the water level gauge height (cm) at Mopti station and I is the inundation area in km^2.

The predicted inundation extents were calculated using observed water levels in the delta and compared to inundation extents derived from MODIS images. A list of MODIS images used to validate the inundation curve is given in Table 6.2. Unfortunately, similarly to Ogilvie et al. (2015), we found that most images captured before September contained a large fraction of clouds and could not be used. Therefore, most of the reference extents used in this paper correspond to the period of receding water.

Table 6.2: List of MODIS images used for validating the relationship between water levels and inundation extent.

Image name	Image date
MOD09A1.A2010273	30 Sep 2010
MOD09A1.A2010321	17 Nov 2010
MOD09A1.A2010337	03 Dec 2010
MOD09A1.A2010353	19 Dec 2010
MOD09A1.A2011001	01 Jan 2011
MOD09A1.A2011033	02 Feb 2011
MOD09A1.A2011057	26 Feb 2011
MOD09A1.A2005305	01 Nov 2005
MOD09A1.A2005337	03 Dec 2005
MOD09A1.A2005353	19 Dec 2005
MOD09A1.A2006041	10 Feb 2006

6.3 Results and Discussion

6.3.1 Hydrodynamic model calibration and validation

The calibration and validation results are presented in the following sections.

6.3.1.1 Discharge and water levels

The calibration and validation results of the model for discharge and water level are given in Table 6.3. NS values are higher than 0.85 in all the simulations, confirming there is good agreement between simulated and observed water levels and discharge. Although, NS values were usually better during the calibration at Mopti and Akka, NS values were higher at Dire during validation for both discharge and water level.

Table 6.3: Comparison of discharge and water level during calibration and validation.

Station	Calibration (2001-2002)				Validation (2008-2009)			
	Discharge		Water level		Discharge		Water level	
	NS	r	NS	r	NS	r	NS	r
Mopti	0.966	0.992	0.939	0.989	0.945	0.988	0.945	0.984
Akka	0.893	0.964	0.953	0.994	0.853	0.949	0.942	0.988
Dire	0.913	0.963	0.913	0.972	0.985	0.995	0.932	0.982

6.3.1.2 Validation of the inundation extent simulated by the hydrodynamic model

Two days (16 October 2001 and 07 October 2008) were selected from the calibration and validation period to derive the reference inundation extent. Table 6.4 provides a short description of the images used in this study.

Table 6.4: List of MODIS images used for calibration and validation.

Image name	Image date	Purpose
MOD09A1.A2001289	16 Oct 2001	Calibration of the model
MOD09A1.A2008281	07 Oct 2008	Validation of the model

The inundation extent was evaluated using the percentage of agreement, under prediction, and over prediction measures as described in the previous section and presented in Table 6.5.

Table 6.5: Inundation extent fit measures.

Fit Measures	Calibration (16 October 2001)	Validation (07 October 2008)
Agreement	69.8%	66.8%
Under prediction	18.5%	22.2%
Over prediction	11.7%	11.0%

Results show a close agreement between the simulated and observed inundation values with a 69.8% and 66.8% agreement for calibration and validation, respectively. It is to be noted that the values of agreements found in this study are relatively low compared to previous studies where authors used high resolution topography (e.g. Bates and De Roo, 2000; Horritt and Bates, 2001) but relatively high compared to the results from other data sparse areas such as Amarnath et al. (2015) who found 38% and Sayama et al. (2012) who found 61% for agreement. Visual representation of the observed and simulated inundation areas on 07 October 2008 are presented in Fig. 6.5.

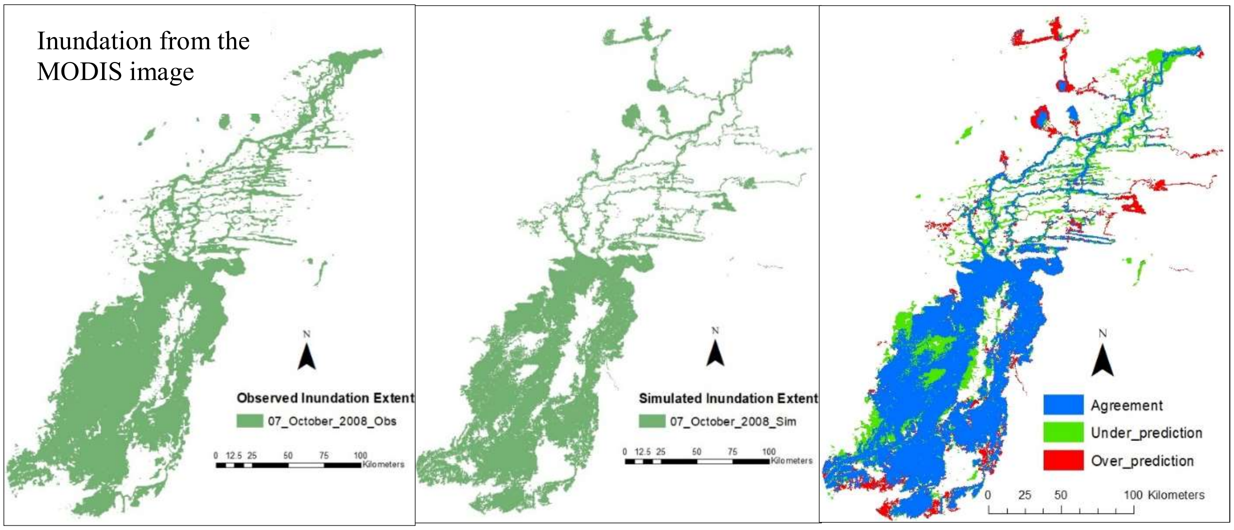

Fig. 6.5: Comparison of the observed and simulated inundation extent on 07 October 2008 during validation

6.3.2 Relationships between dimensionless water level and inundation during rising and receding waters

The simulated inundation extents of 1984-85, 1990-91, 1994-1995, 2001-2002, 2002-2003, 2008-2009 and their corresponding water levels at Mopti were processed to obtain dimensionless water levels and inundation values during rising and receding flood waters. The two timeseries were normalized using Equations 6.6 and 6.7. The rising and receding parts of the flood data were separated, and two curves were fitted to the relationship between scaled water levels and scaled inundation extents, one for the rising flood period and one for the receding period (Fig. 6.6, Table 6.6).

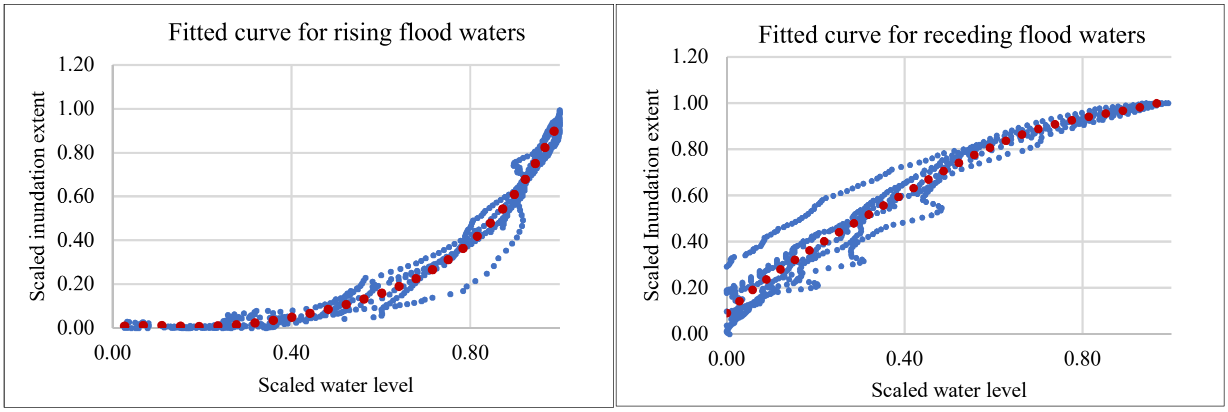

Fig. 6.6: Best fit curve of the relationship between scaled water levels and scaled inundation extent during the period of rising flood waters (left) and receding flood waters (right).

Table 6.6: Best fit curve of the relationship between the scaled water levels and the inundation extent during the period of rising flood waters (left) and receding flood waters (right).

Scale values during rising flood waters		Scale values during receding flood waters	
Water level (H_{sc})	Inundation (I_{sc})	Water level (H_{sc})	Inundation (I_{sc})
0.027	0.006	0.951	1.000
0.181	0.006	0.897	0.969
0.227	0.007	0.837	0.949
0.289	0.015	0.781	0.928
0.359	0.033	0.761	0.920
0.402	0.048	0.707	0.892
0.454	0.070	0.660	0.861
0.495	0.090	0.598	0.813
0.548	0.121	0.553	0.772
0.581	0.142	0.511	0.731
0.623	0.173	0.489	0.707
0.668	0.213	0.447	0.663

0.707	0.254	0.433	0.647
0.734	0.287	0.392	0.601
0.763	0.328	0.344	0.546
0.796	0.381	0.307	0.504
0.825	0.435	0.270	0.461
0.847	0.482	0.223	0.406
0.870	0.535	0.198	0.376
0.882	0.565	0.163	0.334
0.905	0.626	0.128	0.289
0.926	0.686	0.099	0.251
0.951	0.765	0.066	0.203
0.973	0.844	0.052	0.180
0.988	0.897	0.010	0.110
1.000	0.950	0.000	0.090

6.3.3 Estimation of maximum water level at Mopti

To develop a model that can forecast I_{max} and H_{max} from the pool of potential predictors, the timeseries of predictors were split into a calibration period and a validation period. The 1990-2001 and 2002-2009 periods were selected for the calibration and validation of Pool 1 and Pool 2 datasets. In Pool 3, the periods 1979-1998 and 1999-2009 were chosen for the calibration and validation periods, respectively. Forward and backward stepwise regression were applied to the calibration period to determine the best set of predictors in each of the three pools. The p-value used to select a predictor was set to 0.03, while the p-value used to drop a predictor was set to 0.1. Lower p-value was selected to guarantee the proper selection of appropriate predictors and to avoid multicollinearity among the variables. Table 6.7 shows the list of selected predictors for each pool.

Table 6.7: Selected predictor in each Pool.

Predictor	Pool 1	Pool 2	Pool 3
1	Average discharge during August at Kankan ($\bar{Q}_{Aug}^{Kankan}$)	Maximum discharge during September at Koulikoro ($Qmax_{Sep}^{Koulikoro}$)	Average precipitation during April in watershed 31 (PCP_{Apr}^{31})
2	Average discharge during September discharge at KeMacina ($\bar{Q}_{Sep}^{KeMacina}$)	Maximum discharge during September Ke-Macina $Qmax_{Sep}^{Ke\ macina}$)	Average precipitation during June in watershed 29 (PCP_{Jun}^{29})
3	-	-	Average precipitation during July in watershed 21 (PCP_{Jul}^{21})
4	-	-	Average precipitation during August in watershed 13 (PCP_{Aug}^{13})

The equations of the linear regression models (LM) obtained for each dataset pool are as follows:

Pool 1:

$$LM_1 = 264.0822 - 0.0005\bar{Q}_{Aug}^{Kankan} + 0.001223\bar{Q}_{Sep}^{Ke\ Macina} \tag{6.13}$$

Pool 2:

$$LM_2 = 265.08884 - 0.00178Qmax_{Sep}^{Koulikoro} + 0.00069Qmax_{Sep}^{Ke\ Macina} \tag{6.14}$$

Pool 3:

$$LM_3 = 262.7047 - 0.0035293PCP_{Apr}^{31} + 0.0072037PCP_{Jun}^{29} + 0.0.0085746PCP_{Jul}^{21} + 0.0027352PCP_{Aug}^{13} \tag{6.15}$$

The comparison between modeled (from Pools 1 to 3) and observed maximum water levels at Mopti is shown in Fig. 6.7.

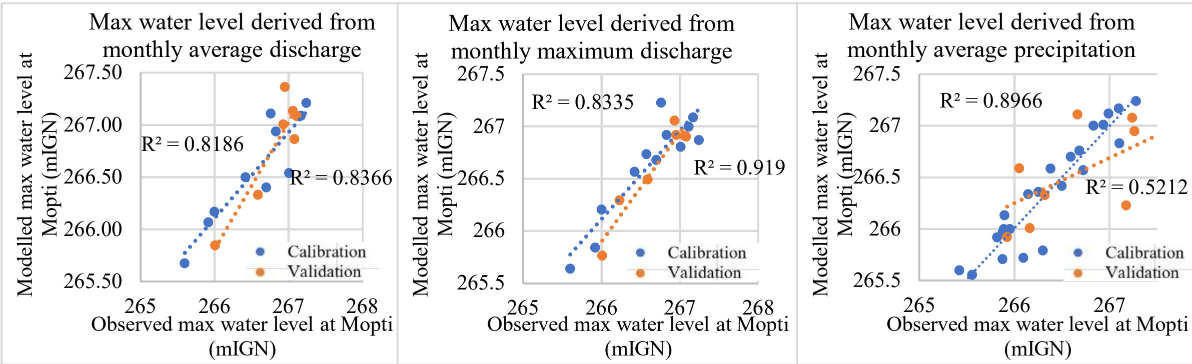

Fig. 6.7: Linear regression model (LM) for Pool 1 (left), Pool 2 (middle), and Pool 3 (right).

The R^2 values for the relationships obtained from pools 1, 2, and 3 are 0.8186, 0.8355 and 0.8966 respectively, during the calibration period, versus 0.8366, 0.919, and 0.5212 during the validation period. The R^2 values were high for both calibration and validation periods (except for pool 3 during the validation period). The outputs of the three linear models were combined through multiple linear regression techniques. We initially intended to include all the best predictors in Pool 1, Pool 2 and Pool 3, directly, into the regression, however, could not be able to do so because the data set contain variable time span. Forcing the data into equal time span led lower R^2 in the regression. Then, we decided to take only the outputs of three linear model (LM_1, LM_2, LM_3) to make the regression equation. The following equation was obtained to estimate the maximum water level at Mopti:

$$H_{max} = -48.4807 + 0.49133 * LM_1 + 0.32663 * LM_2 + 0.36391 * LM_3 \quad (6.16)$$

where H_{max} is the maximum water level at Mopti in mIGN (IGN: datum of Institut national de l'information's). A comparison between the observed and estimated maximum water level using equation 6.16 at Mopti is shown in Fig. 6.8. High R^2 values during both calibration and validation imply the equation can be used for future applications.

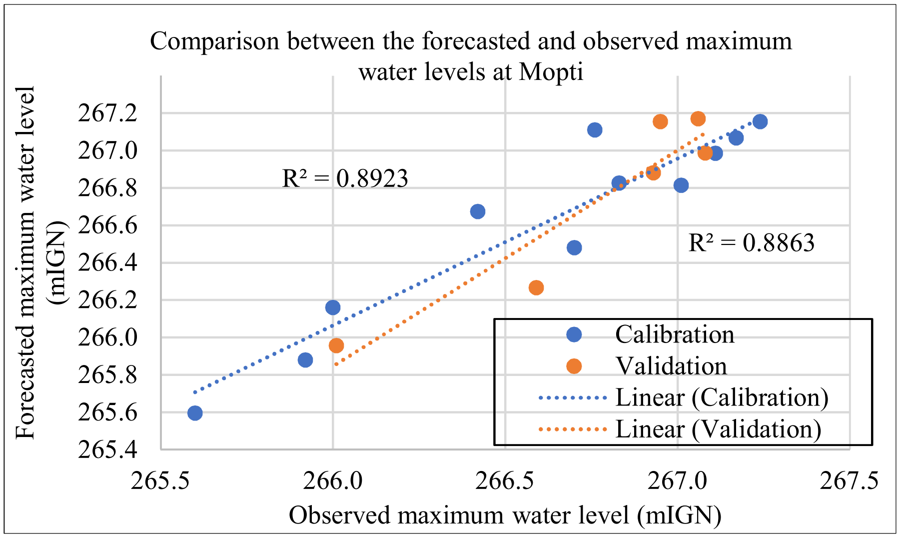

Fig. 6.8: Comparison between the forecasted and observed maximum water levels at Mopti.

The maximum inundation extent is needed to solve equations 6.8 and 6.9. A linear model is established using the relationship between the maximum water level at Mopti and the simulated maximum inundation. The equation is shown below:

$$I_{max} = 7376.862 * H_{max} - 1952780 \quad (6.17)$$

where I_{max} is the maximum inundation extent and H_{max} is the maximum water level at Mopti. Once the maximum water level at Mopti is known, the maximum inundation value can be determined by using Equation 6.17.

Both the maximum water level at Mopti and maximum inundation can be forecasted ahead of time because both the events take place after 30th September. The timing of maximum water level at Mopti and maximum inundation at IND is presented in

. The event of maximum water level at Mopti and maximum inundation takes place well after the day- September 30 of each year. The time between the actual day of occurrence of the peak water level and 30 September is the lead time. The lead time depends on the magnitude of the water level i.e. the higher the maximum water level at Mopti the higher is the lead time.

Table 6.8:: Lead time of the forecasted maximum water level and peak inundation extent

Year	Peak water level at KeMacina		Maximum water level at Mopti			Maximum inundation at IND		
	Water level (mIGN)	Date	Water level (mIGN)	Date	Time lag from Kemacina (day)	Inundation (km2)	Date	Lead time (days) from 30th September
1990-91	273.45	26-Sep	265.92	9-Oct	13	9147	22-Oct	23
2002-03	274.08	28-Sep	266	8-Oct	10	11958	28-Oct	31
2001-02	275.46	21-Sep	266.83	18-Oct	27	15876	30-Oct	30
2008-09	275.13	29-Sep	266.95	23-Oct	24	16755	3-Nov	34
1994-95	275.36	20-Oct	267.17	3-Nov	14	19233	24-Nov	55

6.3.4 Validation of the inundation extent function

The developed relationship between water levels at Mopti and the inundation extent was validated using data from 2010-2011 and 2005-2006. The 2010-2011 hydrological year was a relatively wet year, while 2005-2006 was a relatively dry year. The maximum water level at Mopti and the corresponding maximum inundation were forecasted using equations 6.16 and 6.17, respectively. The predicted inundation extents were compared to the predictions using the equations proposed by Mahe et al. (2011), Zwart et al. (2005), and Mariko (2003) and are shown in Fig. 6.9.

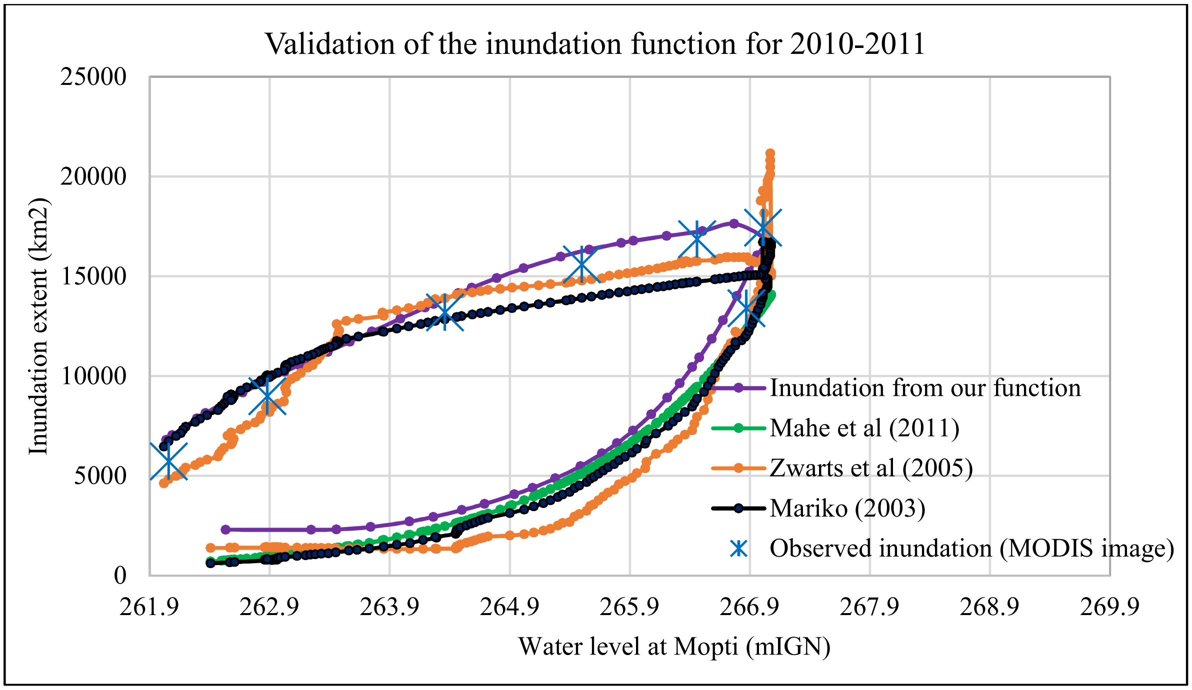

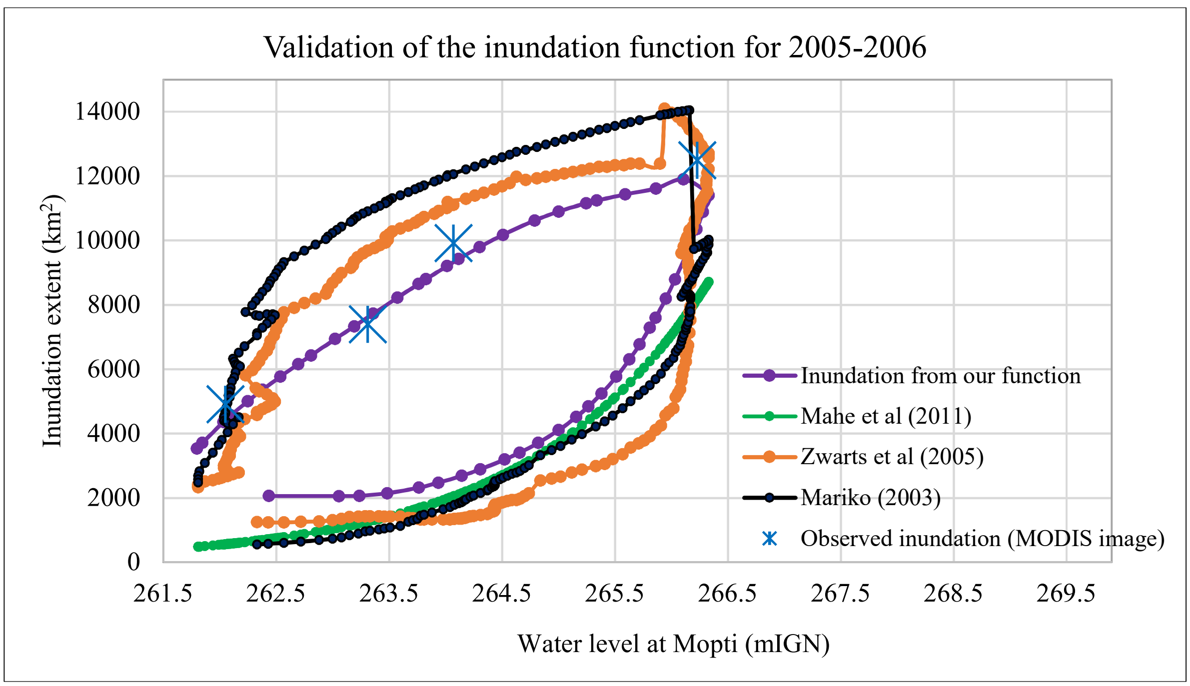

Fig. 6.9: Validation of the inundation extent for 2010-2011 (top) and 2005-2006 (bottom)

Results show Mariko (2003), and Zwart et al. (2005) underestimate the inundation extent during the period of receding water in the wet year (2010-2011) and overestimate it during the dry year (2005-2006). The method developed in this paper better represents the reference inundation obtained from MODIS images in the receding water period. Another advantage of the method proposed in this paper is that the maximum inundation extent is explicitly forecasted, while it is unknown when one uses the formulas derived by Zwarts et al. (2005) and Mariko (2003). The user would therefore not know when to switch from using the equation that represents the rising flood period to the equation that represents the receding period. Bates et al. (1997) also found that the extrapolation of satellite-derived inundation functions is not feasible during high flood periods. Several studies have highlighted the relationship between flood dynamics, particularly the maximum inundation extent, and the quality of ecosystem services in the IND. By explicitly forecasting the maximum inundation extent and providing a more accurate way to estimate flooded areas in the IND using a readily available variable (water level at Mopti), the method developed in this paper can generate useful information for decision-makers. They can, for instance, know how far a flood is likely to travel and inform rice growers of the optimal area to plant in a particular year. They can anticipate the amount and extent of forage that will be available for herders. They will also be able to infer the accessibility of remote villages by road and by boat simply by looking at the measured water levels at Mopti.

6.4 Conclusions

A time-varying relationship between water levels at Mopti station and inundation extent in the IND was developed in this paper. Simulated time series of water levels and inundation extents were first generated using a two-dimensional hydrodynamic model of the IND that was set up, calibrated, and validated for discharge, water level, and inundation extent. The simulated timeseries of water levels and inundated areas were used to build a relationship between water levels and inundation areas. The relationship is conditioned on the maximum water level and maximum flooded area. Finally, stepwise regression was used to develop a non-stationary relationship that can forecast maximum water levels and maximum inundation in the IND using observed streamflow and precipitation. Results show that in addition to explicitly forecasting the maximum inundation extent ahead of time, the inundation extent predicted with the new method is also more accurate than predictions calculated from formulas currently in use for the IND. This study can help provide valuable information to anticipate resource availability and optimize socio-economic activities in the IND.

Chapter 7

Conclusions and recommendation for future works

7.1 Conclusions

In this thesis, we have proposed procedures for the development of 2D hydrodynamic numerical models to simulate variables such as water level, discharge, and inundation extent in a large floodplain in data-sparse regions. The study area is the Inner Niger Delta. Special emphasis set on the derivation of topographic and bathymetric data, given that that they greatly affect the accuracy of the simulation yet are not readily available with the required precision and resolution in the study area. Six different hydrodynamic models of the Inner Niger Delta (IND) in Mali were developed using three different DEMs and two different downstream boundary conditions. The elevation data comes from two global DEMS (SRTM and MERIT) and a DEM derived from satellite imagery and water levels observations using the waterline methods. Given the data scarcity in the area, a considerable amount of input data such as bathymetry, river network, friction coefficient, and inundation extent were derived from secondary sources, leading to a high level of uncertainty in the simulations. The developed six models showed unequal performances in simulating water levels, discharges, and floodplain extent, with none of them outperforming the others in all fronts. Bayesian Model Averaging (BMA) was used to produce a more robust estimate of water levels and discharges using all six model outputs. It was found that specifying water levels as boundary conditions generally lead to better simulations, presumably because the calculation of water levels is more precise than the calculation of discharge in TELEMAC 2D. MERIT DEM is overall the best DEM among the ones considered in this paper as it is a version of SRTM that was post-processed to improve hydrodynamic simulations. Bayesian Model Averaging (BMA) was used to produce a more robust estimate of water levels and discharges using all six model outputs. The results of the BMA allow users to have simulations of water levels and discharge that is more reliable than the ones provided by individual models.

A particularity of the IND is that a severe hysteresis effect is present in stage-discharge relationships at all hydrometric stations. Existing hydrodynamic models of the IND use a static stage-discharge relationship as a downstream boundary condition during both the rise and recession of the flood, leading to potential inaccuracies in the simulation of the flood extent. Horritt (2000) observed that the accuracy of the simulations near the downstream boundary might be strongly affected when a hysteresis effect is present. He also noticed that the impact of the downstream boundary condition for dynamic circumstances would be distinct, and its impact may extend further upstream. In this study, the impact of the inclusion or not of the hysteresis effect in the rating curve at the downstream boundary of a hydrodynamic model of the IND is investigated. Two methods for reproducing the hysteresis effect in the downstream boundary conditions, one based on dimensionless discharges and levels and the other based on the modified Jones formula, were examined. Simulation results are compared using RMSE, ARE, and NS values. It is found that loop rating curve improves the simulation in the downstream area particularly on water level, discharge and inundation simulations. It also allows for the indirect simulation of the connectivity to ecologically important lakes in the IND. Improvement in the results suggests that if an area is subjected to hysteresis effect, hydrodynamic simulation is to perform with looped rating to obtain better simulation results.

Finally, a novel time-varying relationship between water levels at the Mopti station and inundation extent in the Inner Niger Delta (IND) is developed in this thesis. Simulated time-series of water levels and inundation extents were first generated using a two-dimensional hydrodynamic model of the IND that was is set up, calibrated, and validated for discharge, water level, and inundation extent. The simulated time series of water levels and inundated areas are used to build a relationship between water levels and inundation areas. The relationship is conditioned on the maximum water level and maximum flooded area; finally, stepwise regression is used to develop a non-stationary relationship that can forecast maximum water levels and maximum inundation in the IND using observed streamflow and precipitation. Results show that besides explicitly forecasting the maximum inundation extent ahead of time, the inundation extent predicted with the new method is more accurate than the predictions of the formulas currently used for the IND. It has the potential to provide valuable information that can help anticipate resource availability and optimize socio-economic activities in the IND.

7.2 Limitations and constraints of the research

After highlighting all the merits of the techniques taken in this research work, we would also like to point out the limitations and constraints of the research work. Most of the limitations are due mainly to the lack of data available for model development. Three different types of data are recognized as a significant limitation on the performance of the developed models. These are topographic, bathymetric, and flood extent data. Because of the absence of high-resolution data, we had to resort to DEM's such as SRTM and MERIT. Another DEM was derived by combining water level and inundation extent derived from Landsat images. The vertical accuracy of these DEM's is not ideal for floodplain modeling. As observed by Horritt and Bates (2002) that topography is the most important factor for the estimation of flood extent. This resulted in significant inaccuracies in the modeled flood extents.

The bathymetric data used in the thesis is highly uncertain as it was estimated using the geometric equations proposed by Leopold and Maddock (1953). The river bed elevation of four locations such as KeMacina, Mopti, Akka, and Dire are hence approximative. The river bed elevations for the other points in the rivers and channels were estimated by assuming a linear variation based on those four locations.

The mesh size of the model in the northern part of the study area needs to be of finer resolution than the existing one. The existing mesh density is unsuitable for capturing the flood extent as the channel width in-between the east-west running dune is narrower than 300m (Dickens et al. 2018), which is lower than the smallest size of a mesh. Improvement of the flood extent in this region can be achieved if we can use increased mesh density, i.e. each mesh size is smaller than 300m.

The model did not include any infrastructure in the study area. The presence of bridge, culvert, embankment, and any other structural interventions in the domain may affect the flow characteristics. The simulation result can be improved with the inclusion of such structures with their proper dimensions and alignment.

Because of the absence of observed flood extent, Landsat and MODIS images were used for the delineation of flood extent maps. These maps were used for model setup, calibration, and validation purposes. Flood extent could not be derived properly because the resolution of images especially for MODIS image is low (about 500m). The fact that MODIS and Landsat use optical imagery also contributed to decrease the accuracy in the flood extent map. That inaccuracy most likely influenced the quality of calibration and analysis that was done on the satellite-derived inundation extent data.

Evaporation is an important parameter that influences the water balance at IND. A substantial amount of water loss takes place from IND due to evaporation. Evaporation was kept constant throughout the simulation, which may have influenced the accuracy of the result. We kept evaporation constant in our model to simplify the simulations. Exclusion of rainfall from the model may also have influenced the accuracy of the simulation result.

7.3 Recommendation for Future work

There are several other aspects of this work that can be considered to continue the research presented in this thesis:

Inclusion of time-varying evaporation and rainfall into the simulation

In this study, for the sake of simplicity, we have used constant evaporation. Evaporation in IND varies both spatially and temporally. Evaporation is closely proportional to the flood extent. Years with larger flood extent have higher evaporation than years with lower flood extent. The quality of the simulation can be improved by incorporating the yearly variation of the evaporation. While losses can be quantified from inflow and outflow, water level, and simulated inundation extent time series of IND, it has proven to be particularly difficult to separate evaporation from infiltration. Once a better estimate of the spatio-temporal variation of evaporation is obtained, it can be incorporated into the simulation in such a manner that in every time step a new evaporation value is calculated from the simulated water level, and the calculated evaporation can be used as an input for the next computation step. In this case, the TELEMAC source code needs to be modified to include the evaporation function in the simulation.

Rainfall was not considered into the model because that rainfall at the upper Niger basin drives the flooding pattern of the IND. Given that the IND is a large wetland, rainfall over the IND can affect the water balance. Considering rainfall into the model may improve the quality of the result. It is recommended to include the daily time series of rainfall during the simulation. This can be included in the simulation by modifying the TELEMAC source code.

Use of SAR image for the extraction of flood extent

The estimation of the inundated area can be improved by using freely available SAR images such as ENVISAT or high-resolution optical images such as Sentinel-1 and Sentinel-2.

Increasing the mesh resolution for the Northern part

The northern part of the IND contains east-west running dunes in between where the channels are situated. These dunes affect the flood propagation but are difficult to capture in the mesh, given that they are less than 300m wide (Dickens et al. 2018). A higher mesh resolution is needed to better capture the topography/bathymetry at this part.

Bathymetric survey at key locations

Bathymetric information can be improved and enriched by surveying key river cross-sections. It is recommended to collect cross-section data by surveying of the Niger river at least at the key locations such as KeMAcina, Mopti, Akka, Dire. Once cross-section data at upstream and downstream of each of the small channels are available, this would enrich the existing bathymetric data, and thus it helps improve the quality of the simulation result.

Environmental flow calculation

The developed model can be used to estimate environmental flow (hydrodynamic perspective) that is necessary for IND to maintain a habitat for ecosystem production. A time series of annual inundation can be derived from the model simulation. The magnitude of inundation corresponding to a given exceedance probability can be estimated and used for environmental flow estimation. Tennant (1976) recommended 10% of the mean annual flow (MAF) to be the lowest instantaneous flow to sustain short-term survival of aquatic life, while > 30% MAF was recommended to provide flows where the biological integrity of the river ecosystem as a whole was sustained. Here, we can adopt a value of the exceedance probability (say 70%) of inundation extent and determine the corresponding MAF. The maximum of the MAF among the hydrological and hydraulic methods can be selected as the desired environmental flow to be maintained for IND.

Forecasting maximum water level and maximum inundation

As discussed in Chapter 6, maximum inundation can be estimated if the maximum water level (MWL) at Mopti is known. Stepwise regression is applied to screen significant predictors to forecast the MWL. Three types of datasets were chosen for the method and ended up having a model that can forecast the MWL. It is found that MWL correlates with the precipitation of the Inner Niger basin, which is situated in the Sahel region. Several authors (Garric et al. 2002, Sittichok et al. 2014, Gado Djibo et al. 2015) were successful in predicting the precipitation in Sahel. They used datasets such as sea surface temperature (SST) (SST in equatorial Atlantic, equatorial Indian, eastern equatorial Pacific, southern tropical Indian oceans, Atlantic and the Pacific Ocean), southern oscillation index, sea level pressure, relative humidity, air temperature. A potential research topic is a systematic search of the best data sets among the predictors mentioned above using stepwise regression, to predict the maximum water level with a sufficient precision well before it is reached. This kind of information would be extremely useful for the water-dependent community in IND who can then prepare their land for cultivation according to the magnitude of the coming flood.

Chapter 8

References

Abbaspour, K.C. (2007) *User Manual for SWAT-CUP, SWAT Calibration and Uncertainty Analysis Programs*, Swiss Federal Institute of Aquatic Science and Technology, Eawag: Dübendorf, Switzerland. Available online: https://www.eawag.ch/de/abteilung/siam/software/ (accessed on 16 June 2017).

Amarnath, G., Umer, Y.M., Alahacoon, N., Inada, Y., (2015) Modelling the flood-risk extent using LISFLOOD-FP in a complex watershed: case study of Mundeni Aru River Basin. Sri Lanka. Proc. IAHS 370, 131–138, http://dx.doi.org/10.5194/piahs-92-1-2015.

Anusha, N. and Bharathi, B., (2019) Flood detection and flood mapping using multi-temporal synthetic aperture radar and optical data, *The Egyptian Journal of Remote Sensing and Space Sciences*, https://doi.org/10.1016/j.ejrs.2019.01.001

Archer, L., Neal, J.C., Bates, P.C., House, J.I. (2018) Comparing TanDEM-X data with frequently-used DEMs for Flood inundation modeling, *Water Res. Res.* doi:10.1029/2018WR023688.

Archer, D.R., Fowler, H.J. (2008). Using meteorological data to forecast seasonal runoff on the river Jhelum, Paksitan. *Journal of Hydrology, 361*, 10-23

Arnold, J.G., Moriasi, D.N., Gassman, P.W., Abbaspour, K.C., White, M.J., Srinivasan, R., Jha, M.K. SWAT: model use calibration, and validation. *Trans. Asabe, 55*, 1491–1508.

Arnold, J.G., Srinivasan, R., Muttiah, R.S., Williams, J.R. (1998) Large area hydrologic modeling and assessment—Part 1: Model development. *J. Am. Water Resour. Assoc. 34*, 73–89.

Aronica, G., Hankin, B., Beven, K. (1998) Uncertainty and equifinality in calibrating distributed roughness coefficients in a flood propagation model with limited data. *Adv. Water Resour. 22*, 349–365.

Asante, K.O., Artan, G.A., Pervez, S., Bandaragoda, C., Verdin, J.P. (2008) *Technical Manual for the Geospatial Stream Flow Model (GeoSFM): U.S. Geological Survey Open-File Report*, U.S. Geological Survey, Reston, Virginia, pp. 2007–1441, 65p. Available online: https://pubs.usgs.gov/of/2007/1441/pdf/ofr2008-1441.pdf (accessed on 21 September 2018)

Bates, P. D., de Roo, A. (2000) A simple raster-based model for flood inundation simulation, *J. Hydrol., 236*, 54–77, doi:10.1016/S0022-1694(00)00278-X.

Bates, P.D., Anderson, M.G., Hervouet, J.-M., Hawkes, J.C. (1997) Investigating the behavior of two-dimensional finite element models of compound channel flow. *Earth Surf. Process. Landf. 22*, 3–17.

Bates, P. D., Horrit, M. S., Smith C. N., and Mason. D., (1997) Integrating remote sensing observations of flood hydrology and hydraulic modeling, *Hydrol. Process.,* Vol. 11, 1777-1795

Bates PD, Marks KJ, Horritt MS (2003) Optimal use of high-resolution topographic data in flood inundation models. *Hydrological Processes 17*: 537–557.

Bates PD, Wilson MD, Horritt MS, Mason DC, Holden N, Currie A (2006) Reach scale floodplain inundation dynamics observed using airborne synthetic aperture radar imagery: data analysis and modeling. *J Hydrol 328*:306–318. DOI: 10.1016/j.jhydrol.2005.12.028

Bates, P.D. (2012). Integrating Remote Sensing Data with Flood Inundation Models: How Far Have We Got?, *Hydrol. Process., 26*: 2515-2521. doi: 10.1002/hyp.9374.

Beckers, J.V.L., Sprokkereef, E., Roscoe, K.L. (2008) Use of Bayesian Model Averaging to Determine Uncertainties in River Discharge and Water Level Forecasts. In Proceedings of the 4th International Symposium on Flood Defence: Managing Flood Risk, Reliability and Vulnerability, Toronto, Ontario, Canada.

Belaud, G., Cassan, L., Bader, J., Bercher, N., Feret, T. (2010) Calibration of a propagation model in large river using satellite altimetry. In Proceedings of the 6th International Symposium on Environmental Hydraulics, Athens, Greece, 23–25; pp. 23–25.

Bell, V. A., A. L. Kay, R. G. Jones, and R. J. Moore (2007), Development of a high resolution grid-based river flow model for use with regional climate model output, *Hydrol. Earth Syst. Sci.*, 11, 532– 549, doi:10.5194/hess-11-532-2007

Biancamaria, S., Bates, P., Boone, A., Mognard, N. (2009) Large-scale coupled hydrologic and hydraulic modeling of the Ob river in Siberia. *J. Hydrol. Elsevier, 379*, 136–150, doi:10.1016/j.jhydrol.2009.09.054.

Bredesen, A., Brown, C.J. (2019) Comparison of Hydrologic Model Performance Statistics Using Rain Gauge and NEXRAD Precipitation Input at Different Watershed Spatial Scales and Rainfall Return Frequencies for the Upper St. Johns River, Florida USA, *Proceedings*, 7, 11; doi:10.3390/ECWS-3-05806

Brookes, A.N., Hughes, T.J.R. (1982) Streamline Upwind/Petrov-Galerkin formulations for convection dominated flows with particular emphasis on the incompressible Navier-Stokes Equations. *Comput. Methods Appl. Mech. Eng. 32*, 199–259.

CDKN (2014) *The IPCC's Fifth Assessment Report: What's in It for Africa?* Overseas Development Institute/Climate and Development Knowledge Network: London, UK, 35p. Available online: https://cdkn.org/wp-content/uploads/2014/04/AR5_IPCC_Whats_in_it_for_Africa.pdf (accessed on 14 January 2019).

Chelton, D.B., Ries, J.C., Haines, B.J., Fu, L.-L., Callahan, P.S. (2001) Satellite altimetry. *Int. Geophys.* 69, 1–2.

Chen, Z., Luo, J., Chen, N., Ren Xu, R., and Shen, G., (2019) RFim: A Real-Time Inundation Extent Model for Large Floodplains Based on Remote Sensing Big Data and Water Level Observations, Remote Sens. 2019, 11, 1585; doi:10.3390/rs11131585

CILSS (2016) Landscapes of Wet Africa- A Window on a changing world. U.S. Geological Survey, EROS, 47914 252nd St, Garretson, Sd 57030, United States (downloaded on 26 October 2019 from https://eros.usgs.gov/westafrica/node/147)

Cook A and Merwade V (2009) Effect of topographic data, geometric configuration and modeling approach on flood inundation mapping. *Journal of Hydrology 377*: 131-142.

Cracknell, A.P., Hayes, L.W.B., Keltie, G.F. (1987) Remote sensing of the Tay Estuary using visible and near infra-red data: mapping of the inter-tidal zone. *Proc. R. Soc. Edinb. 92B*, 223–236.

Da Silva, J.S., Calmant, S., Seyler, F., Rotunno Filho, O.C., Cochonneau, G., Mansur, W.J. (2010) Water levels in the Amazon basin derived from the ERS 2 and ENVISAT radar altimetry missions. *Remote Sens. Environ. 114*, 2160–2181.

Dadson, S.J., Ashpole, I., Harris, P., Davies, H.N., Clark, D.B., Blyth, E., Taylor, C.M. (2010) Wetland inundation dynamics in a model of land surface climate: Evaluation in the Niger inland delta region. *J. Geophys. Res. 115*, D23114, doi:10.1029/2010JD014474.

Deltares (1995) *D-Flow Flexible Mesh, User Manual,* draft version. Deltares: Delft, the Netherlands, 2015.

de Ferranti, J. (2014). Viewfinder Panorama. Available at: http://www.viewfinderpanoramas.org/dem3.html

Di Baldassarre, G. (2012). *Floods in a Changing Climate: Inundation Modeling* (International Hydrology Series). Cambridge: Cambridge University Press. doi:10.1017/CBO9781139088411

Di Baldassarre G, Schumann G, Bates PD, Freer JE and Beven KJ (2010) Flood-plain mapping: a critical discussion of deterministic and probabilistic approaches. *Hydrology Science Journal 55(*3): 364-376.

Dickens, C., O'Brien, G., Stassen, S., Eriyagama, N., Kleynhans, M., Rowntree, K., Graham, M., Ross-Gillespie, V., MacKenzie, J., Wymenga, E., Mapedza, E., (2018) *E-FLOWS FOR THE UPPER AND INNER NIGER DELTA, PHASE 1: Specialist Reports Hydrology, Hydraulics, Geomorphology, Water Quality.* Report by the International Water Management Institute. CGIAR Research Program on Water, Land and Ecosystems (WLE). 99p.

DLR (2018) Utilization of the TanDEM-X 90m DEM Data Products for Scientific Use. Available at https://tandemx-90m.dlr.de

Domeneghetti, A., Schumann, G.J., Tarpanelli, A. (2019) Preface: Remote Sensing for Flood Mapping and Monitoring of Flood Dynamics. *Remote Sens. 11*, 943.

Domeneghetti, A., Tarpanelli, A., Brocca, L., Barbetta, S., Moramarco, T., Castellarin, A., Brath, A. (2014) The use of remote sensing- derived water surface data for hydraulic model calibration. *Remote Sens. Environ. 149*, 130–141. [CrossRef]

Dottori, F., Martina, M. L. V., and Todini E., (2009) Dynamic rating curve approach to indirect discharge measurement, *Hydrol. Earth Syst. Sci., 13*, 847–863

Draper, D. (1995) Assessment and propagation of model uncertainty. *J. R. Stat. Soc. Ser. B, 57*, 45–97, doi:10.2307/2346087.

Duan, Q., Ajami, N.K., Gao, X., Sorooshian, S. (2007) Multi-model ensemble hydrologic prediction using Bayesian model averaging. *Adv. Water Res. 30*, 1371–1386, doi:10.1016/j.advwatres.2006.11.014.

Dung NV, Merz B, Ba´rdossy A, Thang TD, Apel H (2011) Multi-objective automatic calibration of hydrodynamic models utilizing inundation maps and gauge data. *Hydrol Earth Syst Sci 15*:1339–1354. doi:10.5194/hess-15-1339-2011

Ekeu-wei, I.T., Blackburn, G.A. (2018) Applications of Open-Access Remotely Sensed Data for Flood Modeling and Mapping in Developing Regions. *Hydrology 5*, 39.

European Space Agency (ESA) . Altimetry Instrument Payload. Available online: https://sentinel.esa.int/web/sentinel/missions/sentinel-3/instrument-payload/altimetry (accessed on 26 April 2016).

Farr, T. G., Rosen, P. A., Caro, E., Crippen, R., Duren, R., Hensley, S., et al. (2007). The shuttle radar topography mission. *Rev. Geophys. 45*:RG2004. doi: 10.1029/2005rg000183

Frappart, F., Calmant, S., Cauhopé, M., Seyler, F., Cazenave, A. (2006) Preliminary results of ENVISAT RA- 2- derived water levels validation over the Amazon basin. *Remote Sens. Environ. 100,* 252–264

Fu, L.-L., Alsdorf, D., Rodriguez, E., Morrow, R., Mognard, N., Lambin, J., Vaze, P., Lafon, T. (2009) The SWOT (Surface Water and Ocean Topography) mission: Spaceborne radar interferometry for oceanographic and hydrological applications. Proc. Ocean. Obs. 9, 21–25.

Gado Djibo, A., Seidou, O., Karambiri, H., Sittichok, K., Paturel, J.E., Saley, H.M. (2015). Development and assessment of non-linear and non-stationary seasonal, *Journal of Hydrology: Regional Studies 4,* 134–152, http://dx.doi.org/10.1016/j.ejrh.2015.05.001

Gallien T. W., Sanders, B.F. Flick, R.E. (2014) Urban coastal flood prediction: Integrating wave overtopping, flood defenses and drainage, *Coastal Engineering 91*, 18–28, doi.org/10.1016/j.coastaleng.2014.04.007

Georgakakos, K.P., Seo, D.J., Gupta, H. Schake J. and Butts, M. B., (2004) Characterizing streamflow simulation uncertainty through multimodel ensembles. *Journal of Hydrology, 298* (1-4), 222-241.

Grimaldi, S., Li, Y., Pauwels, V.R.N., Walker, J. P., (2016) Remote Sensing-Derived Water Extent and Level to Constrain Hydraulic Flood Forecasting Models: Opportunities and Challenges, *Surv Geophys 37:*977–1034, DOI 10.1007/s10712-016-9378-y

Guthke, A., Höge, M., Nowak, W. (2017) Bayesian model evidence as a model evaluation metric, Geophysical Research Abstracts, Volume 19, EGU2017-PREVIEW, EGU General Assembly. Available online: https://meetingorganizer.copernicus.org/EGU2017/EGU2017-13390-1.pdf (accessed on 8 August 2019).

Haan, C.T. (2002) *Statistics Methods in Hydrology*, 2nd Edition, Iowa State Univ Press, Ames, Iowa

Haag, A.V. (2015) Coupling A Large-Scale Hydrological Model to a High-Resolution Hydrodynamical Model, A Study of Floods within the Niger Inner Delta as a First Step towards a Potential Global Application. Master's Thesis, Department of Physical Geography and Faculty of Geoscience, Utrecht University, Utrecht, The Netherlands.

Haque, M.M., Seidou, O., Mohammadian, A., Djibo, A.G., Liersch, S., Fournet, S., Karam, S., Perera, E.D.P., Kleynhans, M. (2019) Improving the Accuracy of Hydrodynamic Simulations in Data Scarce Environments Using Bayesian Model Averaging: A Case Study of the Inner Niger Delta, Mali, West Africa. *Water*, *11*, 1766. https://doi.org/10.3390/w11091766

Haque, M.M., Seidou, O., Mohammadian, A. (2019b) Effect of rating curve hysteresis on flood extent simulation with a 2D hydrodynamic model: a case study of the Inner Niger Delta, Mali, West Africa, (Submitted)

Hawker, L., Bates, P., Neal, J., Rougier, J. (2018) Perspectives on Digital Elevation Model (DEM) Simulation for Flood Modeling in the Absence of a High-Accuracy Open Access Global DEM. Front. *Earth Sci. 6*, 233, doi:10.3389/feart.2018.00233.

Herschy, R. W. (1995) *Streamflow Measurement* (second edn). E & FN Spon, London, UK.

Hervouet, J.M. (2007) *Hydrodynamics of Free Surface Flows Modeling with the Finite Element Method*, Wiley: New York, NY, USA.

Hey, R.D., Thorne, C.R. (1986) Stable channels with mobile gravel beds. *J. Hydraul. Eng. 112*, 671–689.

Hoeting, J.A., Madigan, D., Raftery, A.E., Volinsky, C.T. (1999) Bayesian model averaging: A tutorial. *Stat. Sci. 14*, 382–417.

Horritt, M. S. (2000) Calibration of a Two-Dimensional Finite Element Flood Flow Model Using Satellite Radar Imagery, Water Resources Research, Vol. 36, No. 11, pp. 3279-3291. doi:10.1029/2000WR900206

Horritt, M.S., and Bates, P.D., (2001) Predicting floodplain inundation: raster-based modelling versus the finite element approach. Hydrological Process 15,825–842.

Horritt, M., and Bates, P. (2002). Evaluation of 1D and 2D numerical models for predicting river flood inundation. *J. Hydrol. 268*, 87–99. doi: 10.1016/S0022-1694(02)00121-X

Hostache R, Lai X, Monnier J, Puech C (2010) Assimilation of spatially distributed water levels into a shallow-water flood model. Part II: use of a remote sensing image of Mosel River. *J Hydrol 390*:257–268. doi:10.1016/j.jhydrol.2010.07.003

Hunter NM, Bates PD, Horritt MS, De Roo APJ, Werner MGF (2005) Utility of different data types for calibrating flood inundation models within a GLUE framework. *Hydrology and Earth System Sciences 9*: 412-430.

ISO (International Standards Organisation) (1998) *ISO 1100/2: Determination of the Stage–Discharge Relation*. ISO, Geneva, Switzerland.

JAXA (2018) ALOS World 3D-30m (AW3D30), Version 2, Global Digital Surface Model, Earth Observation Research Center (EORC), Japan Aerospace Exploration Agency. Available online: https://www.eorc.jaxa.jp/ALOS/en/aw3d30/index.htm (accessed on 30 December 2018).

Jarihani, A.A., Callow, J.N., McVicar, T.R., Van Niel, T.G., Larsen, J.R. (2015) Satellite- derived Digital Elevation Model (DEM) selection, preparation and correction for hydrodynamic modeling in large, low- gradient and data- sparse catchments. *J. Hydrol. 524*, 489–506.

Jones, B. E. (1916) A method of correcting river discharge for a changing stage. *US Geol. Survey Water Supply Paper 375-E*.

Kaplan, K and Avdan, U. (2017) ISPRS Annals of the Photogrammetry, Remote Sensing and Spatial Information Sciences, Volume IV-4/W4, 2017 4th International GeoAdvances Workshop, Safranbolu, Karabuk, Turkey

Karim, F., Petheram, C., Marvanek, S., Ticehurst, C., Wallace, J., and Gouweleeuw, B., (2011) The use of hydrodynamic modeling and remote sensing to estimate floodplain inundation, 19th International Congress on Modeling and Simulation, Perth, Australia.

Kennedy, R. W. (1984) Discharge ratings at gaging stations. In: *Techniques of Water-Resources Investigations,* Book 3, Chapter 10. US Geol. Survey, Reston, Virginia, USA.

Kernkamp, H. W. J., van Dam, A., Stelling, G. S., de Goede,E. D. (2011) Efficient scheme for the shallow water equations on un-structured grids with application to the Continental Shelf, *Ocean Dynam*., *61*, 1175–1188, doi:10.1007/s10236-011-0423-6.

Koblinsky, C., Clarke, R., Brenner, A., Frey, H. (1993) Measurement of river level variations with satellite altimetry. *Water Resour. Res. 29*, 1839–1848.

Korecha, D., Barnston, A.G. (2006). Predictability of June-September rainfall in Ethiopia. *Monthly Weather Review*, 135, 628-650

Krishnamurti et al (2000) Multimodel ensemble forecasts for weather and seasonal climate. *J. Climate*, 13**,** 4196–4216.

Lai X, Liang Q, Yesou H, Daillet S (2014) Variational assimilation of remotely sensed flood extents using a 2-D flood model. *Hydrol Earth Syst Sci 18*:4325–4339. doi:10.5194/hess-18-4325-2014

Leopold, L.B. (1994) *A View of the River: Cambridge, Mass*, Harvard University Press, Cambridge, Massachusetts, USA.

Leopold, L.B., Maddock, T.J. (1953) The hydraulic geometry of stream channels and some physiographic implications. *U.S. Geol. Surv. Prof. Pap. 252*, 1–57.

Lian, Y., Chan, I., Singh, J., Demissie, M., Knapp, V. and Xie, H. (2007). Coupling of hydrologic and hydraulic models for the Illinois River Basin. *Journal of Hydrology, 344*, 210-222.

Legates, D.R., McCabe, J.G.J. (1999). Evaluating the use of goodness-of-fit measures in hydrologic and hydroclimatic model validation, *Water Resour. Res*., 35, 1, 233-241.

Liersch, S., Fournet, S., Koch, H. (2019) *Assessment of Water Management and Climate Change Impacts on the Water Resources in the Upper Niger and Bani River Basins*, BAMGIRE

Programme Final Report, Potsdam Institute for Climate Impact Research:Potsdam, Germany, Wetlands International: Mali, The Netherlands.

Liersch, S., Fournet, S., Koch, H., Djibo, A.G., Reinhardt, J., Kortlandt, J., Van Weert, F., Seidou, O., Klop, E., Baker, C., Hattermann F., F. (2019) Water resources planning in the Upper Niger River basin: Are there gaps between water demand and supply? *J. Hydrol. Reg. Stud. 21*, 176–194.

Liersch, S., Cools, J., Kone, B., Koch, K., Diallo, M., Reinhardt, J., Fournet, S., Aich, A., Hattermann, F.F., (2012) Vulnerability of rice production in the Inner Niger Delta to water resources management under climate variability and change, *environmental science & Policy, 34, 18- 33*, doi.org/10.1016/j.envsci.2012.10.014

Loveland, T.R., Reed, B.C., Brown, J.F., Ohlen, D.O., Zhu, Z., Yang, L., Merchant, J.W. (2000) Development of a global land cover characteristics database and IGBP DISCover from 1 km AVHRR data. *Int. J. Remote Sens. 21*, 1303–1330, doi:10.1080/014311600210191.

Madigan, D., Raftery, A.E., Volinsky, C., Hoeting, J. (1996) Bayesian model averaging. In Proceedings of the AAAI Workshop on Integrating Multiple Learned Models, Portland, Oregon, pp. 77–83.

Mahé, G., F. Bamba, F., Soumaguel, A., Orange, D. & Olivry, J. C. (2009) Water losses in the Niger River inner delta: water balance and flooded surfaces. *Hydrol. Processes* **23**(22), 3157–3160.

Mahé, G., Orange, D., Mariko, A., Bricquet, J.P. (2011) Estimation of the flooded area of the Inner Delta of the River Niger in Mali by hydrological balance and satellite data. IAHS Publ. vol. 344, pp. 138–143.

Maiga, F. (2019) Hydrological Impacts of Irrigation Schemes and Dams Operation in the Upper Niger Basin and Inner Niger Delta. Master's Thesis, University of Ottawa, Ottawa, Canada.

Malinowski, R., & Schwanghart, W. (2017) Do Remote Sensing Mapping Practices Adequately Address Localized Flooding? A Critical Overview. *Springer Science Reviews*. https://doi.org/10.1007/s40362-017-0043-8

Marchuk, G.I. (1975) *Methods of Numerical Mathematics*, Springer: New York, NY, USA, 316p.

Mariko, A., (2003) Caractérisation et suivi de la dynamique de l'inondation et du couvert végétal dans le Delta intérieur du Niger (Mali) par télédétection. PhD thesis, Université Montpellier 2, France.

Mason, D.C., Davenport, I.J., Flather, R.A., Gurney, C. (1998) A digital elevation model of the inter-tidal areas of the Wash, England, produced by the waterline method. *Int. J. Remote Sens. 9*, 1455–1460, doi:10.1080/014311698215289.

McCuen, R.H., Rawls, W.J. and Whaley, B.L. (1979) Comparative evaluation of statistical methods for water supply forecasting. Water Resources Bulletin American
Water Resources Association, 15, 935-947.

McFeeters, S.K. (1996) The use of the Normalized Difference Water Index (NDWI) in the delineation of open water features. *Int. J. Remote Sens. 17* (7), 1425–1432.

McLachlan, G.J., Krishnan, T. (1997) *The EM Algorithm and Extensions*, Wiley: New York, NY, USA.

Mishra, S.K. & Seth, S.M. (1996) Use of hysteresis for defining the nature of flood wave propagation in natural channels, *Hydrological Sciences Journal, 41*: 2, 153-170, DOI: 10.1080/02626669609491489

Monteith, J.L. (1965) Evaporation and environment. In *The State and Movement of Water in Living Organisms*, Fogg, G.F., Ed., Cambridge University Press: Cambridge, UK, pp. 205–234.

NASA JPL (2013) NASA Shuttle Radar Topography Mission Global 1 arc second, NASA EOSDIS Land Processes DAAC. 2013. Available online: https://earthexplorer.usgs.gov/ (accessed on 1 September 2016).

Nash, J.E. and Sutcliffe, J.V. (1970). River flow forecasting through conceptual models part I - a discussion of principles. *Journal of Hydrology, 10*, 282-290.

Neal, J., Schumann, G., Bates, P. (2012) A subgrid channel model for simulating river hydraulics and floodplain inundation over large and data sparse areas. *Water Resour. Res*. *48*, W11506, doi:10.1029/2012WR012514.

Neitsch, S.L., Arnold, J.G., Kiniry, J.R., Williams, J.R. (2005) *Soil and Water Assessment Tool, Theoretical Documentation: Version 2005*, USDA Agricultural Research Service and Texas A&M Blackl and Research Center: Temple,TX, USA.

Notti, D., Giordan, D., Caló, F., Pepe, A., Zucca, F., Galve, J.P. (2018) Potential and Limitations of Open Satellite Data for Flood Mapping. *Remote Sens. 10*, 1673.

Ogilvie, A., Mahé, G., Ward, J., Serpantié, G., Lemoalle, J., Morand, P., Barbier, B., Diop, A.T., Caron, A., Namara, R., Kaczan, D., Lukasiewicz, A., Paturel, J.-E., Liénou, G., Clanet, J.C., (2010) Water, agriculture and poverty in the Niger River basin. *Water Int. 35* (5), 594–622.

Ogilvie, A., Belaud, G., Delenne, C., Bailly, J., Bader, J., Oleksiak, A., Ferry, L., Martin, D. (2015) Decadal monitoring of the Niger Inner Delta flood dynamics using MODIS optical data. *J. Hydrol. Elsevier, 523*, 368–383, doi:10.1016/j.jhydrol.2015.01.036.

O'Loughlin, F.E., Neal, J., Yamazaki, D., Bates, P.D. (2016) ICESat-derived inland water surface spot heights. *Water Resour. Res. 52,* 3276–3284. [CrossRef]

Opperman, J. Luster, R., McKenney, B., Roberts, M., Meadows A. W. (2010) Ecologically functional floodplains: Connectivity, flow regime, and scale. *Journal of the American Water Resources Association* 46(2):211-226.

OPIDIN (undated) Forecast Tool to Predict the Inundations in the Inner Niger Delta. Available online: https://www.opidin.org/en/home (accessed on 9 August 2019).

Pappenberger, F., Beven, K., Horritt, M., Blazkova, S. (2005) Uncertainty in the calibration of effective roughness parameters in HEC-RAS using inundation and downstream level observations. *J. Hydrol*. *302*, 46–69.

Pappenberger, F., Matgen, P., Beven, K.J., Henry, J.B., Pfister, L., Fraipont, P. (2006) Influence of uncertain boundary conditions and model structure on flood inundation predictions. *Adv. Water*, *29*, 1430–1449.

Patel, S., Hardaha, M. K., Seetpal, M.K, Madankar, K. K. (2016) Multiple Linear Regression Model for Stream Flow Estimation of Wainganga River. *American Journal of Water Science and Engineering. Vol. 2*, No. 1, pp. 1-5. Doi: 10.11648/j.ajwse.20160201.11

Peterson-Overlier, A., (2006) Modeling stage-discharge relationships affected by hysteresis using the Jones formula and nonlinear regression, *Hydrological Sciences Journal-* 51:3, 365-388, DOI: 10.1623/hysj.51.3.365

Ponte, R.M., Wunsch, C., Stammer, D. (2007) Spatial mapping of time-variable errors in Jason-1 and TOPEX/Poseidon sea surface height measurements. *J. Atmos. Ocean. Technol. 24*, 1078–1085.

RRP- River Restoration Program (2016) Reconnecting Rivers to Floodpalians, Returning natural functions to restore rivers and benefit communities, American Rivers, Washington, DC, downloaded from https://s3.amazonaws.com/american-rivers-website/wp-content/uploads/2016/06/17194413/ReconnectingFloodplains_WP_Final.pdf

Raftery, A.E. (1993) Bayesian Model Selection in Structural Equation Models. In *Testing Structural Equation Models*, Bollen, K.A., Long, J.S., Eds., Sage: Beverly Hills, CA, USA, pp. 163–180.

Raftery, A.E., Gneiting, T., Balabdaoui, F., Polakowski, M. (2005) Using Bayesian model averaging to calibrate forecast ensembles. *Mon. Weather Rev. 133*, 1155–1174.

Ramsey, E.W. (1995) Monitoring Flooding in coastal wetlands by using radar imagery and ground-based measurements. *Int. J. Remote Sens. 16*, 2495–2502.

Ramsar (2004), Fact sheet, Inner Niger Delta, Mali, downloaded from https://www.ramsar.org/sites/default/files/documents/library/wwd2004_rpt_mali_press_e.pdf, accessed on 12 January 2018).

Rantz, S. E. *et al*. (1982) Measurement and computation of streamflow, vol. 2. Computation of discharge. US Geol. Survey Water Supply Paper 2175, US Geol. Survey, Reston, Virginia, USA.

Rexer, M., and Hirt, C. (2014). Comparison of free high resolution digital elevation data sets (ASTER GDEM2, SRTM v2.1/v4.1) and validation against accurate heights from the Australian National Gravity Database. *Aust. J. Earth Sci. 61*, 213–226. doi: 10.1080/08120099.2014.884983

Rizzoli, P., Martone, M., Gonzalez, C., Wecklich, C., Borla Tridon, D., Bräutigam, B., et al. (2017). Generation and performance assessment of the global TanDEM-X digital elevation model. *ISPRS J. Photogramm. Remote Sensing 132,* 119–139. doi:10.1016/j.isprsjprs.2017.08.008

Robinson, N., Regetz, J., and Guralnick, R. P. (2014). EarthEnv-DEM90: a nearlyglobal, void-free, multi-scale smoothed, 90m digital elevation model from fused ASTER and SRTM data. *ISPRS J. Photogramm. Remote Sensing 87*, 57–67. doi: 10.1016/j.isprsjprs.2013.11.002

Rodríguez, E., Morris, C.S., Belz, J.E. (2006) A global assessment of the SRTM performance. *Photogramm. Eng. Remote Sens. 72*, 249–260, doi:10.14358/PERS.72.3.249.

Rouse, J., Haas, J.A., Schell, J.A., Deering, D.W., 1973. Monitoring vegetation systems in the Great Plains with ERTS. In: Proceedings 3rd ERTS Symposium. NASA, SP353, Washington DC, USA, pp. 309–317.

Sakamoto, T., Van Nguyen, N., Kotera, A., Ohno, H., Ishitsuka, N., Yokozawa, M. (2007) Detecting temporal changes in the extent of annual flooding within the Cambodia and the Vietnamese Mekong Delta from MODIS time-series imagery. *Remote Sens. Environ. 109*, 295–313.

Sanyal, J., and Lu, XX. (2004) Application of remote sensing in flood management with special reference to monsoon Asia: a review. Natural Hazards 33:283–301.

Sanyal, J., Carbonneau, P., Densmore, A.L. (2013) Hydraulic routing of extreme floods in a. large ungauged river and the estimation of associated uncertainties: A case study of the Damodar River, India. *Natural Hazards 66 (*2), 1153–1177, http://dx.doi.org/10.1007/s11069-012-0540-7.

Sayama, T., Ozawa, G., Kawakami, T., Nabesaka, S., Fukami, K., (2012) Rainfall–runoff–inundation analysis of the 2010 Pakistan flood in the Kabul Riverbasin. Hydrological Sciences Journal 57 (2), 298–312, http://dx.doi.org/10.1080/02626667.2011.644245.

Shamseldin, A. Y., O'Connor, K.M., Liang, G. C. (1997) Methods for combining the outputs of different rainfall–runoff models. *J. Hydrol., 197,* 203–229.

Sanyal, J., Carbonneau, P., Densmore, A. L. (2014) Low-costinundation modeling at the reach scale with sparse data in the Lower Damodar River basin, India, *Hydrological Sciences Journal, 59*:12, 2086-2102, DOI: 10.1080/02626667.2014.884718

Schneider, R., Godiksen, P.N., Villadsen, H., Madsen, H., Bauer-Gottwein, P. (2016) Application of CryoSat- 2 altimetry data for river analysis and modeling. *Hydrol. Earth Syst. Sci.* Discuss. 19, 1–19.

Schöniger, A., Wöhling, T., Nowak,W. (2014) Model selection on solid ground: Rigorous comparison of nine ways to evaluate Bayesian model evidence. *Water Resour. Res*. *50*, 9484–9513, doi:10.1002/2014WR016062.

Schumann G, Hostache R., Puech C., Hoffmann L., Matgen P., Pappenberger F., Pfister L., (2007) High resolution 3-D flood information from radar imagery for flood hazard management. *Geosci Remote Sens IEEE Trans 45*:1715–1725. doi:10.1109/TGRS.2006.888103

Schumann, G.J.-P., Andreadis, K.M., Bates, P.D. (2014) Downscaling coarse grid hydrodynamic model simulations over large domains. *J. Hydrol*. *508*, 289–298, doi:10.1016/j.jhydrol.2013.08.051.

Schwatke, C., Dettmering, D., Börgens, E., Bosch, W. (2015) Potential of SARAL/AltiKa for Inland Water Applications. Mar. Geodesy, 38, 626–643.

Seidou, O. (2019) Development of Models and Tools in Support of the BAMGIRE Program, Final Report, Wetlands International and University of Ottawa: Ottawa, Canada.

Shamseldin, A. Y., O'Connor, K.M., Liang, G. C. (1997) Methods for combining the outputs of different rainfall–runoff models. *J. Hydrol., 197,* 203–229.

Sun, W., Song, H., Cheng, T., Yu, J. (2015) Calibration of hydrological models using TOPEX/Poseidon radar altimetry observations. *Proc. Int. Assoc. Hydrol. Sci.* 368, 3–8.

Steffler, P., J. Blackburn. (2002) *River2D. Two-Dimensional Depth Averaged Model of River Hydrodynamics and Fish Habitat.* Introduction to Depth Averaged Modeling and User's Manual. University of Alberta.Canada.

Stephens EM, Bates PD, Freer JE, Mason DC (2012) The impact of uncertainty in satellite data on the assessment of flood inundation models. *J Hydrol 414–415*:162–173. doi:10.1016/j.jhydrol.2011.10.040

Tadono, T., Ishida, H., Oda, F., Naito, S., Minakawa, K., and Iwamoto, H. (2014). Precise global DEM generation by ALOS PRISM. ISPRS Ann. Photogramm. *Remote Sensing Spat. Inf. Sci*. II 4, 71–76. doi: 10.5194/isprsannals-II-4-71-2014

Taylor, Peter J. (1977) Quantitative Methods in Geography: An Introduction to Spatial Analysis. Houghton Mifflin Harcourt, Boston, Massachusetts (396 pp.).

TELEMAC -2D User Manual (2017), Version 7.2, EDF-R&D.

Tockner, K., Stanford, J.A. (2002) Review of: Riverine Flood Plains: Present State and Future Trends". *Biological Sciences Faculty Publications*. Paper 166.

Tourian, M.J., Tarpanelli, A., Elmi, O., Qin, T., Brocca, L., Moramarco, T., Sneeuw, N. (2016) Spatiotemporal densification of river water level time series by multimission satellite altimetry. *Water Resour. Res. 52*, 1140–1159.

Uddin, K., Matin, M.A., Meyer, F.J. (2019) Operational Flood Mapping Using Multi-Temporal Sentinel-1 SAR Images: A Case Study from Bangladesh. *Remote Sens. 11*, 1581.

Urban, T.J., Schutz, B.E., Neuenschwander, A.L. (2008) A survey of ICESat coastal altimetry applications: Continental Coast, Open Ocean Island, and Inland River. Terr. Atmos. *Ocean. Sci. 19,* 1–19.

USACE (1993) River Hydraulics, Engineering Manual 1110-2-1416, Headquarters, U.S. Army Corps of Engineers, Washington, DC

USACE (2016) HEC-RAS, River Analysis System Hydraulic Reference Manual, Institute for Water Resources, Hydrologic Engineering Center, Davis, CA, USA

USAID (undated) Climate Risk in Mali: Country Risk Profile. Available online: https://www.climatelinks.org/sites/default/files/asset/document/Mali_CRP_Final.pdf (accessed on 12 January 2019).

USDA (1972) Soil Conservation Service. *National Engineering Handbook,* Section 4, Hydrology, US Government Printing Office: Washington, DC, USA.

Vrugt, J.A., Diks, C.G., Clark, M.P. (2008) Ensemble bayesian model averaging using markov chain monte carlo sampling. *Environ. Fluid Mech*. *8*, 579–595, doi:10.1007/s10652-008-9106-3.

Vrugt, J.A., Robinson, B.A. (2007) Treatment of uncertainty using ensemble methods: Comparison of sequential data assimilation and Bayesian Model Averaging. *Water Resour. Res.*, *43*, W01411, doi:10.1029/2005WR004838.

Wang, Q.J., Roberston, D.E., and Chiew, F.H.S. (2009). A Bayesian joint probability modeling approach for seasonal forecasting of stream flows at multiple sites. *Water Resource Research, 45*, 1-18.

Wilks, D.S. (2011). Statistical Methods in the Atmospheric Sciences, third edition. *Oxford: Elsevier Inc.*

Wilson, E.H., Sader, S.A. (2002) Detection of forest harvest type using multiple dates of Landsat TM imagery. *Remote Sens. Environ. 80*, 385–396.

Wilson M. D., and Atkinson P. M (2005) The use of elevation data in flood inundation modeling: A comparison of ERS interferometric SAR and combined contour and differential GPS data, *International Journal of River Basin Management*, *3*: 1, 3-20, DOI: 10.1080/15715124.2005.9635241

Woodhead, S., Asselman, N., Zech, Y., Soares-Frazao, S., Bates, P., Kortenhaus, A. (2007) Evaluation of Inundation Models, FLOODsite Report T08-07-01. Available online: https://ecapra.og/sites/default/files/documents/Flood%20Inundation%20Modeling.pdf (accessed on 6 August 2019).

Xu, H. (2006) Modification of normalized difference water index (NDWI) to enhance open water features in remotely sensed imagery. *Int. J. Remote Sens*. *27*, 3025–3033, doi:10.1080/01431160600589179.

Yamazaki, D., Ikeshima, D., Tawatari, R., Yamaguchi, T., O'Loughlin, F., Neal, J.C., Sampson, C.C., Kanae, S., Bates, P.D. (2017) A high accuracy map of global terrain elevations. *Geophys. Res. Lett. 44*, 5844–5853, doi:10.1002/2017GL072874.

Yan, K., Di Baldassarre, G., Solomatine, D.P., Schumann, G.J.P. (2015) A review of low-cost space-borne data for flood modeling: Topography, flood extent and water level. *Hydrol. Process. 29*, 3368–3387.

Yan, K., Pappenberger, F., Umer, Y. M., Solomatine, D. P.; and Di Baldassarre, G., (2014) "Regional Versus Physically- Based Methods for Flood Inundation Modeling in Data Scarce Areas: An Application To The Blue Nile". *CUNY Academic Works. Available at* http://academicworks.cuny.edu/cc_conf_hic/111

Yan, K., Tarpanelli, A., Balint, G., Moramarco, T., Baldassarre, G.D. (2015) Exploring the Potential of SRTM Topography and Radar Altimetry to Support Flood Propagation Modeling: Danube Case Study. *J. Hydrol. Eng. 20*, 04014048.

Zhu, R., Zheng, H., Wang, E., Zhao, W. (2013) Multi-Model Ensemble Simulation of Flood Events using Bayesian Model Averaging. In Proceedings of the 20th International Congress on Modeling and Simulation, Adelaide, Australia.

Zsuffa, I., Funk, A., Diallo, M. (2013) Hydrodynamic, water quality and habitat modeling in the Inner Niger Delta. WETwin Project

Zwarts, L. (2010) Will the Inner Niger Delta Shrivel up due to Climate Change and Water Use Upstream? A&W Rapport 1537, Altenburg & Wymenga Ecologisch Onderzoek: Feanwâlden, The Netherlands.

Zwarts, L., Frerotte, J. (2012) *Water Crisis in the Inner Niger Delta (Mali), Causes, Consequences, Solutions*, A&W-Report 1832, Altenburg & Wymenga Ecologisch Onderzoek: Feanwâlden, The Netherlands.

Zwarts, L., Van Beukering, P., Kone, B., Wymenga, E. (2005) *The Niger, a Lifeline. Effective Water Management in the Upper Niger Basin. RIZA, Lelystad/Wetlands International, Sévaré*, Institute for Environmental studies (IVM): Amsterdam, The Netherlands, A&W Ecological Consultants: Veenwouden, Mali, The Netherlands.